Functional Films and Fibres based on Liquid Crystal Coatings

Picot, Oliver

Functional Films and Fibres based on Liquid Crystal Coatings

A THESIS SUBMITED TO THE UNIVERSITY OF LONDON FOR THE DEGREE OF DOCTOR OF PHILOSOPHY

August 2014

By

Olivier Picot

School of Engineering and Materials Science

Queen Mary University of London

Mile End Road, London E1 4NS

Declaration

I, Olivier Picot, confirm that the research included within this thesis is my own work or that where it has been carried out in collaboration with, or supported by others, that this is duly acknowledged below and my contribution indicated. Previously published material is also acknowledged below.

I attest that I have exercised reasonable care to ensure that the work is original, and does not to the best of my knowledge break any UK law, infringe any third party's copyright or other Intellectual Property Right, or contain any confidential material.

I accept that the College has the right to use plagiarism detection software to check the electronic version of the thesis.

I confirm that this thesis has not been previously submitted for the award of a degree by this or any other university.

Signature:

Olivier Picot

Date:

28/07/14

Details of collaboration and publications:

Mian Dai, Olivier T. Picot, Nanayaa F. Hughes-Brittain, Ton Peijs and Cees W. M. Bastiaansen, Formation of relief structures on fibres by photo-embossing, *J. Mater. Chem.*, 2011, 21, 15527

Nanayaa F. Hughes-Brittain, Olivier T. Picot, Mian Dai, Ton Peijs, Cees W.M. Bastiaansen, Effect of polymer binder on surface texturing by photoembossing, *Applied Surface Science*, 2012 258, 8609– 8612

Olivier T. Picot, Mian Dai, Ton Peijs and Cees W.M. Bastiaansen, Manufacturing of fibres with new reflective properties and their application in textiles, *Mater. Res. Soc. Symp. Proc.*, 2012, 1403

Nanayaa F. Hughes-Brittain, Olivier T. Picot, Lin Qiu, Carlos Sánchez , Ton Peijs and Cees W.M. Bastiaansen, Photoembossing for surface texturing of films and fibres for biomedical applications, *Mater. Res. Soc. Symp. Proc.*, 2012, 1418

Olivier T. Picot, Rafael Alcalá, Carlos Sánchez, Mian Dai, Nanayaa F. Hughes-Brittain, Dirk J. Broer, Ton Peijs and Cees W. M. Bastiaansen, Manufacturing of surface relief structures in moving substrates using photoembossing and pulsed-interference holography, *Macromol. Mater. Eng.*, 2013, 298, 33–37

Mian Dai, Olivier T. Picot, Julien M. N. Verjans, Laurens T. de Haan, Albertus P. H. J. Schenning, Ton Peijs, and Cees W. M. Bastiaansen, Humidity-responsive bilayer actuators based on a liquid-crystalline polymer network, *ACS Appl. Mater. Interfaces*, 2013, 5, 4945-4950

Olivier T Picot, Mian Dai, Dirk J. Broer, Ton Peijs and Cees W.M. Bastiaansen, A new approach towards reflective films and fibers using cholesteric liquid crystal coatings, *ACS Appl. Mater. Interfaces*, 2013, 5, 7117-7121

Olivier T. Picot, Mian Dai, Emiliano Billoti, Dirk J. Broer, Ton Peijs, and Cees W. M. Bastiaansen, Real time optical strain sensor based on a cholesteric liquid crystal network, *RSC Advances*, 2013, 3, 18794-18798

Olivier T. Picot, Cees W. M. Bastiaansen, Christopher Reynolds, Ton Peijs, (2011), *Process for coating a curved article*, WO 2012084200 A1

Olivier T. Picot, Mian Dai, Cees W. M. Bastiaansen, (2012), *Continuous process for preparation of a substrate with a relief structure*, WO 2013072350 A1

Olivier T. Picot, Cees W. M. Bastiaansen, Emiliano Bilotti, Ton Peijs, (2013), *Optical strain sensor*, WO2013113877 A1.

Acknowledgements

I would first like to thank my supervisors Profs Cees Bastiaansen and Ton Peijs for giving me the opportunity to carry out this PhD in their group. They have been very helpful and supportive and I enjoyed their guidance and the intensive discussions throughout the three years. I also wish to thank Dr. Emiliano Bilotti and Christopher Reynolds for their involvement in the project.

I also thank Carlos Sánchez and Rafael Alcalá for welcoming me in their group in Zaragoza University and there precious input in this work.

In Eindhoven, I would like to thank Prof. Dick Broer for his expertise and comments on liquid crystals. I also wish to thank Tom Bus for his help carrying out experiments in TU/e. Many thanks go to Mian Dai with whom it has been a pleasure to collaborate with.

I would like to thank the staff in the School of Engineering and Materials as well as Nanoforce Technology Ltd. for use of their facilities. I thank the Dutch Polymer Institute for the financial support through the project #679.

My special thanks go to my partner Charline Sellam and my family for their great support.

Abstract

This thesis aims to produce functional polymer fibres and films using liquid crystal networks or photoembossing. The work focuses on visual effects in fibres, optical sensing properties and, actuation and morphing properties. In the first part we focused on changing the perception of textiles by generating structural colours based on diffraction and/or reflection of light. For the former, a micro-structuring technique is combined with a contactless patterning technique: pulsed holography. The results show that diffractive features could be generated on static or moving polymer films allowing for large area patterning. The use of a contactless patterning technique also suggests its potential application for curved surfaces such as fibres. In the second approach, reflective colours are generated using a self-organising cholesteric liquid crystal (CLC) coating. The coating is applied in a one step process though spray coating of a liquid crystal monomer mixture on the polymer substrate followed by photopolymerization. Reflectivity measurements and optical microscopy show that a well-defined liquid crystalline and planar alignment is obtained. In the case of films, a strong angular dependent reflection is obtained. In comparison fibres shown lower reflectivity with an angular dependent colour in a single dimension along the fibre direction which originates from the planar cholesteric alignment on a curved surface. The second part of the project was aimed at detecting strain optically in polymer films and fibres. Here, we used the same process to produce reflective films and studied the optical response to uniaxial deformation. Results showed a colour shift as function of strain that was dependent on the mechanical behaviour of the substrate giving real time information of the deformation in the substrate. In the final part the thesis, we explored shape change in

response to light of a bilayer photoresponsive film for adaptive textile applications. Here we showed that bending could be generated by coating a photoresponsive LC layer on an oriented polymer substrate. Bending is attributed to a photo induced contraction that occurs in the coating. The resulting response was strongly dependent on the substrate thickness and stiffness, thermo-mechanical properties and the concentration of chromophore in the LC layer.

Table of Contents

List of figures

List of tables

List of publications

Mian Dai, Olivier T. Picot, Nanayaa F. Hughes-Brittain, Ton Peijs and Cees W. M. Bastiaansen, Formation of relief structures on fibres by photo-embossing, *J. Mater. Chem.*, 2011, 21, 15527

Nanayaa F. Hughes-Brittain, Olivier T. Picot, Mian Dai, Ton Peijs, Cees W.M. Bastiaansen, Effect of polymer binder on surface texturing by photoembossing, *Applied Surface Science*, 2012 258, 8609– 8612

Olivier T. Picot, Mian Dai, Ton Peijs and Cees W.M. Bastiaansen, Manufacturing of fibres with new reflective properties and their application in textiles, *Mater. Res. Soc. Symp. Proc.*, 2012, 1403

Nanayaa F. Hughes-Brittain, Olivier T. Picot, Lin Qiu, Carlos Sánchez , Ton Peijs and Cees W.M. Bastiaansen, Photoembossing for surface texturing of films and fibres for biomedical applications, *Mater. Res. Soc. Symp. Proc.*, 2012, 1418

Olivier T. Picot, Rafael Alcalá, Carlos Sánchez, Mian Dai, Nanayaa F. Hughes-Brittain, Dirk J. Broer, Ton Peijs and Cees W. M. Bastiaansen, Manufacturing of surface relief structures in moving substrates using photoembossing and pulsed-interference holography, *Macromol. Mater. Eng.*, 2013, 298, 33–37

Mian Dai, Olivier T. Picot, Julien M. N. Verjans, Laurens T. de Haan, Albertus P. H. J. Schenning, Ton Peijs, and Cees W. M. Bastiaansen, Humidity-responsive bilayer actuators based on a liquid-crystalline polymer network, *ACS Appl. Mater. Interfaces*, 2013, 5, 4945-4950

Olivier T Picot, Mian Dai, Dirk J. Broer, Ton Peijs and Cees W.M. Bastiaansen, A new approach towards reflective films and fibers using cholesteric liquid crystal coatings, *ACS Appl. Mater. Interfaces*, 2013, 5, 7117-7121

Olivier T. Picot, Mian Dai, Emiliano Billoti, Dirk J. Broer, Ton Peijs, and Cees W. M. Bastiaansen, Real time optical strain sensor based on a cholesteric liquid crystal network, *RSC Advances*, 2013, 3, 18794-18798

Olivier T. Picot, Cees W. M. Bastiaansen, Christopher Reynolds, Ton Peijs, (2011), *Process for coating a curved article*, WO 2012084200 A1

Olivier T. Picot, Mian Dai, Cees W. M. Bastiaansen, (2012), *Continuous process for preparation of a substrate with a relief structure*, WO 2013072350 A1

Olivier T. Picot, Cees W. M. Bastiaansen, Emiliano Bilotti, Ton Peijs, (2013), *Optical strain sensor*, WO2013113877 A1.

Chapter 1

General introduction

1.1 Functional textiles

Traditionally, textiles are produced from either natural fibres or synthetic fibres, or a combination of both.[1] While natural fibres, sourced from animals or plants have been used since the beginning of textiles, synthetic fibres appeared less than 100 years ago with the development of nylon.[2] Today synthetic fibres represent more than half of the global supply of fibres, with polyesters and polyamides being the most produced.[3] Textiles are used in various fields such as sport, fashion, medicine but also in architecture or military. Today there is a growing interest in creating multi-functional fibres, for use in fabrics and textiles that can sense, respond, see, hear or even communicate. Thanks to on-going developments in technology and progress in the field of materials, textiles with diverse functions have already been produced. Some examples are self-cleaning textiles, temperature regulating textiles, sensing

textiles, display textiles, self-actuating textiles, luminescent textiles or e-textiles (integrating electronics and computing elements).[4-14] The development of functional textiles requires, by definition, integrating new functionalities into the textile itself. Successful approaches have been developed, such as breathable waterproof clothing based on porous polytetrafluoroethylene (PTFE) membranes. The main feature of the membrane is to repel water droplets while allowing moist vapour to be transported through. However it is usually layered with other fabrics to create synergistic effects with added comfort or durability. Other approaches using the textile as a substrate to attach sensors or electronic elements (for instance wearable computers) have also been demonstrated although here there is little integration and as a result, weight or flexibility of the textile can be hampered.[10] This can be addressed by integrating desired functionalities directly into the constituting fibres. To date, the main approach has been to combine processes or materials from the field of electronics or optics with fibre spinning processes.[15] For instance Yoel Fink and co-workers used thermal drawing to produce functional fibres. In this process a cylindrical preform is heated and drawn to form kilometre long fibres with a diameter of hundredths of microns. The properties of these fibres come from the materials selected for the preform. The researchers showed that by combining a high glass temperature polymeric thermoplastic and a high refractive index glass into a layered structure, they could successfully produce infrared reflecting fibres.[16] Furthermore, by selecting the appropriate materials for the preform; thermal, electrical, optical and acoustic properties were also introduced into fibres using this approach.[17-20] In this thesis we aim to create optical, sensing and/or responsive functionalities in synthetic fibres. To this effect, we use materials and processes from the electronics and display

industry, liquid crystals or photoembossing, and combine them with the fibre itself or during the spinning process.

1.2 Liquid crystals

Liquid crystals (LC) are a class of material that have a state of matter between the solid phase and the liquid phase, called the liquid crystalline phase. They consist of rigid anisotropic molecules. According to their geometry, they are defined as calamitic or rod-like, discotic and bent-core.[21] In this work, the molecules used are calamitic LCs. An example is shown in (Figure 1.1). They have a distinctive elongated shape and their structure usually consists of a rigid core formed by cyclic compounds to which are attached flexible spacers and in some cases a lateral substituent.[22]

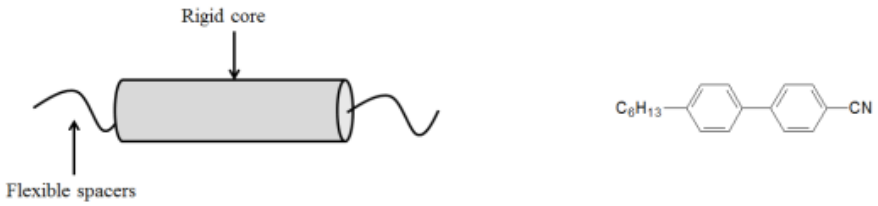

Figure 1-1 Representation of a calamitic liquid crystal molecule with a general representation of the associated structure.

The different phases can be described according to the order of the molecules. In the isotropic liquid phase, molecules have no orientational or positional order while in the solid crystalline phase they possess both orders. In the liquid crystalline phase,

molecules are not as ordered as in a crystal, yet they have some degree of positional or orientational order (Figure 1.2).

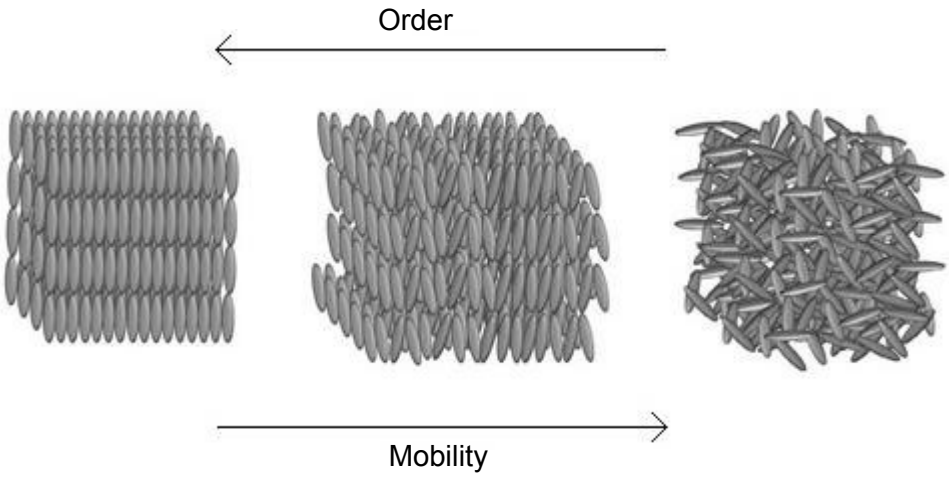

Figure 1-2 Schematic representations of the crystalline phase, liquid crystalline phase and isotropic phase, respectively.

Phase transition can be observed in LC materials as a function of temperature changes. Such LCs are called thermotropic.[23] On the other hand, we also distinguish lyotropic LCs where the phase transitions occurs in solution as a function of the concentration of the LC molecules.[23] Depending on the degree of order several liquid crystal phases have been identified and are classified into two categories: nematic or smectic (Figure 1.3). In the nematic phase, molecules have only orientational order along the director, i.e. they tend to be parallel to a common axis called the director and denoted by the unit vector $\underline{n}$. The smectic phase is a phase of higher order in comparison with the previous one and therefore it is usually obtained at temperatures below the nematic phase. In this phase molecules are generally organised in layers with a specific spacing *d* between each layer. The thickness can vary from the full

length of the molecule to twice this length.[24] In each layer, there is only orientational order. Depending on the orientation of the director, different type of smectic phases can be observed. The most common types of smectic phases are smectic A where the molecules are orthogonal to the layer plane, and smectic C which can be described as a tilted form smectic A.

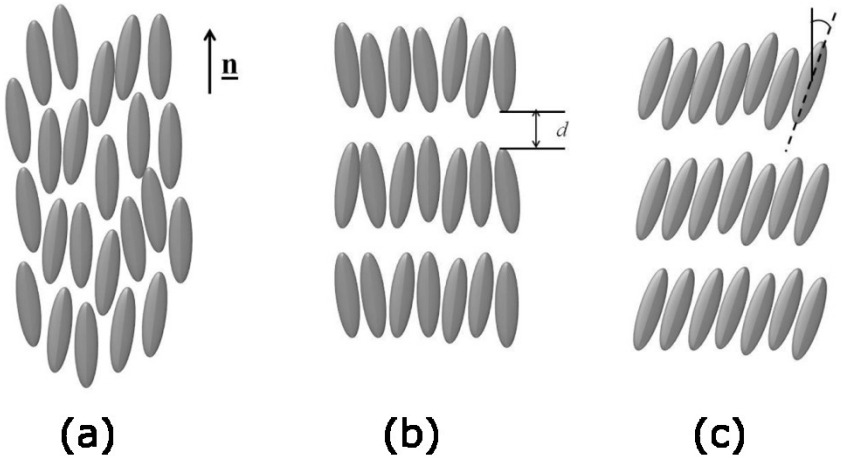

Figure 1-3 Schematic representation of different liquid crystal phases: (a) nematic, (b) smectic A and (c) smectic C.

When a chiral substituent is attached to the LC or a chiral molecule is added to the liquid crystal mixture itself, a chiral liquid crystal is obtained. The LC phases obtained are mainly the cholesteric liquid crystalline phase (CLC) or chiral nematic liquid crystalline phase, and the chiral smectic phase. The chiral molecule induces a twist in director of the LC molecules resulting in a helical structure (Figure 1.4). The latter is characterized by its pitch *P* which is defined as the length, over which a complete rotation of the mesogen is obtained, and its handedness can be left or right.

Typical values of the spatial period *P* range from a few microns to hundredths of nanometres.

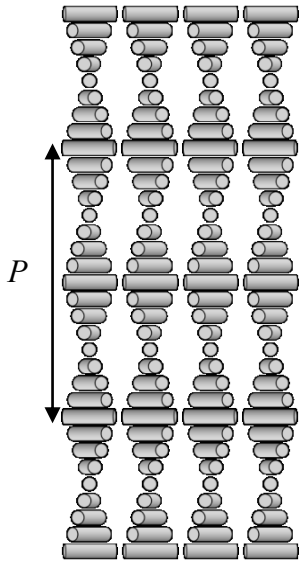

Figure 1-4 Illustration of the helical order in the cholesteric liquid crystalline phase.

This description of LC phases is qualitative, but in some cases it is more convenient to use the order parameter *S* which quantifies the orientational order of the molecules. It is defined by Equation 1.1, where θ is the angle between the director $\underline{n}$ (Figure 1.5) and the long axis of the molecule.

$$S = \langle (3\cos^2\theta) - 1 \rangle / 2 \qquad (1.1)$$

The brackets represent an average over time of one molecule or the average of many molecules at the same time. In a perfectly ordered crystal, *S* is equal to 1. Typical in the LC phase *S* will vary from 0.8 to 0.3 as temperature increases (Figure 1.5).[25] At the liquid crystal-isotropic phase transition temperature, *S* drops to 0 as there is no orientational order in the isotropic phase.

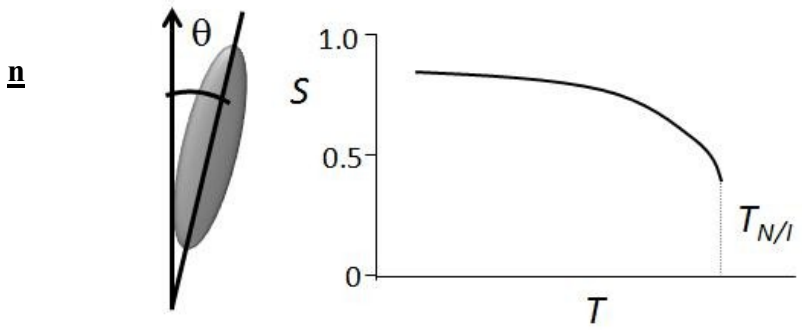

Figure 1-5 Schematic representation of the angle θ and the change in order parameter (S) as a function of temperature

1.3 Liquid crystal polymers

Liquid crystal polymers are a class of polymer that uses low molecular weight LC molecules as monomer units. Main chain or side chain polymers are obtained depending on how the monomer units are attached to the polymer backbone (Figure 1.6). In a main chain LC polymer, the liquid crystal units are attached head-to-tail by the polymer backbone. Main chain LC polymers usually have high strength and high modulus and also good heat resistant properties (i.e. high glass transition temperature and melting point).[22, 26] Side chain polymers have the LC units attached to the side of the polymer backbone as pendant groups. As opposed to main chain LC polymers, side chain LC polymers show mesogenic behaviour over a wide range of temperatures owing to the higher freedom of the LC units.[27] A third type of liquid crystal polymer is the liquid crystal network. Similar to a side-chain LC polymer, the mesogenic units are attached on both sides to the polymer backbone, yielding a densely cross-linked polymer.

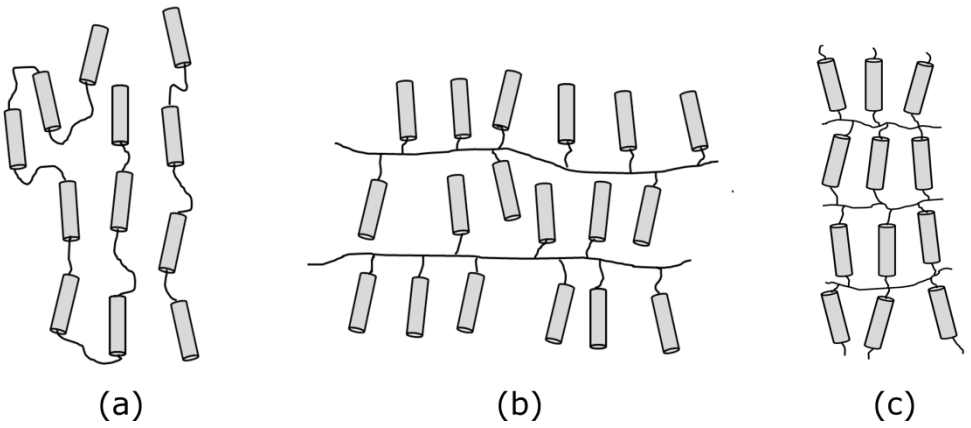

Figure 1-6 Schematic representation of main chain (a) and side chain (b) liquid crystal polymers and a liquid crystal network (c).

1.4 Photoembossing

The photoembossing process is a microstructuring process that allows surface relief structures to be created with a defined pattern. The technique uses a photopolymer blend consisting of a polymeric binder, a multifunctional acrylate monomer, a photoinitiator and optional additives such as inhibitors or chain transfer agents.[28-30] The mixture is processed from solution with a volatile solvent and a thin solid film is obtained, after solvent evaporation, on a rigid or flexible substrate (Figure 1.7a). The relief structure is then generated in three steps (Figure 1.7b, c and d): (i) the film is exposed to patterned UV light to locally activate the photoinitiator, (ii) the film is heated and (iii) the film is further cured by exposing it to a flood UV exposure and a second heating step. The relief structure develops after the patterned UV exposure by heating the film above a threshold temperature. This threshold is often a discrete thermal transition like the glass transition to increase monomer mobility and enhance

polymerization. Before heating and after the first exposure, the film is in the glassy state and both monomer diffusion and chemical reactions are strongly suppressed. After heating the film, the polymerization reaction and the subsequent consumption of monomer in the exposed areas provides a driving force for the diffusion of the reactive species from the non-exposed areas to the exposed areas and the resulting mass transport generates the relief structures.[29, 31, 32]

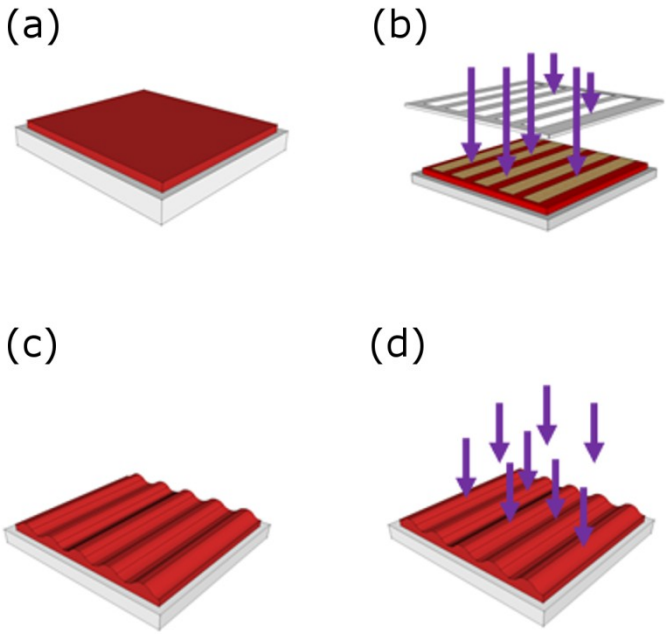

Figure 1-7 Schematic representation of the photoembossing process which consist of (a) photopolymer film preparation, (b) patterned UV light exposure, (c) heating step and (d) UV flood exposure.

1.5 Outline of the thesis

The aim of the work is to create films and fibres with new functionalities. In the first part, the purpose is to change the visual perception of textiles. Traditionally,

inorganic or organic dyes are used to produce colours in textiles which are based on the absorption of light. Here we will demonstrate two processes to obtain visual effects based on diffraction and/or reflection of visual light. Chapter 3 shows how diffractive gratings can be generated on fibres in a continuous process by combining pulsed interference holography with photoembossing. In Chapter 4, reflective optics will be introduced by coating a cholesteric liquid crystal mixture onto oriented polymer substrates. The process will be demonstrated on both flat films and fibres with a round cross-section and the effect of the substrate geometry on the perceived colour will be investigated.

Secondly, the work is aims to develop fibres with an integrated optical strain sensing capability. Using the same process as described in Chapter 4, an optical strain sensor is demonstrated in Chapter 5. Here, a uniaxially oriented polyamide 6 substrate is coated with a CLC layer and the sensing behaviour is investigated by measuring the optical response under uniaxial deformation.

The final part of this work aims at developing films or fibres that respond to environmental triggers such as light, via bending. Here we use liquid crystalline networks comprising azobenzene moieties to generate a light induced actuation of the film or fibre. In Chapter 6 bi-layer films consisting of an oriented polymer substrate and the aforementioned LC network are produced. We show that a uniaxial contraction is generated in the LC layer and consequently a bending response of the bi-layer is obtained. The relationship between thermo-mechanical properties of the substrate and the resulting deformation is discussed.

1.6 References

1 T. Hongu, G. O. Phillips, "*New fibres"*, Ellis Horwood, New York, 1990, p. 1-5.

2 K. K. Chawla, "*Fibrous materials"*, Cambridge University Press, Cambridge, England ; New York, 1998, p. 1-5.

3 J. E. McIntyre, Textile Institute (Manchester England), "*Synthetic fibres : nylon, polyester, acrylic, polyolefin"*, CRC Press ; Woodhead Pub., Boca Raton Cambridge, England, 2005, p. 1-15.

4 B. Gauvreau, N. Guo, K. Schicker, K. Stoeffler, F. Boismenu, A. Ajji, C. Dubois, M. Skorobogatiy, *2009 Conference on Lasers and Electro-Optics and Quantum Electronics and Laser Science Conference (Cleo/Qels 2009), Vols 1-5* **2009**, 461.

5 S. Mondal, *Appl Therm Eng* **2008**, *28*, 1536.

6 J. L. Hu, H. P. Meng, G. Q. Li, S. I. Ibekwe, *Smart Mater Struct* **2012**, *21*.

7 J. L. Hu, S. J. Chen, *J Mater Chem* **2010**, *20*, 3346.

8 R. Zhang, H. Deng, R. Valenca, J. H. Jin, Q. Fu, E. Bilotti, T. Peijs, *Sensor Actuat a-Phys* **2012**, *179*, 83.

9 C. Mattmann, F. Clemens, G. Troster, *Sensors-Basel* **2008**, *8*, 3719.

10 G. Cho, "*Smart clothing : technology and applications"*, CRC Press, Boca Raton, FL, 2010, p. 1-8.

11 J. Kiwi, C. Pulgarin, *Catal Today* **2010**, *151*, 2.

12 K. S. Liu, L. Jiang, *Annu Rev Mater Res* **2012**, *42*, 231.

13 http://www.sensingtex.com/index.php/en/.

14 K. Cherenack, L. van Pieterson, *J Appl Phys* **2012**, *112*.

15 A. F. Abouraddy, M. Bayindir, G. Benoit, S. D. Hart, K. Kuriki, N. Orf, O. Shapira, F. Sorin, B. Temelkuran, Y. Fink, *Nat Mater* **2007**, *6*, 336.

16 S. D. Hart, G. R. Maskaly, B. Temelkuran, P. H. Prideaux, J. D. Joannopoulos, Y. Fink, *Science* **2002**, *296*, 510.

17 S. Egusa, Z. Wang, N. Chocat, Z. M. Ruff, A. M. Stolyarov, D. Shemuly, F. Sorin, P. T. Rakich, J. D. Joannopoulos, Y. Fink, *Nat Mater* **2010**, *9*, 643.

18 M. Bayindir, A. E. Abouraddy, J. Arnold, J. D. Joannopoulos, Y. Fink, *Adv Mater* **2006**, *18*, 845.

19 M. Bayindir, O. Shapira, D. Saygin-Hinczewski, J. Viens, A. F. Abouraddy, J. D. Joannopoulos, Y. Fink, *Nat Mater* **2005**, *4*, 820.

20 O. Shapira, A. Stolyarov, N. D. Orf, K. Kuriki, A. F. Abouraddy, J. D. Joannopoulos, Y. Fink, *Opt. Photon. News* **2007**, *18*, 26.

21 S. Kumar, "*Chemistry of Discotic Liquid Crystals : from Monomers to Polymers"*, CRC Press, Boca Raton, **2011**, p. 1-14.

22 X. Wang, Q. Zhou, "*Liquid Crystalline Polymers"*, World Scientific Pub. Co., River Edge, N.J., 2004, p. 6.

23 S. Chandrasekhar, "*Liquid Crystals"*, 2nd edition, Cambridge University Press, Cambridge England ; New York, NY, USA, 1992, p. 1-14.

24 R. A. Pethrick, "*Polymer Structure Characterization : from Nano to Macro Organization"*, RSC Publishing, Cambridge, U.K., 2007, p. 68-123.

25 P. J. Collings, M. Hird, "*Introduction to Liquid Crystals Chemistry and Physics"*, Taylor & Francis, London ; Bristol, PA, 1997, p. 10-14.

26 T. Scharf, "*Polarized Light in Liquid Crystals and Polymers"*, Wiley-Interscience, Hoboken, N.J., 2007, p. 127-129.

27 J. W. S. Hearle, Textile Institute (Manchester England), "*High-performance Fibres"*, CRC Press ; Woodhead Pub., Boca Raton Cambridge, England, 2001, p. 23-58.

28 J. Perelaer, K. Hermans, C. W. M. Bastiaansen, D. J. Broer, U. S. Schubert, *Adv Mater* **2008**, *20*, 3117.

29 K. Hermans, F. K. Wolf, J. Perelaer, R. A. J. Janssen, U. S. Schubert, C. W. M. Bastiaansen, D. J. Broer, *Appl Phys Lett* **2007**, *91*.

30 C. DeWitz, D. J. Broer, *Polymer Preprint* **2003**, *44*, 236.

31 C. Sanchez, B. J. de Gans, D. Kozodaev, A. Alexeev, M. J. Escuti, C. van Heesch, T. Bel, U. S. Schubert, C. W. M. Bastiaansen, D. J. Broer, *Adv Mater* **2005**, *17*, 2567.

32 T. Meyer, J. Keurentjes, "*Handbook of Polymer Reaction Engineering*", Wiley-VCH, Weinheim, 2005, p. 995-1013.

Chapter 2

Liquid crystal networks

2.1 Alignment of LC networks

In the nematic phase, the molecules intrinsically align along a preferred axis and polydomain morphologies with different orientation in each domain are usually obtained. In order to obtain a LC film with monodomain morphology, a driving force is necessary to align the mesogens. Owing to the strong dipole of mesogens, the orientation of the director can be controlled with electric or magnetic fields.[1-2] Another route is through surface alignment which is usually done by coating the substrate with a polymer layer followed by mechanical rubbing.[1-4] Common polymers used for the coating are polyimide (PI) or polyvinylalcohol (PVA). Different molecular organisations can be obtained in nematic LC film (Figure 2.1).

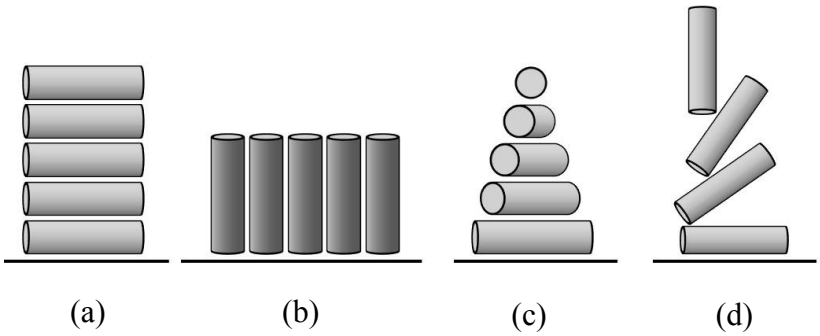

Figure 2-1 Representation of various molecular organisations: (a) planar, (b) homeotropic, (c) twisted and (d) splay.

In the planar alignment, molecules are parallel to the surface while in a homeotropic alignment the director is perpendicular. The twisted nematic (TN) is obtained when the director rotates by 90^{o} between the top and bottom surface. The splay alignment is a hybrid alignment between planar and homeotropic. In the case of cholesteric or chiral nematic LCs (or CLCs), three specific organisations are encountered depending on the orientation of the cholesteric helix with respect to the surface of the film (Figure 2.2a to c). The planar texture or Grandjean texture, is found when the helix axis is perpendicular to the surface while the fingerprint texture is obtained if the helix axis is parallel to the surface. Finally the focal conic texture is a multidomain organisation with the helix axis tilted randomly with respect to the surface. The different alignments found in the CLC phase can easily be identified by optical microscopy.

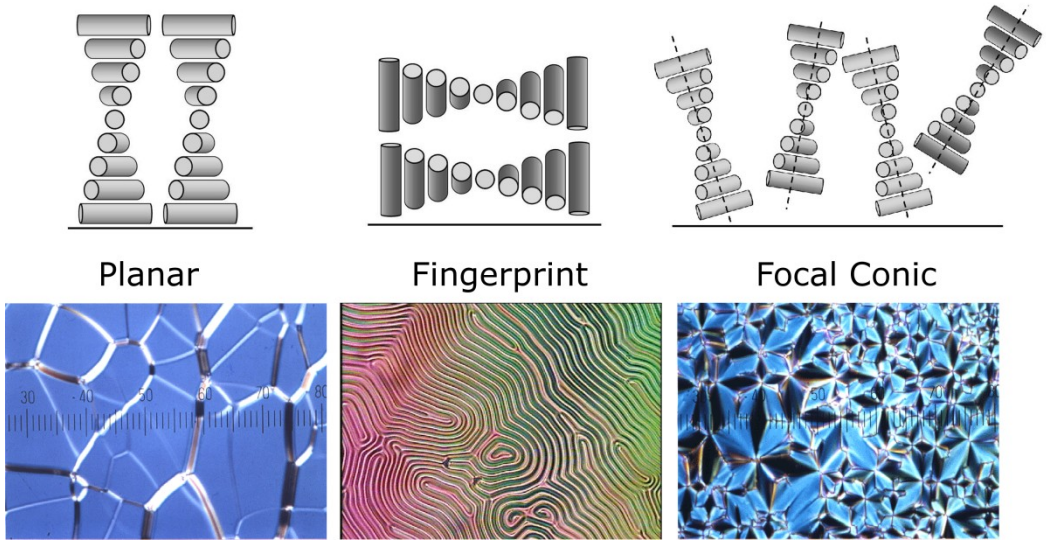

Figure 2-2 Representation and optical microscopy images of the three main CLC alignments with the corresponding texture as seen by optical microscopy (Courtesy of Ingo Dierking).[5]

2.2 Cross-linked liquid crystalline networks

In cross-linked liquid crystalline networks, the monomers are attached by each end to the polymer backbone. As a result, mobility is greatly decreased and the phase transitions disappear.[6] Ordered liquid crystal networks can be obtained by aligning the LC monomers in the desired mesophase on a substrate followed by a polymerization step to "lock in" the molecular order. Liquid crystal networks were first obtained by thermally initiated bulk polymerization of diacrylate functionalized LC monomers, resulting in a highly ordered LC polymer.[7] However, the use of temperature hampers processing as the LC phases are also temperature dependent. A more versatile route based on photoinitiated polymerization of liquid crystal

monomers is usually preferred.[8-12] Here, a photoinitiator is dissolved in the monomer mixture and polymerization is initiated upon exposure to a specific wavelength of light, which corresponds to the absorption wavelength of the photoinitiator. This process is illustrated in Figure 2.3.

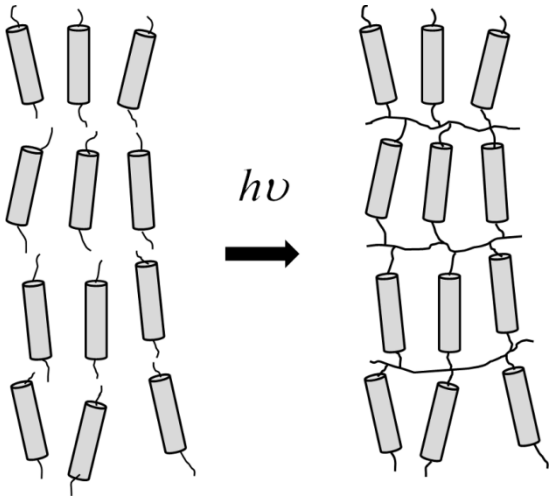

Figure 2-3 Formation of a liquid crystal network through photoinitiated polymerization of liquid crystal monomers.

Figure 2.4 shows the chemical structure of a diacrylate monomer that is widely used for cross-linked LC material.[13] Here x represents the length of the spacer and stands for the number of carbon atoms in the aliphatic chain and R indicates the side group attached to the LC core that is usually a hydrogen atom or a methyl group.

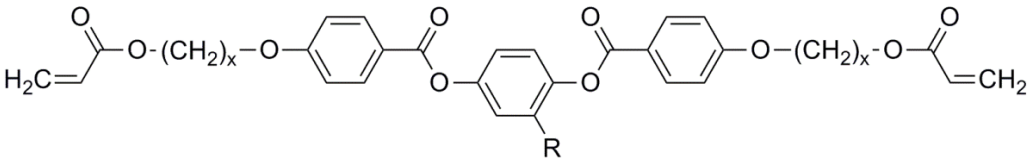

x	R
2	CH_3
3	H
4	
6	
10	

Figure 2-4 General molecular structure of an LC acrylate monomer with common spacer length and side groups

The properties of the mesogens greatly depend on the spacer length and the substituent group. For instance introducing a methyl group on the mesogen unit decreases both crystalline-nematic and nematic-isotropic transitions. Additionally, it suppresses the smectic transition upon cooling. Table 2-1 gives an overview of the phase transitions for common LC acrylate monomers. Overall, the melting temperature tends to decrease with increasing spacer length and a smectic phase is present for spacer length longer than 6 methyl groups ($x > 6$).

Table 2-1 Common LC monomers of the CxR family with their phase transitions upon heating[6, 8, 12]

Spacer length	Substituent	Phase transitions
4	H	**C** 96 **S** 112 **N** 137 I
6	H	**C** 108 (**S** 88)[a] **N** 155 I
6	CH_3	**C** 86 **N** 116 **I**
8	H	**C** 82 **S** 108 **N** 148 **I**
10	H	**C** 87 **S** 112 **N** 137 **I**

[a] visible during cooling

Acrylate based monomers have high reactivity which allows for quick cross-linking.[14-15] However, oxygen present in air inhibits the reaction and therefore photopolymerization is usually carried out in oxygen free atmosphere.[16] Other reactive groups which are not as sensitive to air, such as epoxides, thiol-enes or oxetanes, have also been used to functionalize LC monomers and produce cross-linked LC networks.[7]

2.2.1 Thermomechanical properties of LC networks

After polymerization of the monomers the liquid crystalline behaviour is lost, *i.e.* the phase transitions are suppressed. As encounter with oriented polymers, LC networks exhibits strong anisotropy in mechanical and optical properties.[17] As in their monomer form, spacer length and side groups will also influence the properties of the polymers. Typically, the glass transition temperature of these materials is above room temperature. In LC cross-linked systems, the glass transition temperature is

greatly influenced by the cross-link density of the network.[18] Hikmet *et al.* showed that increasing the length of the flexible spacer results in higher mobility in the network with the glass transition temperature shifting toward lower temperatures.[6, 19] Equally the same effect was observed in films formed from a mixture of di-acrylate and mono-acrylate LC monomers in different ratios. Spacer length also affects the mechanical properties of the material. For instance, Young's modulus of a LC polymer film with a planar alignment, measured parallel to the orientation direction, decreased by a ~56% when the number of methyl groups in the spacer increased by a factor of 2 (Table 2-2).[19]

Table 2-2 Various properties of LC polymer film with a planar alignment[19]

Spacer length	Substituent	Tg (C^o)	E (GPa)[a]
4	H	118	4.8
6	H	83	2.6
6	CH_3	83	2.6
8	H	71	2.1
10	H	55	1.6

[a] Measured at 25^{o}C

2.3 Cholesteric liquid crystal networks

The cholesteric liquid crystal phase is readily obtained by adding a chiral component to a nematic liquid crystal to generate the helical structure. The pitch length depends on the concentration (*C*), the helical twisting power (*HTP*) which the ablity to induce

a twist in the LC orientation and the enantiomeric excess (*ee*) of the dopant (Equation 2.1).[20]

$$P = (HTP \times C \times ee)^{-1} \quad (2.1)$$

The enantiomeric excess expresses the ratio of one enantiomer over the other, *i.e.* in a right handed chiral compound this would represent the amount of left handed molecules present. Additionally, the sign of *ee* gives the handedness: positive is right handed and negative is left handed.[21-22]

2.3.1 Optical properties of chiral LCs

The periodic modulation of the refractive index caused by the rotation of the director gives unique optical properties. When light is incident to a CLC film with a planar texture, reflection of a portion of light takes place (Figure 2.6).[21]

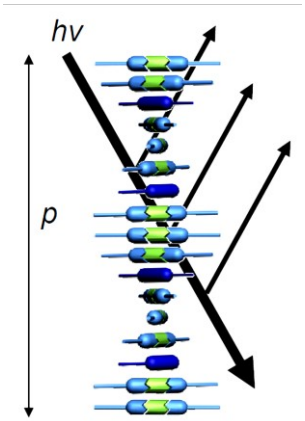

Figure 2-6 Schematic representation of the light reflection in a CLC structure. The pitch *P* is indicated. (reproduced from [13])

At normal incidence with respect to the helical axis, the reflected wavelength is centred on a specific value (λ_0) and is given by Equation 2.2:[23]

$$\lambda_0 = \bar{n}P \qquad \text{with } \bar{n} = \frac{(n_e+n_o)}{2} \tag{2.2}$$

where $\bar{n}$ is the average refractive index of the polymer, n_e and n_o the extraordinary and ordinary refractive index, and P is the pitch of the helix. The width of the reflection band ($\Delta\lambda$) is proportional to the birefringence (Δn) of the polymer and is given by Equation 2.3:[23]

$$\Delta\lambda = \lambda_0 \frac{\Delta n}{\bar{n}} \qquad \text{with } \Delta n = (n_e - n_o) \tag{2.3}$$

The reflected light is circularly polarized with its handedness matching the one of the helix. For instance a right handed helix will reflect right handed circular polarized light and transmit left handed circularly polarized light.

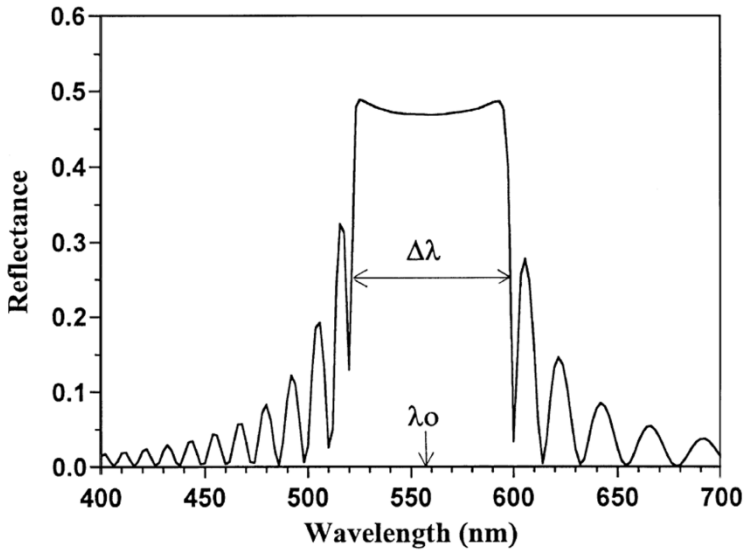

Figure 2-7 Reflection spectrum as a function of wavelength for non-polarized light. (reproduced from [24])

A typical reflection spectrum is shown, with the central wavelength λ_0, the reflection band width $\Delta\lambda$. The polarization selectivity of the reflected wavelength limits the maximum reflection of incident un-polarized light to 50%. The additional fringes outside of the reflection band are due to interference of light induced by the interfaces between the CLC and the media surrounding the CLC *i.e.* air and glass.[25] Under oblique incidence with respect to the helical axis, the reflection band shifts according to Bragg's law (Equation 2.4):[23]

$$\lambda_0 = \bar{n} P_0 cos\theta \qquad (2.4)$$

Where θ is the incident angle, the reflected wavelength is blue shifted, *i.e.* λ decreases towards the blue/violet part of the spectrum.

2.4 Responsive CLC networks

Materials that show dynamic colour changes such as thermochromic or photochromic dyes have been very attractive for various applications ranging from eyewear, smart textiles or sensors.[26-29] In LC polymer networks, mobility is hindered by the cross-links. With such materials colour changes require a co-operative response of the polymer network. As there is a strong coupling between the polymer backbone and the LC orientation, any changes in the polymer can transfer to the LC organisation. Three different changes can occur in CLC networks:

- Compression or shrinkage of the CLC layer leads to a pitch decrease and a blue shift of the reflection band.
- Swelling of the polymer results in a pitch increase and a red shift.
- A reduction in order results in a narrowing and disappearance of the reflection band caused by the change in birefringence Δn of the polymer.

The followings sections will deal with different CLC polymer sensors based on the above mentioned mechanism.

2.4.1 Solvent/Gas sensitive CLCs

Van Oosten *et al.* investigated the optical response of a CLC film to trimethylamine gas.[13] Hydrogen bonds were introduced into the polymer network and typically two non-liquid crystalline monomers that can pair by hydrogen bonding are used.[33] The paired molecules have a rod-like conformation and show liquid crystalline behaviour.[34] In their study, authors used a mixture of monomer 6OBA and 6OBA-M

and methyladipic acid (MAA) to form a chiral trimer (Figure 2.8). A diacrylate monomer was also added as a cross-linking agent and increases the mechanical stability of the film .The sensor was produced though inkjet printing followed by photopolymerization in the chiral nematic phase.

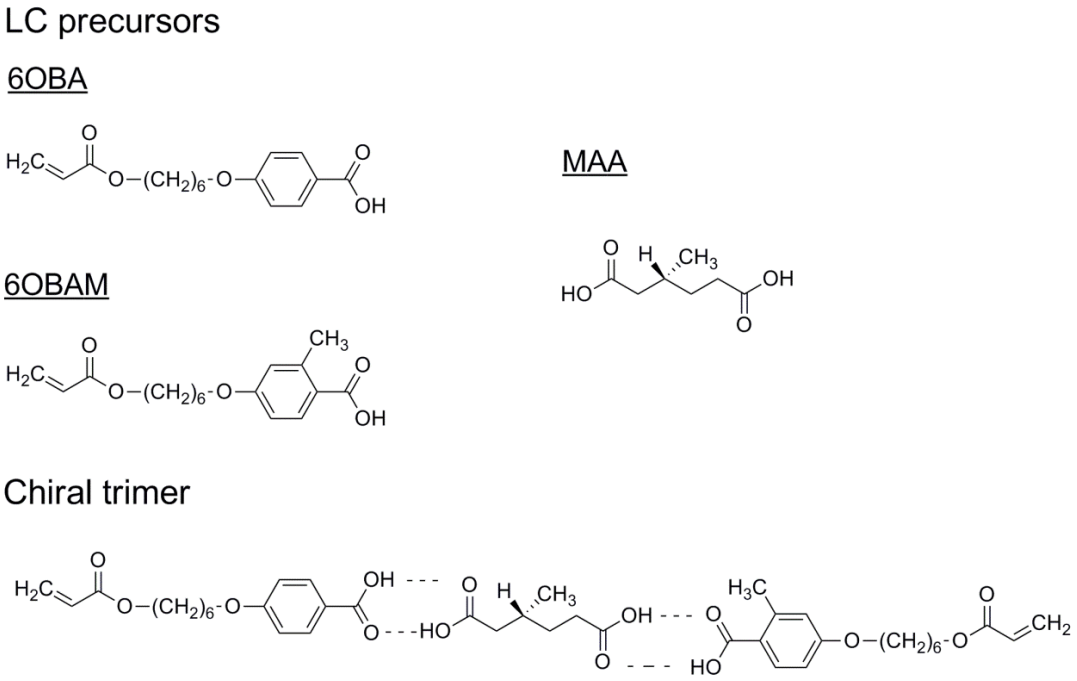

Figure 2-8 Molecular structure of the different monomers and one of the possible trimers obtained in the mixture of monomers formed by hydrogen bonding.

Exposure to trimethylamine fumes from a 45% solution in water, led to a decrease in the reflection band by 25% with a slight red shift. The decrease in reflection was attributed to a reduction in order induced by the breakage of the H-bonds under the action of the strongly basic gas. Swelling of the network caused the pitch length to increase resulting in a red shift of the reflection band. This reflection band was partially recovered after drying the film. The film was also responsive to solvents. The authors demonstrated that immersing the sensor in an aqueous solution of 1%

4,4' dipyridyl resulted in a red shift of the reflection band. Here the pitch length increased due to a swelling of the network caused by the complexation of the 4,4' dipyridyl with the hydrogen bonds.

2.4.2 Humidity optical sensor

Based on the same concept of hydrogen bonded CLC networks, Schenning *et al*. produced a humidity sensor.[35] In their work they used a combination of the same monomers 6OBA and 6OBA-M shown previously, mixed with the diacrylate (C6M) and monoacrylate (C6BP) (Figure 2.8). As a chiral compound they used the chiral LC monomer LC756 (BASF). The sensor was also produced though inkjet printing followed by photopolymerization. The formed polymer was then immersed into an aqueous solution of potassium hydroxide (0.5 $mol.L^{-1}$) to convert the polymer into a salt and thereby making it hygroscopic. Exposure of the sensor for 5 min to water vapour resulted in a swelling of the polymer salt accompanied by a colour change from green to yellow-orange. The film was sensitive enough to detect relative humidity as low as 3%.

2.4.3 Temperature sensitive CLCs

The humidity sensor presented above was also demonstrated to allow temperature sensing. As the polymer salt is hygroscopic, temperature induced evaporation of absorbed water led to pitch decrease resulting in a blue shift that was reversible in time. The CLC sensor produced by Van Oosten also showed an optical response to temperature. Heating the CLC film above 130 ^{o}C, hydrogen bonded MAA

evaporated from the film, resulting in an irreversible blue shift of the reflected colour. As the colour is irreversible, this type of sensor is particularly suitable for time integrating temperature sensing applications. Although the need for high temperature is limits the applications. Vacarro et al. demonstrated a time integrating optical sensor in a CLC polymer hydrogen bonded network.[36] In their work, the CLC network reflecting in the visible region is mechanically embossed above the glass transition temperature (*Tg*~ 50 ^{o}C), thus reducing the pitch length and shifting the reflection band to lower wavelengths. When the material is heated above the glass transition temperature, the pitch length is restored through the shape memory of the polymer. As a result a permanent red shift of the reflection band can be observed. Reported results showed that temperature changes between 41 ^{o}C and 55 ^{o}C were successfully detected.

2.5 Responsive LC networks: actuators

The previous section focused on optical responses of LC networks with a cholesteric alignment. Here the interest is on LC networks responding through mechanical deformations to external stimulus such as light, pH or humidity and temperature. Mechanical deformation of liquid crystal network was first predicted theoretically in 1975, by De Gennes for liquid crystal elastomer (LCE).[37] He proposed that LCEs could contract in the direction of the director axis in response to heat as an effect of both the rubber elasticity of the polymer network and the reorientation of the LC unit in the different phases. This was then proven experimentally in 1994, by Finkelmann.[38] Since this pioneering work, reversible mechanical deformation has been reported in several other LC based materials in response to various stimuli such

as light, electricity, pH or humidity. The following section will describe the mechanisms involved in light, water and temperature induced actuation in a liquid crystal network.

2.5.1 Light driven actuation

2.5.1.1 Photoisomerisation and photocontraction

Light induced deformation in liquid crystal network is very attractive as it can be remotely controlled and can produce a considerable and rapid response.[39] Light induced actuation is typically obtained by introducing photosensitive molecules or additives in the LC network such as azobenzenes, carbon nanotubes and spiropiran.[40-44] Azobenzenes are by far the most studied class of photosensitive molecules for photoresponsive LC networks.[41] Azobenzenes are composed of two aromatic rings linked by a N=N (Figure 2.9a). The aromatic rings provide stiffness to the azobenzene resulting in liquid crystalline behaviour.[45]

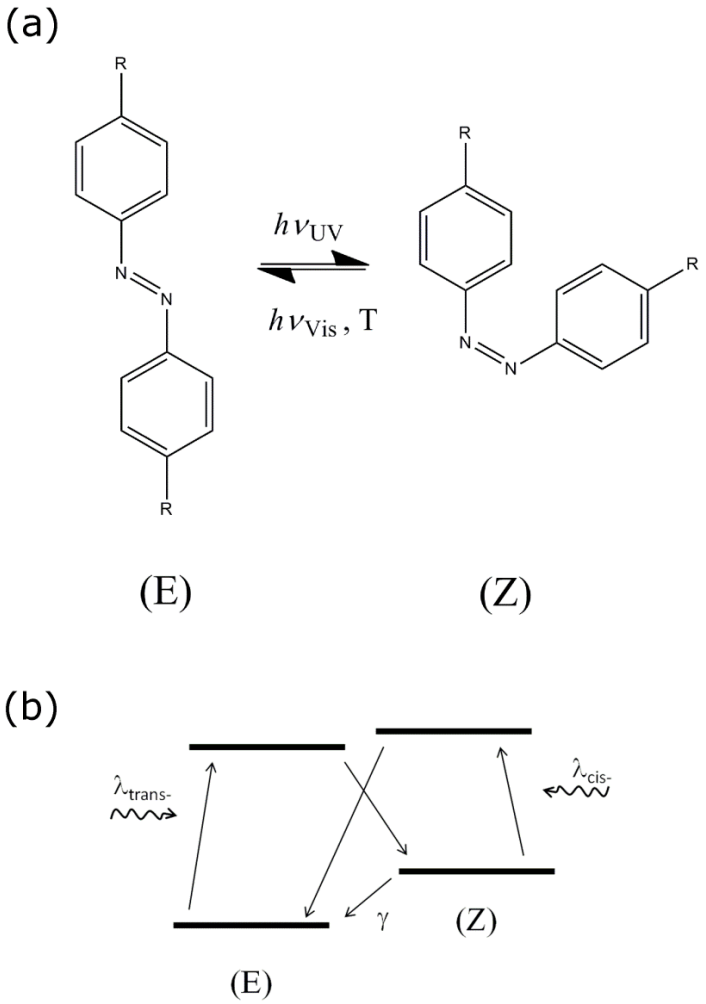

Figure 2-9 (a) Photoisomerisation of an azobenzene. (b) Simplified state levels for the different azobenzene conformations. λ_{trans-} and λ_{cis-} correspond to the absorption wavelength of the *trans*- and *cis*- state while γ represents thermal relaxation.[13, 46]

Azobenzene type molecules can undergo photoisomerisation from the *trans*-configuration to the *cis*-configuration when exposed to a specific wavelength of light.[47] Upon absorption of a photon of light, the molecule in the *trans*-state is excited to a higher energy level from where it can go the *cis*-state (Figure 2.9b). Absorption of a photon corresponding to the *cis*-state will cause the isomer to go back to the *trans*-state. As the *trans*-isomer is much more stable than the *cis*-, the

back-isomerisation process can also occur spontaneously in the dark or by heating (thermal relaxation).[48] The change in conformation is characterized by the angle of the N=N bond going from 60° for the *trans*-state to -60° for the *cis*-state.[13, 49] This results in a decrease of the distance between the 4- and 4'- carbon (Figure 2.10).[47, 50]

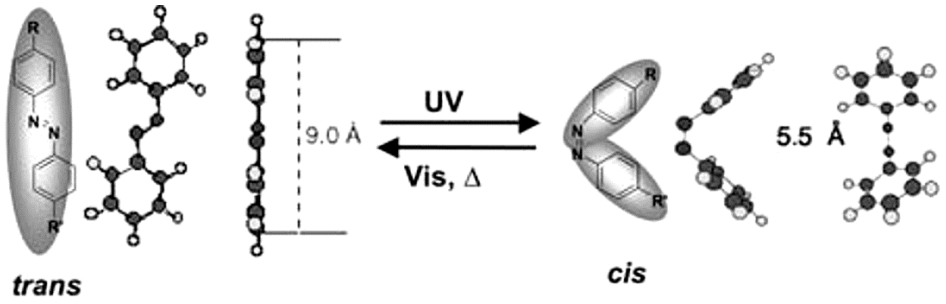

Figure 2-10 Photoisomerisation mechanism of an azobenzene. (reproduced from [47])

Different substituents can be attached at one or both ends of the azobenzene which will change the geometry or the physico-chemical properties such as the absorption or emission of the molecule.[48] For instance electron donor groups such as NH_2 or OH attached to the aromatic ring (in positions 4 and/or 4'), significantly decreases the energy transition of the azobenzene thereby shifting the absorption peak of the molecule towards higher wavelengths.[51]

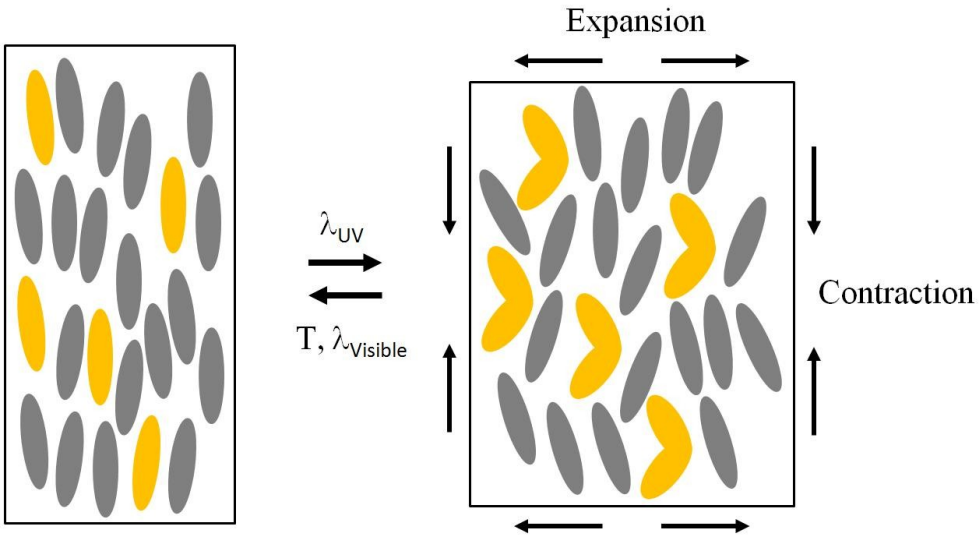

Figure 2-11 Mechanism of photoinduced deformation. The change in molecule conformation leads to a reduction of order in the LC network.[13]

Azobenzenes are readily incorporated in LC networks. In the *trans*-state they can align with the mesogen units. Photoisomerisation leads to a subtle disruption of the LC order. Although the loss of order is much smaller than in low molar systems, the strong interaction between the azobenzene and the polymer results in a large contraction along the molecular axis. On a macroscopic scale, this translates into a change in volume of the LC network that contracts along the alignment direction and expands in the perpendicular direction (Figure 2.11).

2.5.1.2 Photoinduced bending

Photoinduced bending in LC networks was first reported by Ikeda and co-workers.[52] They showed that a uniaxially aligned monodomain LC film prepared from an azo-

containing LC monomer and a azo-diacrylate cross-linker, would bend towards the actinic source when exposed to UV light. The film then bent away from the light source when exposed to visible light. The proposed mechanism governing the bending is as follows. Due to the high concentration of azobenzene in the *trans*-state, a gradient in intensity is generated through the thickness of the film when it is exposed to UV light. As a result, photocontraction along the alignment direction occurs only in the surface area of the film causing it to bend towards the light source. This behaviour is analogous to a bimetal thermostat where a difference in thermal expansion in a bimetal strip leads to bending upon heating.[53] As mentioned previously, contraction is generated along the molecular axis while expansion is obtained perpendicular to this direction. Films prepared with a homeotropic alignment showed a different response. UV exposure led to an isotropic expansion of the exposed surface of the film causing it to bend away from the light source.[54] In both cases the observed bending is due to a difference in deformation between the top surface and bottom surface of the film which is induced by the UV intensity gradient.

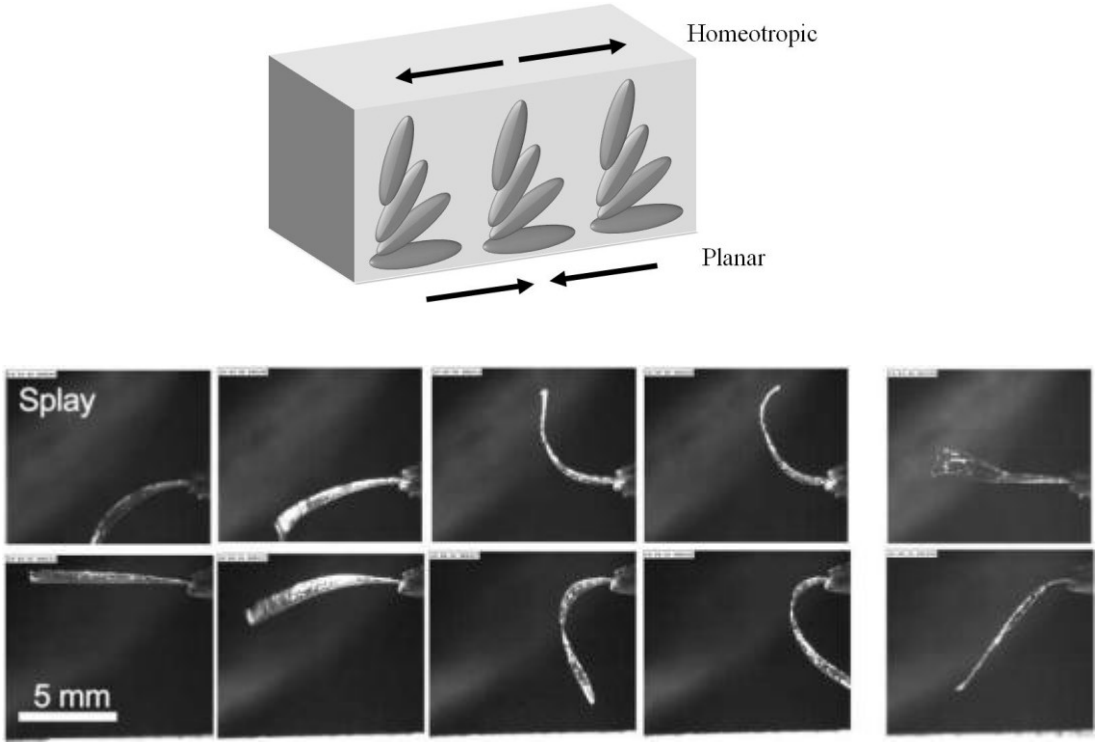

Figure 2-12 (a) Schematic of the contraction and expansion in a splay alignment. (b) Response of a splay LC film when exposed to UV light from different sides (top series: planar and bottom series: homeotropic). The pictures on the far right are taken after 40s recovery in the dark. Reproduced from [55].

Another approach consists of generating and controlling macroscopic bending through the alignment of the mesogens. Here the deformation gradient is based on different alignments on the top and bottom surfaces rather than an intensity gradient, therefore much lower azo-dye concentrations can be used (<10%). Van Oosten *et al.* prepared films with only 2% of a cross-linkable azo-LC monomer and showed that large bending could be obtained in films with a splay alignment (Figure 2.12).[55] When exposing the side with molecules aligned parallel to the film surface, the film bent towards the light. Exposing the opposite side (molecules aligned perpendicular to the film surface) resulted in the opposite response. In comparison, films with a

planar alignment showed almost no bending. The low dye concentration resulted in an almost total conversion of the *trans*-population to the *cis*-state, thereby solely generating contraction in the film. They further demonstrated that by inducing a 90° twist in the LC alignment, coiling could be generated rather than uniaxial bending.[56] Finally, controlled bending is also achieved with light polarization based on UV dichroism of the azobenzene, *i.e.* the absorption of the molecule depends on its orientation with respect to the polarization direction of the incident light. Yu *et al.* successfully demonstrated polarization controlled bending in a multidomain azo-LC film.[57] Their film bent towards the actinic light resulting from the contraction of the top surface of the film, however the bending direction changed when rotating the polarization of the light source. As absorption is higher in domains oriented parallel to the polarization direction, they provide the driving force in the bending over the other domains.

2.5.2 Thermally induced actuation

Oriented liquid crystal networks show anisotropic thermal expansion. Heating of a monodomain ordered LC network leads to a positive linear thermal expansion in the direction perpendicularly to the alignment. A negative linear thermal expansion is observed in the direction parallel to the alignment. This behaviour is ascribed to an increased mobility of the LC units as a function of temperature, resulting in a loss of order.[19, 58] Although the network restricts the mobility of the mesogen, the subtle change in orientation is enough to induce a length change on the macroscopic scale. The mechanism is depicted in Figure 2.13. The angle θ between the main alignment

direction and the molecular axis is found to increase as a function of temperature. As a result the end-to-end distance between cross-links decreases ($L_0 < L_T$) and the material contracts along the orientation direction.

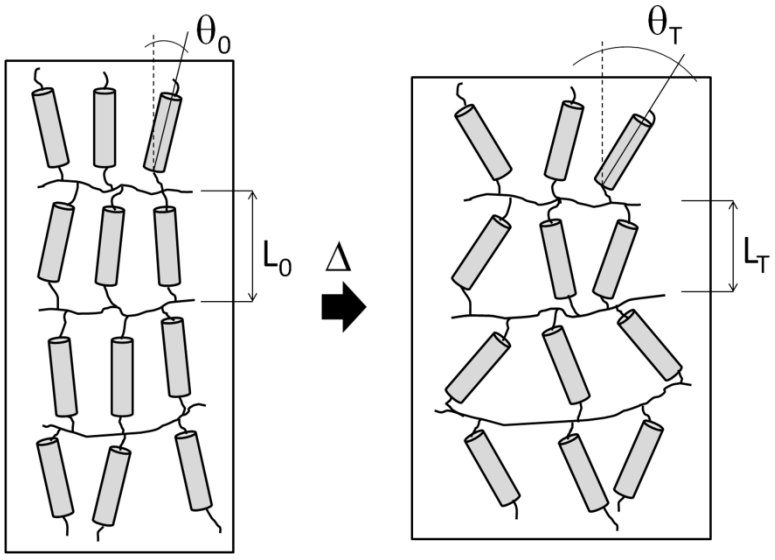

Figure 2-13 Schematic representation of the thermally induced length change in a uniaxially aligned LC network.[13, 58]

Unlike azo-LC films where bending can be generated through an UV intensity gradient, thermal gradients are difficult to obtain in micron thick LC films. Mole *et al*. showed that large bending was successfully achieved in free standing LC films by introducing a gradient in the mesogen alignment.[59]

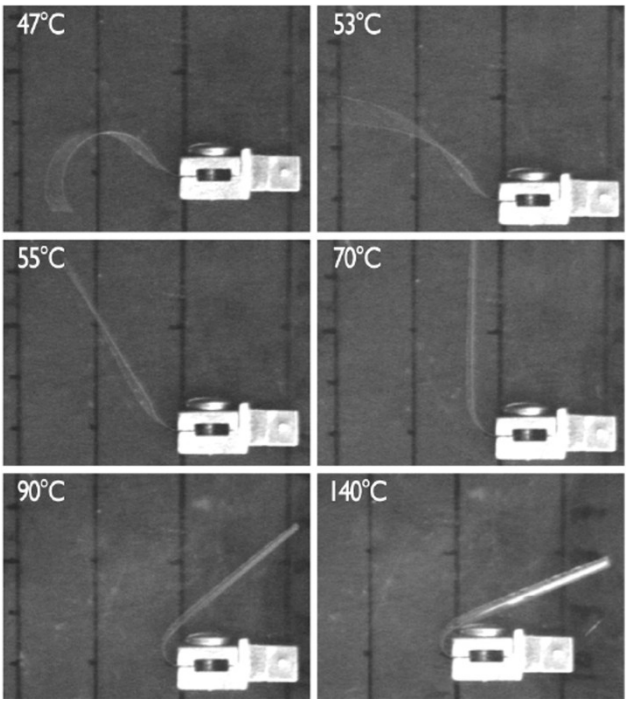

Figure 2-14 Thermal response of LC film with TN alignment. Reproduced from [59]

Figure 2.14 shows a typical response in a film with a twisted nematic alignment. In this specific structure, the director gradually rotates through the thickness of the film such that the molecules at the top of the film are oriented with an angle of 90^{o} compared to the molecules at the bottom of the film. Upon heating, the top part of the film will contract along the length direction while the bottom part of the film will expand in the same direction. This contraction/expansion deformation causes the film to curl up. However, it is worth noting that in this alignment there is a competition between top and bottom contractions, resulting in a saddle-shape deformation.

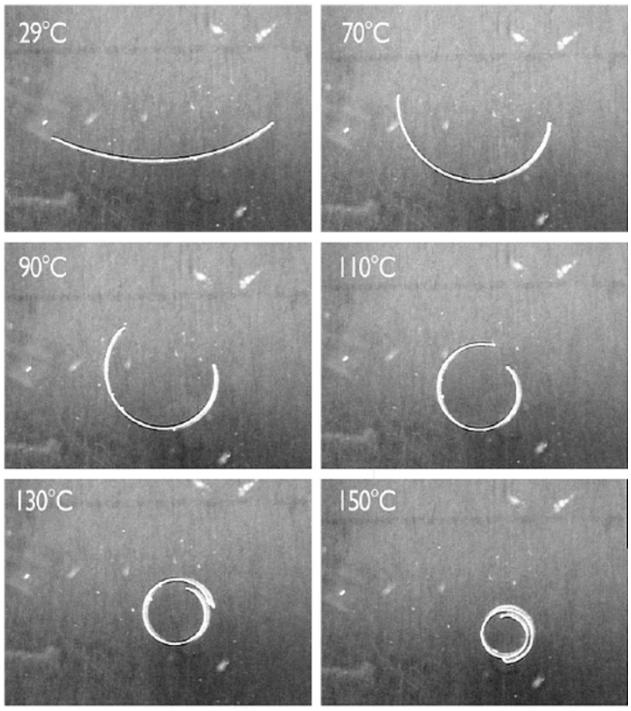

Figure 2-15 Bending behaviour of a free standing LC film with a splay alignment. Reproduced from [59]

Splay alignment circumvents this competition between top and bottom which allows for a more predictable deformation. Figure 2.15 shows the response of a film with a splay organisation. The heating results in a smooth deformation with contraction in the top part of the film (planar) and expansion in the bottom part (homeotropic).

2.5.3 Humidity responsive LC actuators

Polymers that move in response to moisture are of particular interest for comfort enhancement in textiles applications such a medical wear or protective wear.[60-61] Water triggered LC actuators are readily obtained by introducing hydrogen bonds in

the polymer backbone.[62] As mentioned previously (section 2.4.2), two non-liquid crystalline monomers that can pair by hydrogen bonding are used. Harris *et al.* demonstrated that such monomers could be aligned and cross-linked to form ordered LC networks.[33] However, the formed bonds are strong enough to withstand immersion in water. It has been shown that immersing the ordered LC film in an alkaline solution can break the H-bonds and convert the polymer to a polymer salt resulting in a hygroscopic material which is much more sensitive to humidity and other chemical solvents. The process is shown in Figure 2.16.

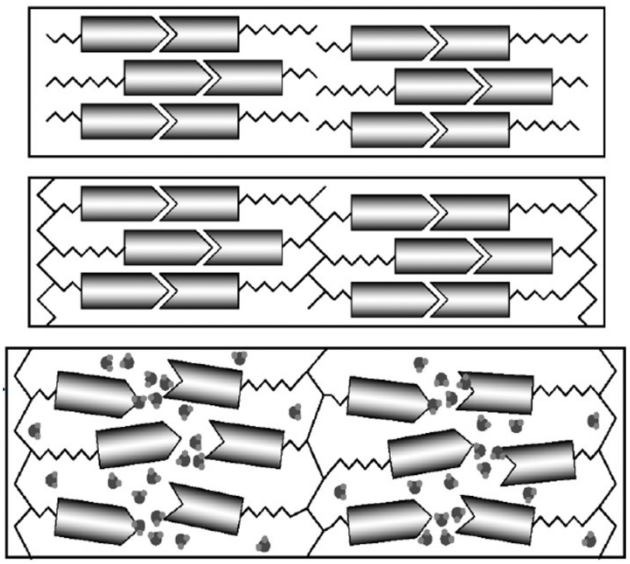

Figure 2-16 Illustration of the H-bond network formation.[32]

In their work, Harris *et al.* "activated" the polymer by immersing it in a solution of KOH (pH=13) for 10 to 20 s. During this step carboxylic acid groups were converted into potassium carboxylate groups, forming a hygroscopic network. A consequence of breaking the H-bonds is the loss in order which is accompanied by a deformation

of the LC film. Here the immersion time was short enough to break only a fraction of the hydrogen bonds and preserve some order in the network. Interestingly, these systems do not show the usual expansion/contraction deformation encountered in light sensitive or thermal sensitive LC networks. Upon exposure to water, a uniaxially planar aligned film expands in both direction (parallel and perpendicular to the alignment direction) with a larger expansion in the perpendicular direction. On the other hand, introducing a gradient in the mesogens alignment allowed large bending to be generated when exposed to water vapour.

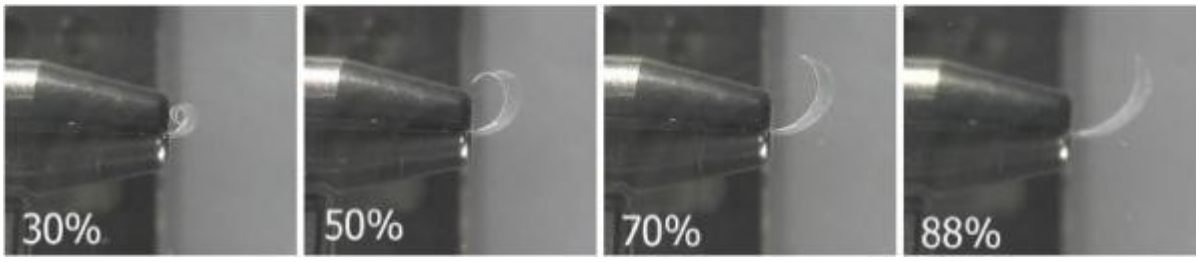

Figure 2-17 Response of a twisted nematic film to relative humidity. Reproduced from [62].

Figure 2.17 shows the response of a twisted nematic LC film to water vapour. The film was also found to respond to toluene vapour, ethanol vapour, xylene vapour, acetone vapour, isopropanol vapour and methanol vapour.[63] Such films can also be "deactivated" by immersing them in an acidic solution. The hydrogen bonds are restored and the original dimension is regained. As a consequence the responsiveness is lost as the film is no longer hydrophilic.

2.6 Summary

In this chapter we have shown how liquid crystalline polymer networks can be used as functional materials such as optical sensors or actuator. By a simple photopolymerization step of aligned reactive mesogens, highly organised polymers can be produced with properties directly related to the molecular structure and their organisation. For instance, LC molecules with a cholesteric arrangement enabled optical monitoring of gases and solvents. Additionally, LC polymers may exhibit large deformations such as bending or curling triggered by UV light, humidity and/or temperature. The following chapters will demonstrate how liquid crystalline networks can be used as a "toolbox" to produce synthetic fibres with new functionalities.

2.7 References

1 K. Takatoh, "Alignment technologies and applications of liquid crystal devices", in *Liquid crystals book series*, Taylor & Francis, London, 2005.

2 S. Ishihara, *J. Disp. Technol.* **2005**, *1*, 30.

3 J. M. Geary, J. W. Goodby, A. R. Kmetz, J. S. Patel, *J. Appl. Phys.* **1987**, *62*, 4100.

4 N. A. J. M. Vanaerle, M. Barmentlo, R. W. J. Hollering, *J. Appl. Phys.* **1993**, *74*, 3111.

5 http://www.mc2.chalmers.se/pl/lc/engelska/gallery/gallery.html#anchor1125970.

6 D. J. Broer, R. G. Gossink, R. A. M. Hikmet, *Angew. Makromol. Chem.* **1990**, *183*, 45.

7 G. P. Crawford, D. J. Broer, S. *Zumer, "*Cross-linked liquid crystalline systems : from rigid polymer networks to elastomers"*, CRC Press, Boca Raton, FL, 2011, p. 3-48

8 D. J. Broer, J. Boven, G. N. Mol, G. Challa, *Makromol. Chem.* **1989**, *190*, 2255.

9 D. J. Broer, H. Finkelmann, K. Kondo, *Makromol. Chem.* **1988**, *189*, 185.

10 D. J. Broer, R. A. M. Hikmet, G. Challa, *Makromol. Chem.* **1989**, *190*, 3201.

11 D. J. Broer, G. N. Mol, *Makromol. Chem.* **1989**, *190*, 19.

12 D. J. Broer, G. N. Mol, G. Challa, *Makromol. Chem.* **1991**, *192*, 59.

13 C. L. van Oosten, "Responsive liquid crystal networks", TU/e, Eindhoven, 2009.

14 E. Andrzejewska, *Prog. Polym. Sci.* **2001**, *26*, 605.

15 C. Decker, *Prog. Polym. Sci.* **1996**, *21*, 593.

16 C. Decker, A. D. Jenkins, *Macromolecules* **1985**, *18*, 1241.

17 I. M. Ward, "*Structure and properties of oriented polymers"*, Applied Science Publishers, London, 1975, p. xv.

18 P. Xie, R. Zhang, *J. Mater. Chem.* **2005**, *15*, 2529.

19 R. A. M. Hikmet, D. J. Broer, *Polymer* **1991**, *32*, 1627.

20 M. Mitov, *Adv. Mater.* **2012**, *24*, 6260.

21 J. Lub, D. J. Broer, R. T. Wegh, E. Peeters, B. M. I van der Zande, *Mol. Cryst. Liq. Cryst.* **2005**, *429*, 77.

22 D. Leung, S. O. Kang, E. V. Anslyn, *Chem. Soc. Rev.* **2012**, *41*, 448.

23 W. D. Stjohn, W. J. Fritz, Z. J. Lu, D. K. Yang, *Phys. Rev. E* **1995**, *51*, 1191.

24 D. K. Yang, X. Y. Huang, Y. M. Zhu, *Annu. Rev. Mater. Sci.* **1997**, *27*, 117.

25 N. W. Roberts, J.-P. S. Guillou , H. F. Gleeson , I. Kirar , S. J. Watson, E.O. Arikainen, *Mol. Cryst. Liq. Cryst.* **2004**,*411*, 57.

26 J. M. Hu, S. Y. Liu, *Macromolecules* **2010**, *43*, 8315.

27 M. Aldib, R. M. Christie, *Color Technol.* **2013**, *129*, 131.

28 M. Aldib, R. M. Christie, *Color Technol* **2011**, *127*, 282.

29 R. A. Evans, T. L. Hanley, M. A. Skidmore, T. P. Davis, G. K. Such, L. H. Yee, G. E. Ball, D. A. Lewis, *Nat. Mater.* **2005**, *4*, 249.

30 T. J. White, M. E. McConney, T. J. Bunning, *J. Mater. Chem.* **2010**, *20*, 9832.

31 B. Bahadur, "*Liquid crystals : applications and uses"*, World Scientific, Singapore ; London, 1991.

32 R. S. Pindak, C. C. Huang, J. T. Ho, *Phys. Rev. Lett.* **1974**, *32*, 43.

33 K. D. Harris, C. W. M. Bastiaansen, J. Lub, D. J. Broer, *Nano Lett.* **2005**, *5*, 1857.

34 X. Lu, C. He, A. C. Griffin, *Macromolecules* **2003**, *36*, 5195.

35 N. Herzer, H. Guneysu, D. J. D. Davies, D. Yildirim, A. R. Vaccaro, D. J. Broer, C. W. M. Bastiaansen, A. Schenning, *J. Am. Chem. Soc.* **2012**, *134*, 7608.

36 D. J. D. Davies, A. R. Vaccaro, S. M. Morris, N. Herzer, A. Schenning, C. E. M. Bastiaansen, *Adv. Funct. Mater.* **2013**, *23*, 2723.

37 P.G.de Gennes *C. R. Acad. Sci. Paris* **1975**, *281b*, 101.

38 J. Kupfer, H. Finkelmann *Macromol. Chem. Phys.* **1994**, *195*, *1353.*

39 C. L. van Oosten, D. Corbett, D. Davies, M. Warner, C. W. M. Bastiaansen, D. J. Broer, *Macromolecules* **2008**, *41*, 8592.

40 H. Finkelmann, E. Nishikawa, G. G. Pereira, M. Warner, *Phys. Rev. Lett.* **2001**, *87*.

41 T. Ikeda, J.-i. Mamiya, Y. Yu, *Angew. Chem. Int. Edit.* **2007**, *46*, 506.

42 J. E. Marshall, Y. Ji, N. Torras, K. Zinoviev, E. M. Terentjev, *Soft Matter* **2012**, *8*, 1570.

43 N. Torras, K. E. Zinoviev, J. E. Marshall, E. M. Terentjev, J. Esteve, *Appl. Phys. Lett.* **2011**, *99*.

44 M. L. Bossi, D. H. Murgida, P. F. Aramendia, *J. Phys. Chem. B* **2006**, *110*, 13804.

45 C. J. Barrett, J. I. Mamiya, K. G. Yager, T. Ikeda, *Soft Matter* **2007**, *3*, 1249.

46 Y. Zhao, T. Ikeda, "*Smart light-responsive materials : azobenzene-containing polymers and liquid crystals"*, Wiley, Hoboken, N.J., 2009, p. xviii.

47 H. Yu, T. Ikeda, *Adv. Mater.* **2011**, *23*, 2149.

48 H. M. D. Bandara, S. C. Burdette, *Chem. Soc. Rev.* **2012**, *41*, 1809.

49 T. Hugel, N. B. Holland, A. Cattani, L. Moroder, M. Seitz, H. E. Gaub, *Science* **2002**, *296*, 1103.

50 G. S. Kumar, D. C. Neckers, *Chem. Rev.* **1989**, *89*, 1915.

51 Griffith.J, *Chem. Soc. Rev.* **1972**, *1*, 481.

52 Y. L. Yu, M. Nakano, T. Ikeda, *Pure Appl. Chem.* **2004**, *76*, 1467.

53 S. Timoshenko, *J. Opt. Soc. Am.* **1925**, *11*, 233.

54 M. Kondo, Y. Yu, T. Ikeda, *Angew. Chem. Int. Edit.* **2006**, *45*, 1378.

55 C. L. van Oosten, K. D. Harris, C. W. M. Bastiaansen, D. J. Broer, *Eur. Phys. J E* **2007**, *23*, 329.

56 K. D. Harris, R. Cuypers, P. Scheibe, C. L. van Oosten, C. W. M. Bastiaansen, J. Lub, D. J. Broer, *J. Mater. Chem.* **2005**, *15*, 5043.

57 Y. L. Yu, M. Nakano, T. Ikeda, *Nature* **2003**, *425*, 145.

58 D. J. Broer, G. N. Mol, *Polym Eng Sci* **1991**, *31*, 625.

59 G. N. Mol, K. D. Harris, C. W. M. Bastiaansen, D. J. Broer, *Adv. Funct. Mater.* **2005**, *15*, 1155.

60 J. Hu, S. Chen, *J Mater. Chem.* **2010**, *20*, 3346.

61 H. Jinlian, M. Harper, L. Guoqiang, I. I. Samuel, *Smart Mat.and Stru.* **2012**, *21*, 053001.

62 D. J. Broer, C. M. W. Bastiaansen, M. G. Debije, A. P. H. J. Schenning, *Angew. Chem. Int. Edit.* **2012**, *51*, 7102.

63 K. D. Harris, C. W. M. Bastiaansen, D. J. Broer, *Macromol. Rapid. Comm.* **2006**, *27*, 1323.

Chapter 3

Pulsed photoembossing for diffractive optics in films and fibres

3.1 Introduction

The ability to control the surface structure of thin polymer films at a micro- and nanoscale has led to many applications in the area of photonics, organic electronics, micromechanics and also tissue engineering.[1-4] Different techniques are used to create surface relief structures such as mechanical embossing, or micro- and nano-imprinting.[4-7] A new promising technique for the production of surface relief structures is photoembossing.[3,8-16] The technique uses a self-developing material to generate the relief structures and therefore does not require expensive moulds or wet etching steps. As a consequence photoembossing is a convenient and cost-effective

technique for creating surface relief structures especially for low cost, large area applications.

The photoembossing process uses a photopolymer blend consisting of a polymeric binder, a multifunctional acrylate monomer, a photoinitiator and optionally additives such as inhibitors or chain transfer agents.[9-11] These mixtures are processed from solution using a volatile solvent and a thin solid film is obtained, after solvent evaporation, on a rigid or flexible substrate. The relief structure is then generated in three steps: (i) the film is exposed to patterned UV light to locally activate the photoinitiator, (ii) the film is heated and (iii) the film is further cured by exposing it to a flood UV exposure and a second heating step. The relief structure develops after patterned UV exposure by heating the film above a threshold temperature. This threshold is often a discrete thermal transition like the glass transition to increase monomer mobility and enhance polymerization. Before heating and after the first exposure, the film is in the glassy state and both monomer diffusion and chemical reactions are strongly suppressed. After heating, the polymerization reaction and the subsequent consumption of monomer in the exposed areas provides a driving force for the diffusion of the reactive species from the non-exposed areas to the exposed areas and the resulting mass transport generates the relief structures.[8, 10, 12] Though photoembossing is convenient and cost effective compared to other patterning techniques, it is in its current form, performed as a discontinuous process with static substrates. This limits production speeds and in-line processing like roll-to-roll. In order to generate a high throughput in large scale applications, an in-line photoembossing process, is envisaged and demonstrated in this chapter.

The classical approach of photoembossing relies on a photomask to generate a UV-light pattern. However, the use of a photomask in combination with moving

substrates such as encountered in a roll-to-roll process could be a costly technological challenge. On the other hand, generating light patterns on a photoresist can also be achieved using interference holography. In the simplest case, a linearly polarized laser beam is split in two coherent laser beams with the same intensity. These are made to interfere at a certain angle (2θ) in the sample region. As a result, a line interference pattern with a period of $\lambda/2\sin\theta$, λ being the wavelength of light.[17, 18, 19] This patterning technique enables to achieve submicron scale periodicities of the light patterns provided that the wavelength of the laser light can be selected in the UV region.[19] More complex structures such as two-dimensional lattices can be prepared using multiple beam holography or several exposure steps before heating.[12, 20] Here, we report the use of interference holography with a continuous wave (CW) laser and a nanosecond (ns) pulsed laser using both static and moving substrates to simulate processing conditions in a roll-to-roll process.

3.2 Experimental

3.2.1 Photopolymer preparation

Polybenzyl methacrylate (PBMA) (Scientific Polymer Products, weight-average molecular weight (Mw) 70.000 $g.mol^{-1}$), dipentaerythritol penta-/hexa-acrylate (Aldrich) and Irgacure 369 photoinitiator (Ciba) were used as received. Photopolymer solutions were prepared by dissolving the binder PBMA and the monomer in a 1:1 weight ratio and adding 5 wt.% of photoinitiator, in propylene glycol monomethyl ether acetate (PGMEA). The final photopolymer:PGMA ratio

was 1:1 in weight. The obtained solution was spin coated on glass substrates, and the solvent was evaporated at 80 °C for 10 min to give films with an average thickness of 10 μm.

3.2.2 Surface relief structuring

Photoembossed films were made with two types of lasers: an argon continuous wave (CW) laser with a wavelength of λ=351 nm and a pulsed Nd:Yag laser coupled to second and third harmonic modules emitting 4 ns pulses of 355 nm linearly polarized light with vertical polarization (repetition rate 10 Hz). In both setups, CW and pulsed laser, the beam was split into equal intensity beams which were made to interfere on the substrate (Figure 3.1). Than angle between the two interfering beams was 2.5° resulting in a grating period of about 8 μm.

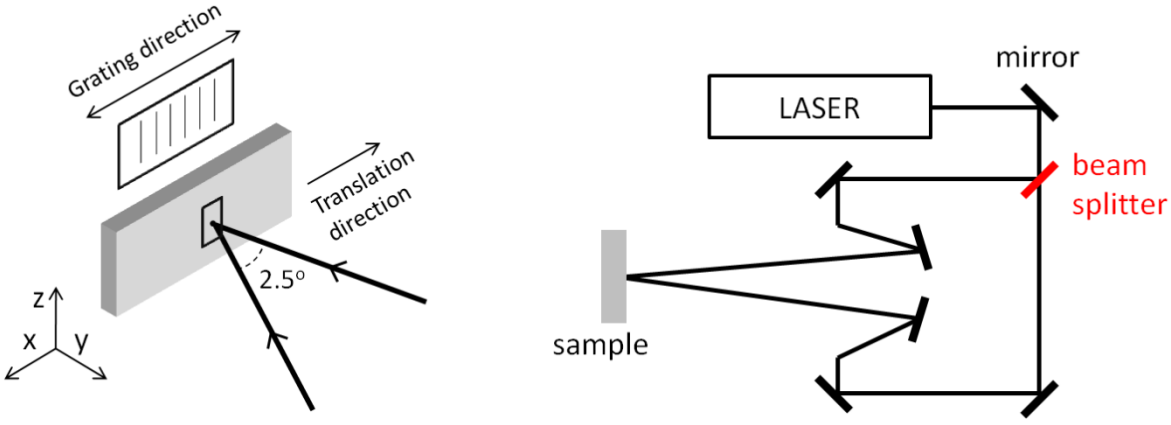

Figure 3-1 Schematic of the holography setup

The exposure of the film to the UV pattern is performed in two conditions: one with a static substrate and one with a moving substrate (translational motion) at a speed ($\dot{\varepsilon}$) of 0.05 $m.s^{-1}$. In the latter case the displacement of the substrate is done in a direction parallel to the grating vector. After exposure, the samples were heated to 80 ^{o}C during 10 min for development.[8] The obtained structures were fixed using a flood exposure with a UV Exfo Mercury lamp (100 $mW.cm^{-2}$) and a 350-500 nm filter, for 10 min at RT and a subsequent heating step at 80 ºC.[8]

3.2.3 Measurements

The height of the relief structures was measured using a NMDT AFM in semi-contact mode. Repeatability was verified by producing multiple samples, the heights were measured and scatter in the experimental data is represented by error bars in the figures. IR spectra were obtained in absorption mode using a Nicolet 8700 FT-IR spectrometer.

3.3 Results and discussion

Surface relief structures on photopolymer films are obtained by combining photoembossing with interference holography. In a first set of experiments, an interference pattern is generated with two coherent, equal intensity, linearly

polarized beams coming from a CW laser. In Figure 3.1, the height of the relief structures is plotted as a function of exposure energy for a static substrate ($\dot{\varepsilon}$ = 0 m.s^{-1}) and a moving substrate ($\dot{\varepsilon}$ = 0.05 m.s^{-1}) simulating conditions in a roll-to-roll process. Relief structures are obtained with the static substrate. But moving the substrate (translational motion) during the exposure to an interference pattern from a continuous wave laser does not produce any surface relief structures as expected. The absence of relief structures on the surface of the moving substrates is directly related to the displacement of the substrate during exposure, as light modulation sweeps the film along the grating vector direction, leading to a homogeneous dose all over the exposed area, i.e. the whole area is exposed to the same light dose.

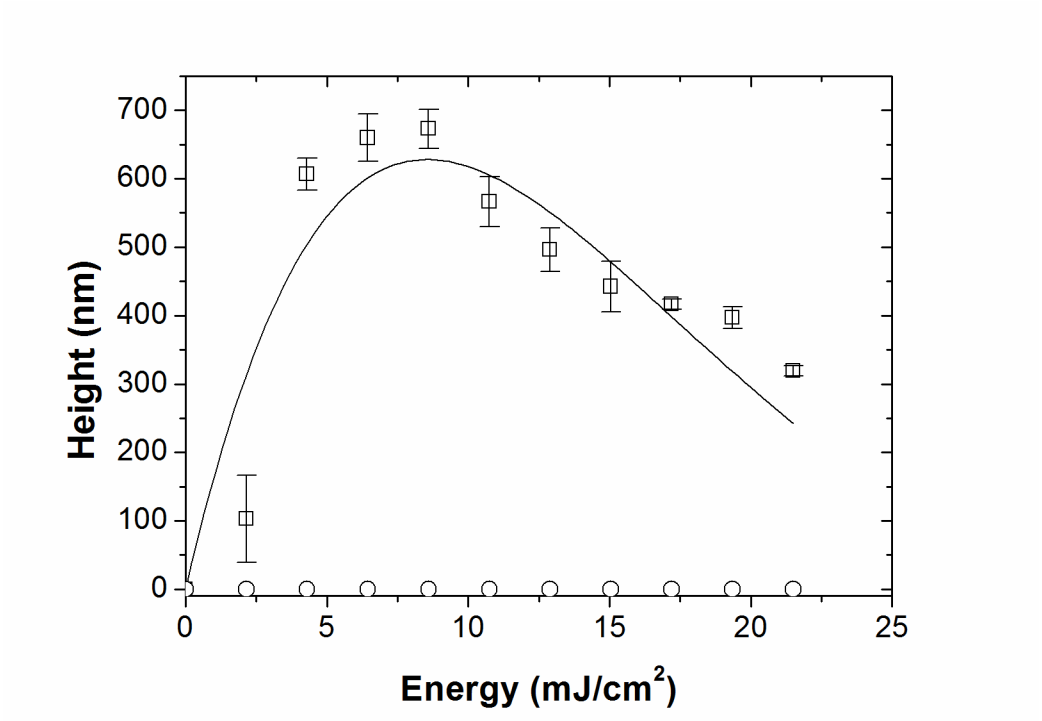

Figure 3-1 Relief height as function of energy dose. Exposure with continuous wave interference pattern in combination with a static ($\dot{\varepsilon}$ = 0 m.s^{-1}) (□) and a moving ($\dot{\varepsilon}$ = 0.05 m.s^{-1}) (○) substrate.

In a subsequent set of experiments, interference patterns are generated with a 4 ns pulsed laser. Again, a comparison is made between static and moving substrates (Figure 3.2). It is shown that the pulsed laser experiments produce now the desired relief structures in both static and dynamic substrates in contrast with the experiments done using a continuous laser (see Figure 3.1). Moreover, FT-IR experiments indicated that degradation phenomena are hardly present in both CW and pulsed laser exposed samples.

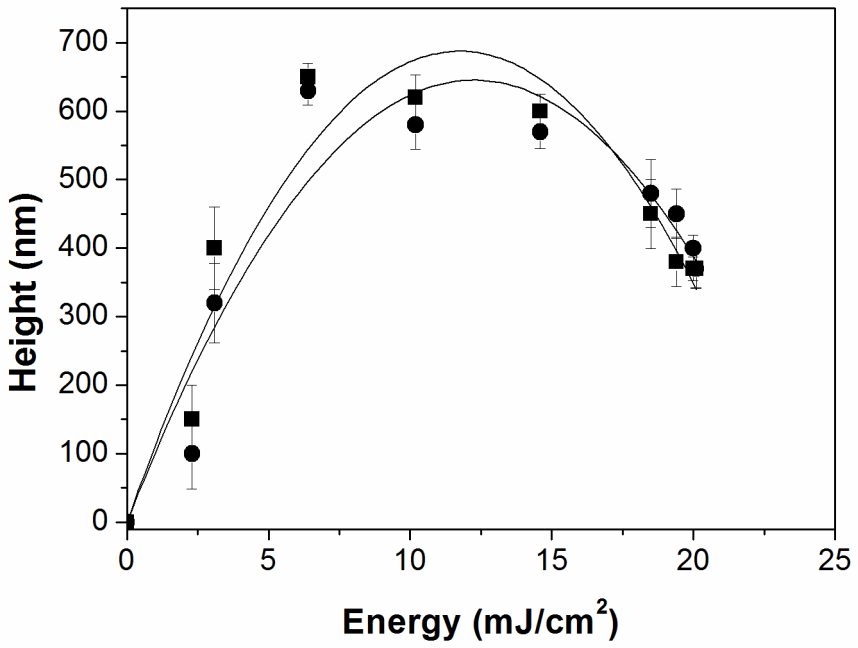

Figure 3-2 Relief height as function of energy dose. Exposure with a pulsed laser interference pattern (single pulse) in combination with a static ($\dot{\varepsilon} = 0$ m.s^{-1}) (■) and a moving ($\dot{\varepsilon} = 0.05$ m.s^{-1}) (●) substrate.

In order to generate a well-defined pattern of radicals and therefore relief structures on a moving substrate, the exposure time needs to be short enough to obtain a small

displacement of the substrate during exposure compared to the grating pitch. The displacement of the substrate during the exposure to a pulsed interference pattern is given by Equation (3.2):

$$l = \dot{\mathcal{E}} \times t \tag{3.2}$$

where l is the displacement of the substrate, $\dot{\mathcal{E}}$ the speed of the substrate and t is the pulse duration. In our experiments, $\dot{\mathcal{E}}$ = 0.05 m.s^{-1} and t = 4.10^{-9} s and, therefore, the substrate displacement during the pulsed exposure is only 0.20 nm. We employed an interference pattern with a pitch of 8000 nm which illustrates that the displacement of the substrate during exposure is small in comparison with the pitch. The sample can be considered to be nearly static during the 4 ns duration of the pulse and therefore similar relief modulation is obtained in moving and static substrates.

The above-described experimental data seem to indicate that pulsed laser interference holography is an excellent tool for generating relief structures in typical continuous film production lines. Actually, Figure 3.3 shows two sets of gratings recorded on a photopolymer coated flexible substrate using our pulsed laser holographic setup working at 10 Hz repetition rate. The exposed area was set to be square by putting a fixed window (5 × 5 mm) in the interference region. The lateral size of the window and the speed of the substrate are such that consecutive pulses cover a continuous line of stitched holographic gratings (without overlapping or unexposed areas).

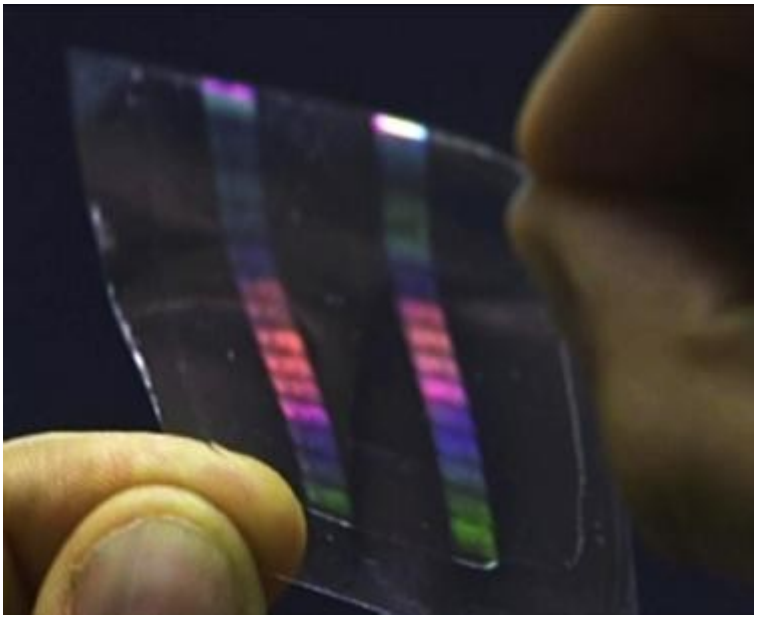

Figure 3-3 Two sets of square shaped gratings recorded using a pulsed holographic setup working at 10 Hz repetition rate. The exposed area was limited by a 5 mm side square aperture and the sample was moved at a linear speed of $\dot{\varepsilon} = 0.05$ m.s^{-1},leading to a set of stitched gratings. The process was repeated twice on the flexible substrate resulting in two stripes of holograms.

However, a few remarks are appropriate with respect to the experimental results presented here. In Figure 3.4, a typical AFM profile is shown of a surface relief structure generated in a moving substrate using a pulsed laser. A typical sinusoidal-like shape of the relief structure is observed and the height of the structure is in the order of hundreds of nanometers, which gives a rather low aspect ratio (height/pitch).

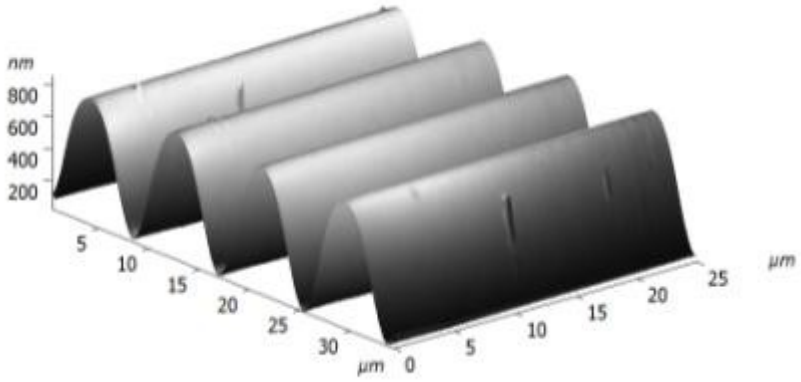

Figure 3-4 Representative AFM-profile of a surface relief structure produced with pulsed laser interference holography and a moving substrate.

In previous studies, it was already shown that this is predominantly related to the processing conditions (air environment, etc.) and/or to the chemical composition of the photopolymer.[8,16] Aspect ratio can be improved dramatically and relief shape modified using optimized binders, monomers, additives and/or illumination conditions.[8, 10, 11, 16] It is anticipated that the general trends observed in these studies also apply to the systems presented here and that the shape and dimensions of the relief structures can be substantially improved. More importantly, the speed of the substrate in this study was only 0.05 $m.s^{-1}$ and it seems interesting to estimate the maximum line speeds that are feasible in a roll-to-roll process. Equation (3.3) expresses the maximum speed of the substrate $\dot{\varepsilon}_{(max)}$ in order to fully cover a moving film with surface relief structures without overlapping of contiguous gratings. This speed is a function of the repetition rate of the laser f_{pulse} , the diameter of the laser beam d_{beam} and the beam expansion factor k. The size of the beam at the interference region where the sample is placed is denoted as $d_{hologram}$.

$$\dot{\mathcal{E}}_{(\max)} = f_{pulse} \times d_{beam} \times k \qquad \text{with} \quad k = \frac{d_{hologram}}{d_{beam}} \tag{3.3}$$

The laser used here produces light pulses with a $6x10^{-3}$ m diameter beam and a repetition rate of 10 Hz (see experimental section), limiting the maximum speed of the substrate, without beam expansion (k = 1), to $6x10^{-2}$ m.s^{-1}. This maximum speed of the substrate can be increased in a variety of ways. For instance, the laser beam can be expanded with the proper optical components. However, the energy at the film should be kept high enough to generate a high modulation surface relief grating. The laser beam used in our experiments can be expanded by a factor 3.5 leading to the optimum energy (~8 mJ.cm^{-2}) for generating relief structures (with maximum height; see Figure 3.2) when the laser works at full energy. This leads to a maximum line speed of $2.1x10^{-1}$ m.s^{-1}. Of course, a further reduction in the optimum energy for photoembossing via photopolymer optimization allows to increase $d_{hologram}$ and consequently the maximum line speed. The use of a more powerful or higher repetition rate laser could also lead to further increases in maximum line speeds.

3.4 Conclusions

It was shown that surface relief structures could be generated by photoembossing in a moving photopolymer film using pulsed laser interference holography. This experimental observation indicates that relief structures can be produced in a

continuous operation such as needed in a roll-to-roll process. At optimized conditions, the relief structures are nearly identical to the structures obtained for a static substrate. The system is insensitive to vibrations due to short time exposure in comparison to CW recordings, being this an interesting aspect for industrial applications. It is also shown that the maximum speed of the substrate is rather low and limited by the laser specifications. Several routes are proposed for increasing line speeds such as photopolymer optimization, the use of higher energy and higher frequency lasers and the reduction of the laser energy required for photoembossing.

3.5 References

1 J. M. Ziebarth, A. K. Saafir, S. Fan, M. D. McGehee, *Adv. Funct. Mater.* **2004**, *14*, 5, 451.

2 M-S. Kim, J- S. Kim, J.C. Cho, M. Shtein, J. Kim, L. J. Guo, J. Kim *Appl. Phy. Lett.* **2007**, *90*, 123113.

3 K. Hermans, M. van Delden, C.W.M. Bastiaansen, D. J. Broer, *J. Micromech. Microeng.* **2008**, *18*, 095022.

4 F. Chiellini, R. Bizzarri, C. K. Ober, D. Schmaljohann, T. Yu, R. Solaro, E. Chiellini, *Macromol. Rapid. Commun.* **2001**, *22*, 1284.

5 G. Fichet, N. Stutzmann, B. V. O. Muir, W. T. S. Huck, *Adv. Mater.* **2002**, *14*, 47.

6 J. Giboz, T. Copponex, P. Mélé, *J. Micromech. Microeng.* **2007**, *17*, R96.

7 L. J. Guo, *Adv. Mater.***2007**, *19*, 495.

8 C. Sánchez, B.-J. de Gans, D. Kozodaev, A. Alexeev, M. J. Escuti, C. van Heesch, T. Bel, U. S. Schubert, C. W. M. Bastiaansen, D. J . Broer, *Adv. Mater.* **2005**, *17*, 2567.

9 C. DeWitz, D.J. Broer, *Polym. Preprint* **2003**, *44*, 236.

10 K. Hermans, F. K. Wolf, J. Perelaer, R. A. J. Janssen, U. S. Schubert, C. W. M. Bastiaansen, D. J . Broer, *Appl. Phys. Lett.* **2007**, *91*, 174103.

11 J. Perelaer, K. Hermans, C. W. M. Bastiaansen, D. J. Broer, U. S. Schubert, *Adv. Mater.* **2008**, *20*, 3117.

12 T. Meyer, J. Keurentjes, *Handbook of Polymer Reaction Engineering vol.2*, Wiley-VCH, Weinheim,Germany **2005**.

13 N. Adams, B. De Gans, D Kozodaev, C. Sánchez, C.W.M. Bastiaansen, D.J. Broer, U.S. Schubert, *J. Comb. Chem.* **2006**, *8*, 184.

14 B.-J. de Gans, C.Sánchez, D. Kozodaev, D. Wouters, A. Alexeev, M. J. Escuti, C.W.M. Bastiaansen, D. J. Broer, U. S. Schubert, *J. Comb. Chem.* **2006**, *8*, 228.

15 K. Hermans, I. Tomatsu, M. Matecki, R. P. Sijbesma, C.W.M. Bastiaansen, D.J. Broer, U.S. Schubert, *Macromol. Chem. Phys.* **2008**, *209*, 2094.

16 K. Hermans, *PhD*, University of Technology (Eindhoven, NL), April, **2009.**

17 D. Xia, Z. Ku, S.C. Lee, S.R.J. Bruek, *Adv. Mater.* **2011**, *23*, 147.

18 T. Zhai, X. Zhang, Z. Pang, F. Dou, *Adv. Mat.* **2011**, *23*, 1.

19 S. R. J. Brueck, *Proc. IEEE* **2005**, *93*, 10, 1704.

20 M. Campbell, D.N. Sharp, M.T. Harrison, R.G. Denning, A.J. Turberfield, *Nature* **2000**, *404*, 53.

Chapter 4

Reflective fibres based on CLC coatings

4.1 Introduction

Colour has been essential for fibres since the early use of textiles and fabrics. Conventionally, organic and/or inorganic dyes or pigments are used to generate the colour based on absorption or scattering of visible light. However, colours can also be produced based on the selective reflection of light for instance, as can be seen in beetles.[1-3] Here, the produced colours are very bright and intense, and change drastically with viewing angle or illuminating conditions (for instance polarization direction).[3] Driven by consumers demand for textiles with unique appearances we explore a new route to introduce reflection-based optical effects into oriented fibres or films using a cholesteric liquid crystal (CLC) coating.[4, 5] In a CLC, molecules are arranged into a helical structure giving unique optical properties to the material. They selectively reflect one specific circular polarization direction of light and

transmit the other.[6] In other words, at normal incidence the reflected light is circularly polarized with the same handedness as the cholesteric helix and a maximum reflection of 50% is obtained.[6, 7] The reflected light also changes with the viewing angle. A blue shift of the reflected light is observed in planar CLC films at oblique incidence, *i.e.* when the angle between the incident light and the cholesteric helix increases.[8, 9] The reflected wavelength is determined by the average refractive index of the liquid crystalline polymer and the pitch *P* of the helix. In a CLC film, controlling the planar alignment of the molecules at the surface of the substrate is the key to obtaining a well-defined reflection band. The most common and inexpensive way to align liquid crystal is by mechanically rubbing the surface of the substrate.[10] More interestingly, polymer substrates stretched over 100%, such as polyvinyl alcohol or cellulose, have been shown to align nematic liquid crystal molecules along the stretching direction.[11] However, the present work aims at applications in apparel and textiles where polyamide 6 (PA6) is one of the main polymers used to produce synthetic fibres.[12] In this chapter we demonstrate a process for the production of oriented PA6 films and fibres with angular dependent colours through spray coating of CLCs. The alignment is characterized and the resulting optical properties are evaluated for the coated films and fibres.

4.2 Experimental

4.2.1 Materials

PA6 oriented films were purchased from Goodfellow. PA6 monofilaments were produced by melt spinning fibre grade PA6 pellets (Durethan B35F, Lanxess).

Monomers C3M and C6M (Merck) were mixed in a 1:4 weight ratio.[14] The chiral mesogen LC756 – BASF (5.2 wt.%) was added to the monomer mixture to obtain a green reflection band. A small amount (1 wt.%) of 1-hydroxycyclohexyl phenyl ketone (Sigma Aldrich) was added as a photoinitiator. The monomers and photoinitiator were dissolved in xylene (1:2.5 weight ratio).

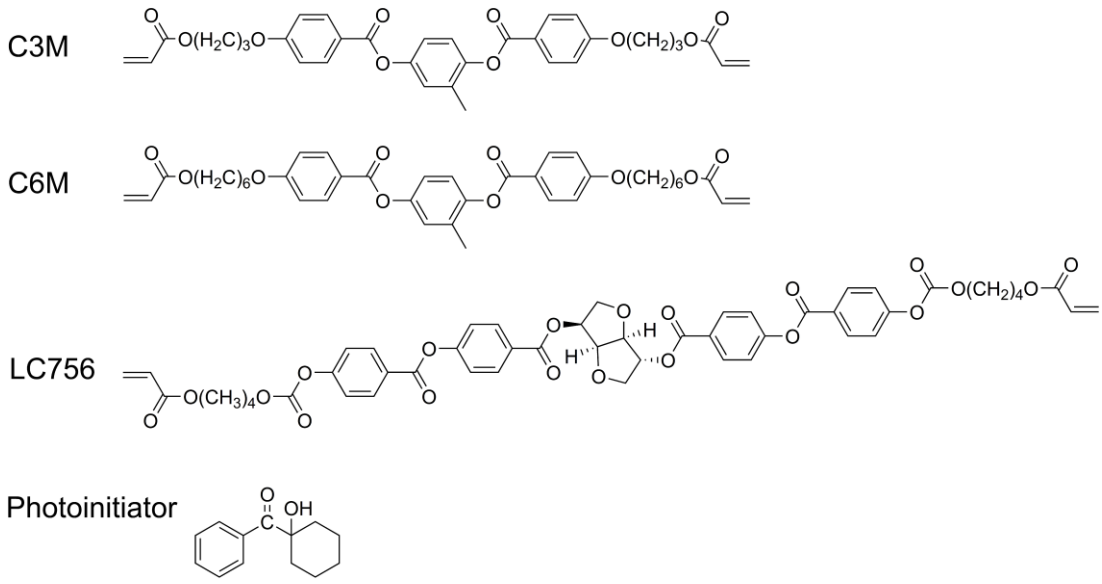

Figure 4-1 Molecular structures of the monomers and the photoinitiator composing the cholesteric liquid crystal mixture.

4.2.2 Reflective film preparation

PA6 films were washed with isopropanol and dried with compressed air. The films were then taped to a substrate and the liquid crystal mixture was applied using an Iwata painting airbrush with air as a gas carrier (flow rate = 2 mL.min^{-1} and nozzle to film distance = 10 cm). The films were annealed to 80 ^{o}C in an oven for 60 s to remove residual traces of solvent and successively cooled to room temperature and

photopolymerized in the nematic phase. The photopolymerization was performed using a mercury lamp (EXFO Omnicure S2000, λ= 350-450 nm) in a nitrogen atmosphere for 200 s. Tapes with a CLC coating on both sides were produced by repeating the procedure above.

4.2.3 Reflective fibre preparation

PA6 pellets were dried over night at 110 ^{o}C and melt-spun using a single screw extruder with monofilament die (spinning temperature = 260 ^{o}C). Oriented filaments were obtained after drawing the fibres to a draw ratio of 3 at 80 ^{o}C. The fibres were then prepared and coated following the same process as the double-sided coated tape. A continuous coating process was also designed where a monofilament was unwound and guided through the spray of two airbrushes. After the coating step, the fibre was guided through an oven and then through a nitrogen box to cure the CLC layer under UV light. The speed was adjusted to obtain a residency time of 30 s for both the annealing and curing step (as shown in Figure 4.2).

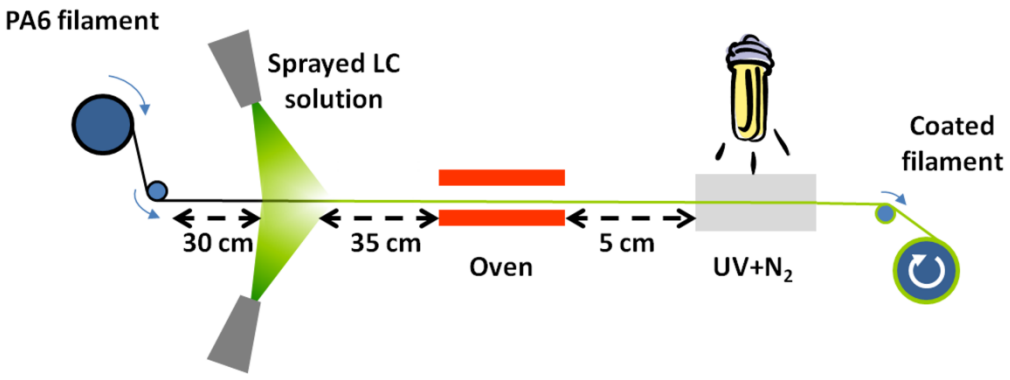

Figure 4-2 Schematic illustration of the in-line fibre coating setup.

4.2.4 Characterization

Transmission measurements were performed using a Perkin Elmer Lambda 950 UV-VIS spectrophotometer. Left and right circular polarisers were used for the measurement on the single side coated PA6 film. The phase transition temperatures of the non-polymerized LC mixture were determined using differential scanning calorimetry (DSC) characterization with a heating and cooling rate of 5 $^{o}C.min^{-1}$ (Mettler Toledo). Optical microscopy was done with a Leica optical microscope. SEM images were taken using a FEI Inspect with secondary electron detector. Photographs of the fibres were taken with a digital camera

4.3 Results

4.3.1 Oriented films

Experiments were first carried out on a uniaxially oriented PA6 film in order to investigate the alignment of the polymerized mesogens and reflective properties of the coating. The CLC mixture used to coat the substrates was produced by adding a chiral mesogen to a nematic LC host (Figure 4.1).[13, 14]

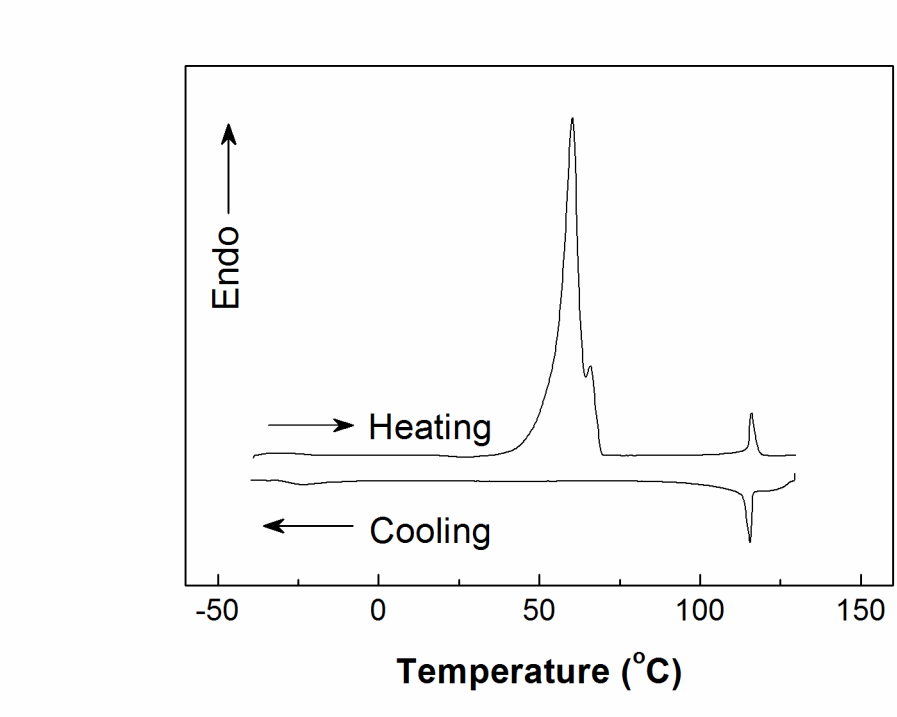

Figure 4-3 DSC thermogram of the mixture RM82/RM257 during the 1st heating and 1st cooling.

The transition temperatures of the LC host (C3M/C6M) were determined by DSC. The blend showed a first nematic transition upon heating to 60 °C followed by the isotropic transition at 115 °C. During cooling, the mixture showed a broad temperature range in which the mixture is nematic (Figure 4.3). The liquid crystalline diacrylates used here enable the formation of a cross-linked network upon polymerization while preserving the CLC order.[15,16] Optical microscopy observations of the coating showed the characteristic oily streak morphology, typical of a CLC planar texture (Figure 4.4).[17]

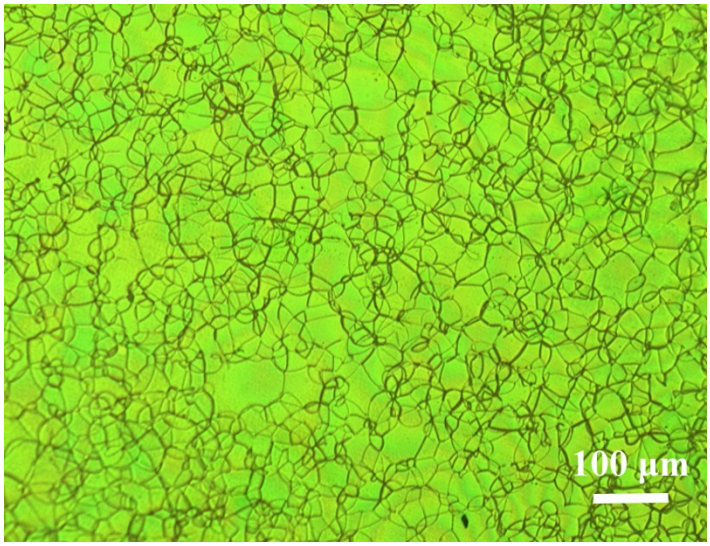

Figure 4-4 Microscopy image in reflection mode without polarizer of a green reflecting film, showing the characteristic oily streak morphology of a CLC film with a planar alignment.

The reflection band was characterized by measuring the transmittance of the film in the visible spectrum (400-800 nm) for two different polarization states, *e.g.* left- and right-handed circularly polarized light (Figure 4.5a). Measurements done with right-handed circularly polarized light (RHCPL) showed a strong reflection band centred at λ_0 = 535 nm and a width $\Delta\lambda$ = 65 nm (measured at the half-height of the peak). The reflection, almost completely absent in left-handed circularly polarized light (LHCPL) confirmed the right hand helical arrangement of the LC molecules.[18] When the incident light was at an oblique incidence, the reflection band shifted towards lower wavelengths. (Figure 4.5b) which is expected in CLC films with a planar texture.[8]

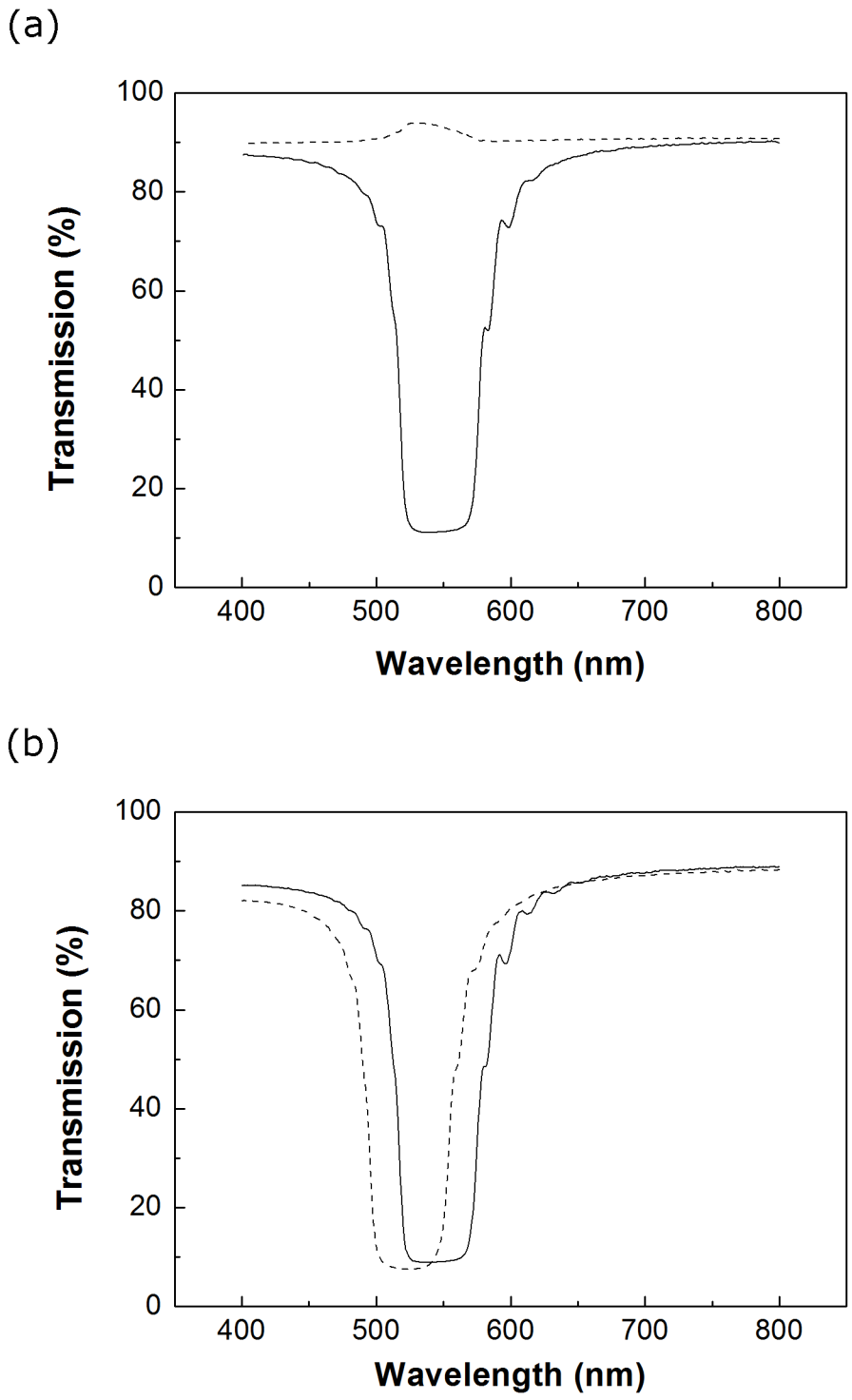

Figure 4-5 (a) Transmission spectrums recorded for the same film for right-handed circular polarized light (—) and left-handed circular polarized light (---) at normal incidence. (b) Influence of the incident angle for right-handed circular polarized light. Film perpendicular to the beam (—) and tilted by 30^{o} (---).

The reflection of a CLC film under non-polarized light is less than 50%, though it can be increased by introducing a half wave optical retardation between two CLC films of identical handedness.[19] Here, it is attempted to use the oriented PA6 substrate as an optical retarder and increase the reflection of the film by coating both sides of the substrates with the same CLC. The reflective properties of the double-side coated film were measured with non-polarized light and compared to a single-side coated film.

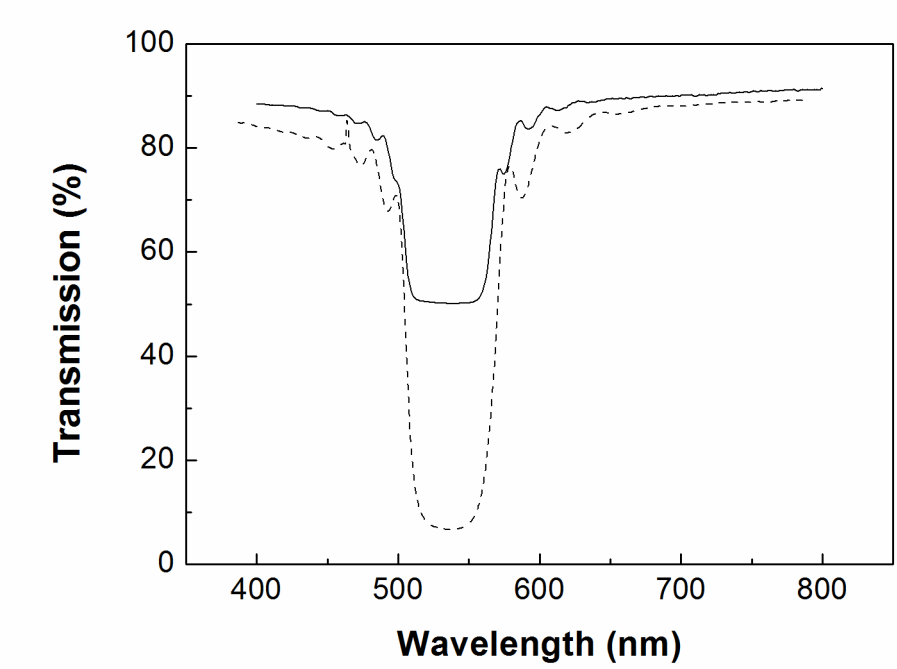

Figure 4-6 Transmission spectrums of a single-side coated PA6 film (—) and double-side coated PA6 film (---) obtained for non-polarized light.

Spectrums are shown in Figure 4.6. The double-side coated film showed a reflectivity of 80% which is 40% higher compared to the single-side coated film. To

verify the optical retardation of the substrate, the birefringence of the pure PA6 oriented film was calculated following the method described by Escuti and co-workers.[20] It was found that the 25 μm thick PA6 film had a birefringence $\Delta n = 0.01$. Based on this result the retardation could be estimated to be 250 nm which is indeed close to half-wave retardation of the reflected wavelength ($\lambda_0 = 535$ nm).

4.3.2 Oriented fibres

Reflective fibres were produced by coating stretched PA6 monofilaments following the same process as above and using the same CLC mixture. SEM observations of the fibres' cross-section showed a conformal coating around the fibre with a thickness of 6-10 μm (Figure 4.7a).

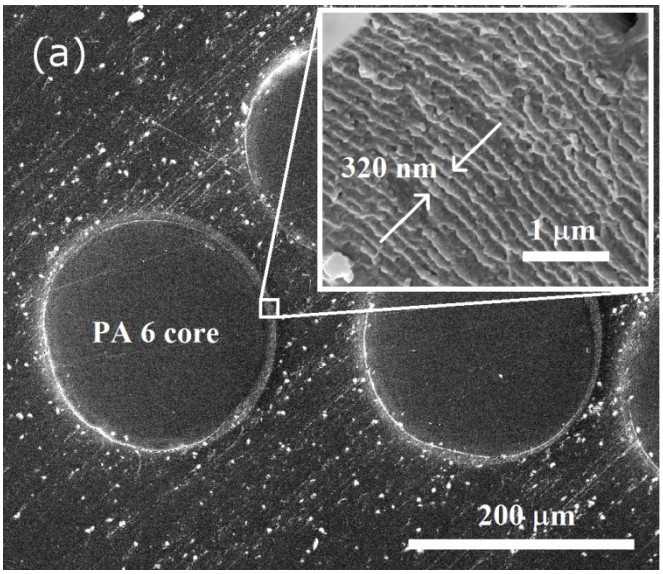

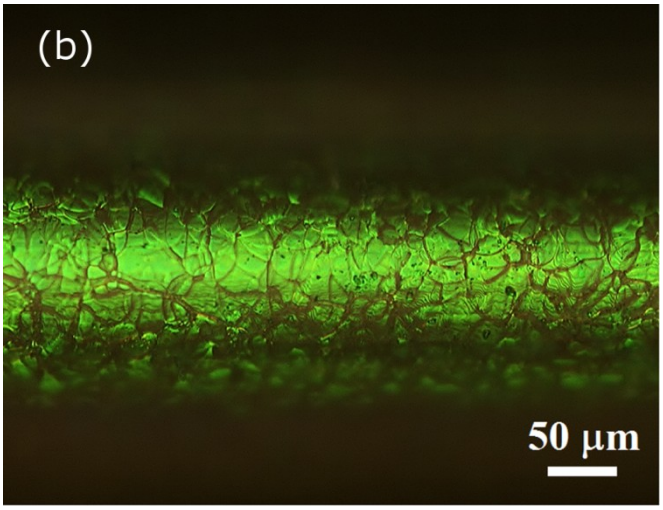

Figure 4-7 (a) SEM cross-sectional images of coated PA6 fibres. The inset shows the layered structure of the LC coating. The succession of bright and dark lines corresponds to half the pitch. Here a complete pitch is measured. (b) Microscopy image in reflection mode of the green reflecting fibre. The image is focused on the top part of the fibre.

In the close-up view of the coating (inset); the layered morphology of the CLC consisting of a succession of bright and dark lines, can be seen. Optical microscopy images of the CLC layer showed the characteristic oily streaks indicating a planar alignment (Figure 4.7b). The filaments with a diameter of 200 μm had a reflection band in the green region of the spectrum, as measured by UV-VIS spectroscopy (Figure 4.8). A broad reflection band $\Delta\lambda$ = 96 nm with a maximum reflection of 30% for non-polarized light was measured originating from the curved geometry of the fibre.

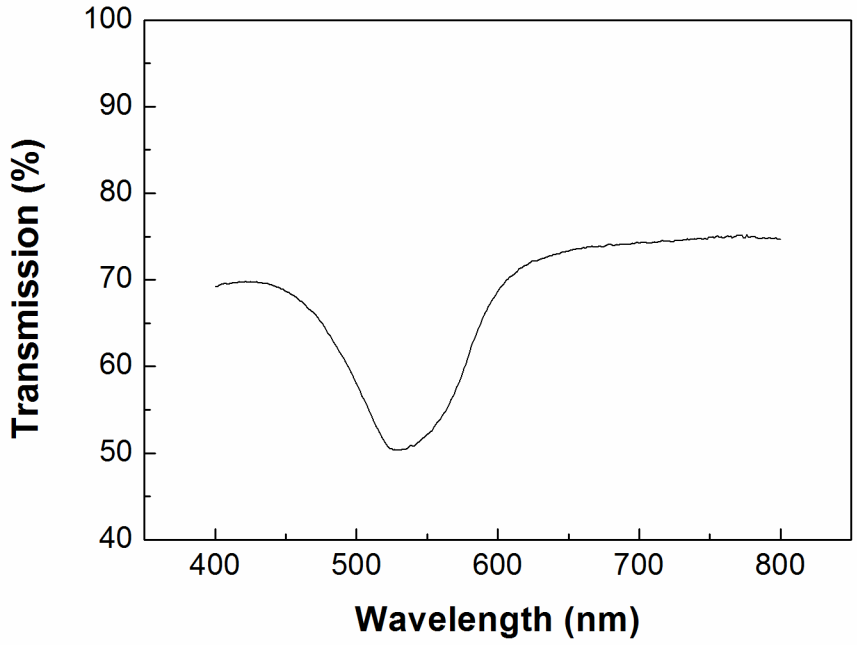

Figure 4-8 Transmission spectrum of the coated fibres obtained for non-polarized light at normal incidence. The baseline is shifted due to incident light scattered by the fibres.

In fact, optical microscopy observations showed that the reflection was green in the middle of the fibre only and blue closer to the edges (Figure 4.9a). The CLC has a planar alignment, with the helix axis perpendicular to the fibre surface. Therefore the angle between the incoming light and the helix (denoted θ) is expected to increase from the middle of the fibre towards the edges (Figure 4.9b) which causes the blue shift at the edges. Similar observations were reported for CLC microcapsules.[21]

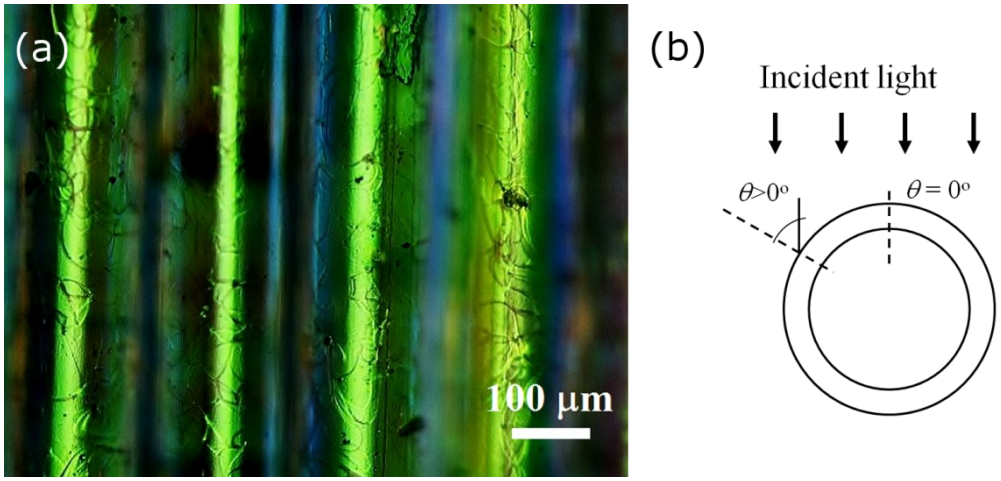

Figure 4-9 (a) Microscopy image in reflection mode of an array of coated fibres with non-polarized light. (b) Representation of the coated fibre with the CLC helixes normal to the incident light $\theta = 0^{o}$ and at an angle $\theta > 0^{o}$.

Finally the effect of the viewing position on the perceived colour was investigated. Photographs were taken at different angles, respectively perpendicular (α) and parallel (β) to the fibre axis (Figure 4.10a). From the pictures it is clear that an increase in the radial angle α did not change the perceived colour which is due to the symmetric geometry of circular cross-section fibres (Figure 4.10b and Figure 4.10c). On the other hand, a blue shift was observed when β increased (Figure 4.10b and Figure 4.10d). These results indicate that the observed colour is only influenced by the viewing angle along the fibre axis.

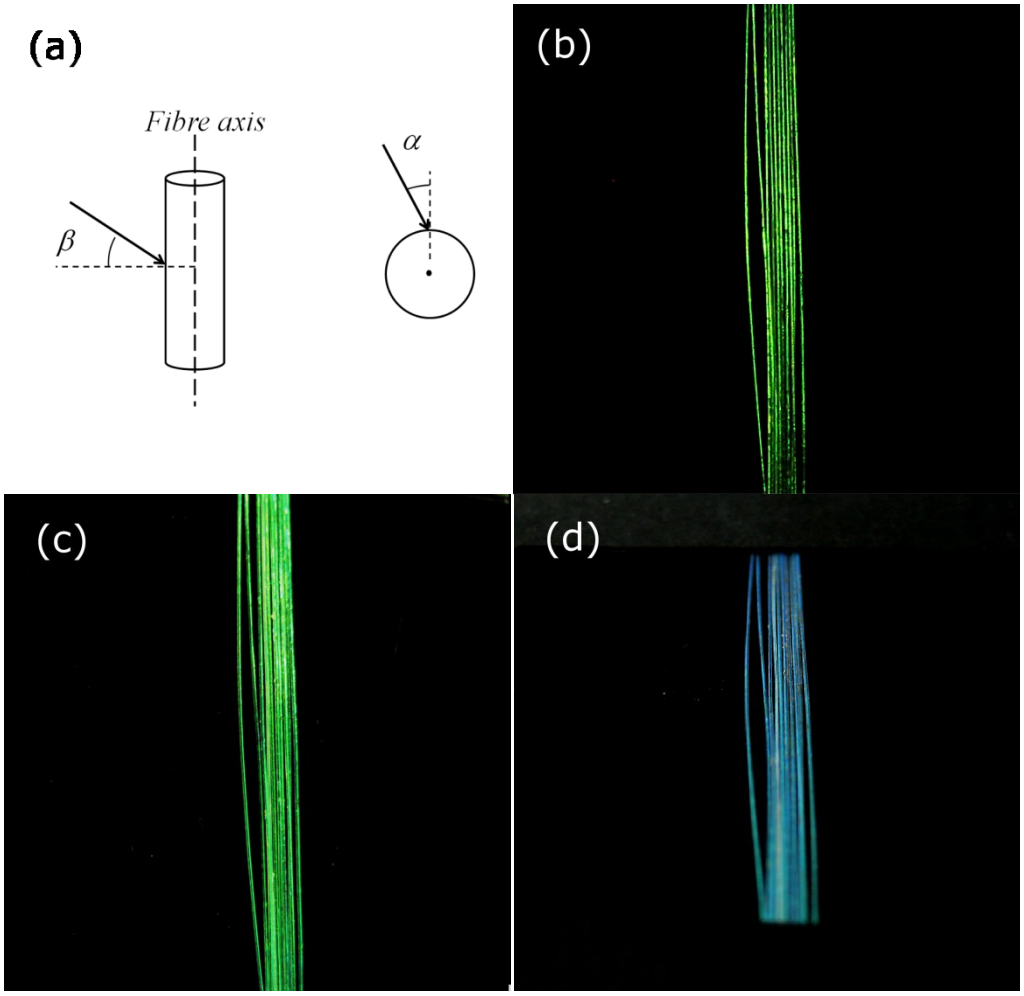

Figure 4-10 (a) Schematic representation of the different viewing angles. Pictures of the array of fibres are taken at different viewing angles α and β: (b) $\alpha = 0^o$ and $\beta = 0^o$, (c) $\alpha = 30^o$ and $\beta = 0^o$, (d) $\alpha = 0^o$ and $\beta = 60^o$. Pictures are taken against a black background.

4.3.3 Textiles application

The optical properties of the coated fibres suggest applications in fashion and apparel. In order to demonstrate the feasibility of integrating these fibres into conventional fabrics it was woven with a black cotton thread. Figure 4.11 shows a close up view of a 5 x 5 cm fabric woven in a Harness-Satin 8 weave pattern. For

this specific weave pattern, 87.5% of the reflective fibres are located on the top part of the fabric, giving a green aspect to the fabric.

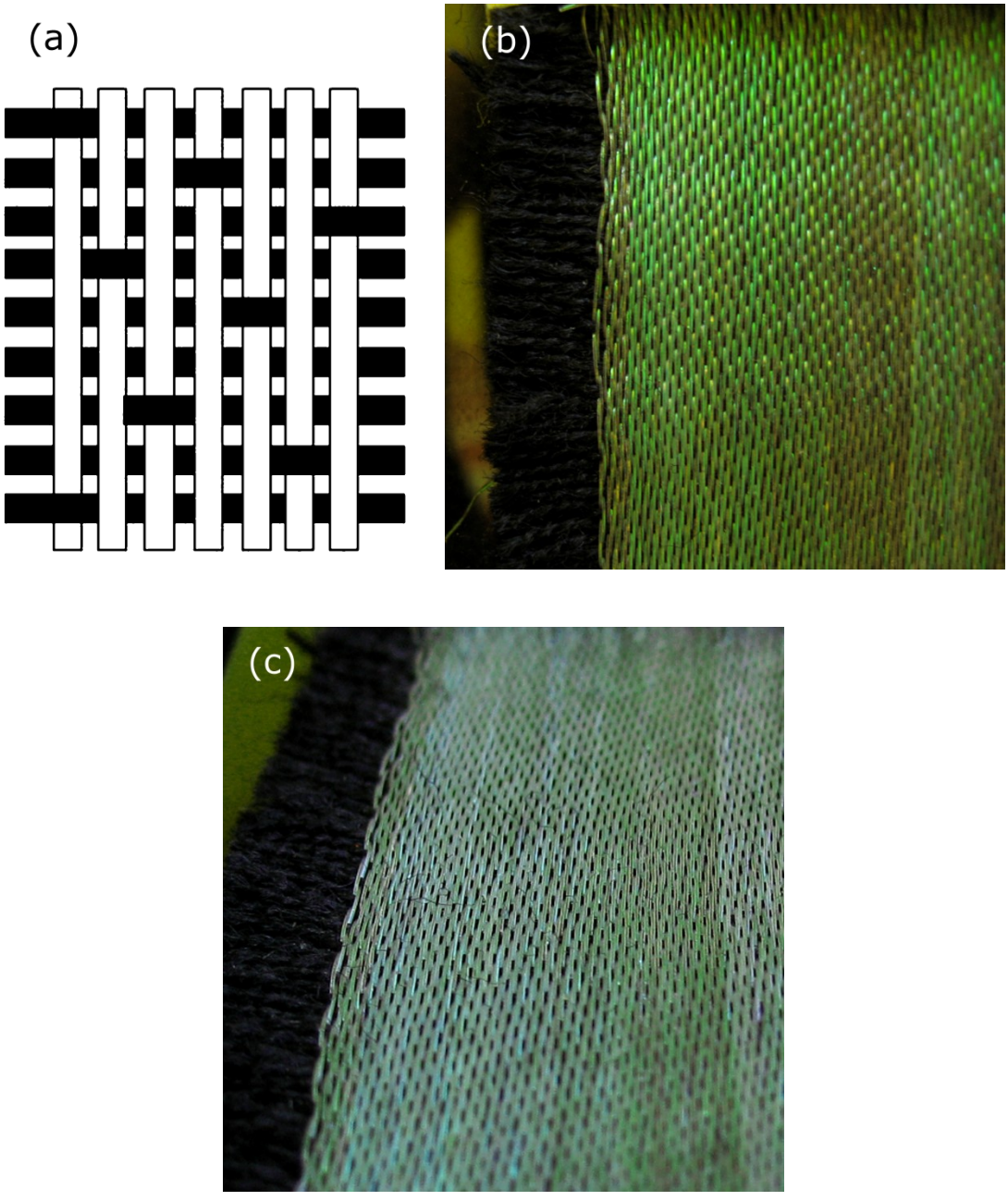

Figure 4-11 (a) Illustration of the weaving pattern. The lengthwise fibres (warp fibres) are represented in white while the fibres in the transverse direction (weft

fibres) are in black. (b) Woven fabric composed of the reflective fibre (warp fibres) and a black cotton yarn (weft fibres). (c) The fabric as seen from oblique incidence.

As expected when observing the fabric from a different angle, the colour shifts to the lower wavelength region of the spectrum (Figure 4.11c). However, the colour shift is rather weak in comparison with the neat fibres (see section 4.3.2). This weaker colour shift is attributed to the crimp in the fabric induced by the weaving, *i.e.* fibres do not lie perfectly straight but are deformed owing to the interlacing in the fabric. As a result, when tilting the fabric, the angle between the incident light and the cholesteric helix does not change as drastically as for the neat monofilament (Figure 4.10b and d) or for a flat film (Figure 4.5b). Reducing the crimp in the fabric, by changing the weaving pattern for instance would help to overcome the low angle dependence and enhance the colour change. However, this example does show the possibility of obtaining new visual effects in textiles depending on illumination conditions, weave pattern, and/or viewing angle.

4.4 Discussion

The experiments performed on oriented tapes showed that a well-aligned CLC layer and consequently a narrow reflection band are obtained with the spray deposition process. The high reflection obtained in double-side coated tapes would suggest that flat fibres or tapes could be used in textiles, for instance in clothing applications. On the other hand, round cross-sections are far more common in textiles.[12] We showed

here that the curved geometry of a round fibre changes the reflection band as well as the perception of the fibre, with a blue shift under oblique incidence observed in one dimension only. Although in this work, we demonstrated the potential to generate colours using a green reflecting CLC coating it should be noted that also other colours can be easily generated by changing the chiral dopant concentration.[22] Hence the reflection band could be tuned to produce fibres that reflect UV or infrared radiations thereby broadening the field of application of the process. For instance, fibres reflecting infrared radiation could be used as heat reflectors to manage body heat loss in low temperature weather conditions.[23] Experiments were also performed using polyethylene terephthalate (PET) as a substrate. Here, uniaxially oriented films and fibres with a reflective CLC coating were produced in the same way as the PA6 films/fibres. Characterization of these films and fibres showed that a planar alignment (Figure 4.12a) and narrow reflection band were also obtained for PET substrates (Figure 4.12b).

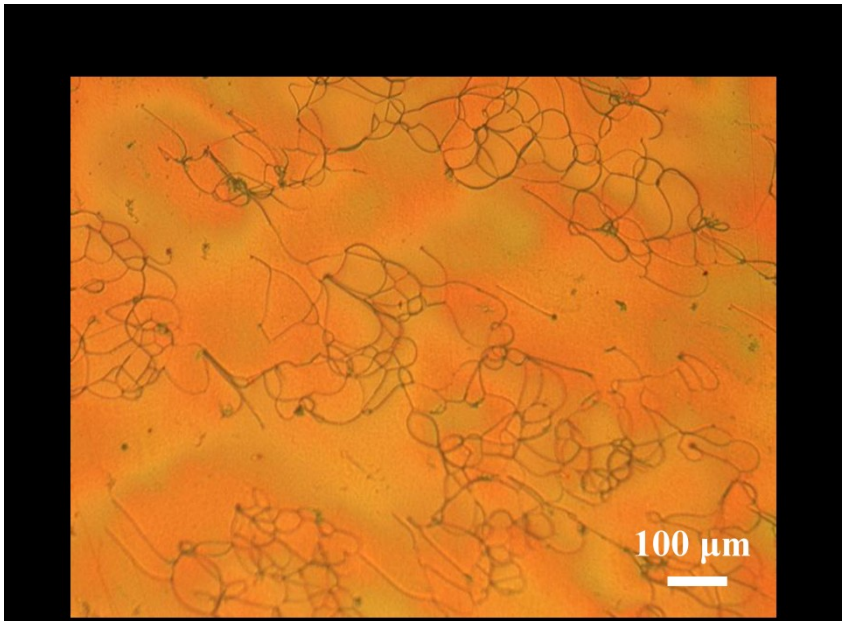

(b)

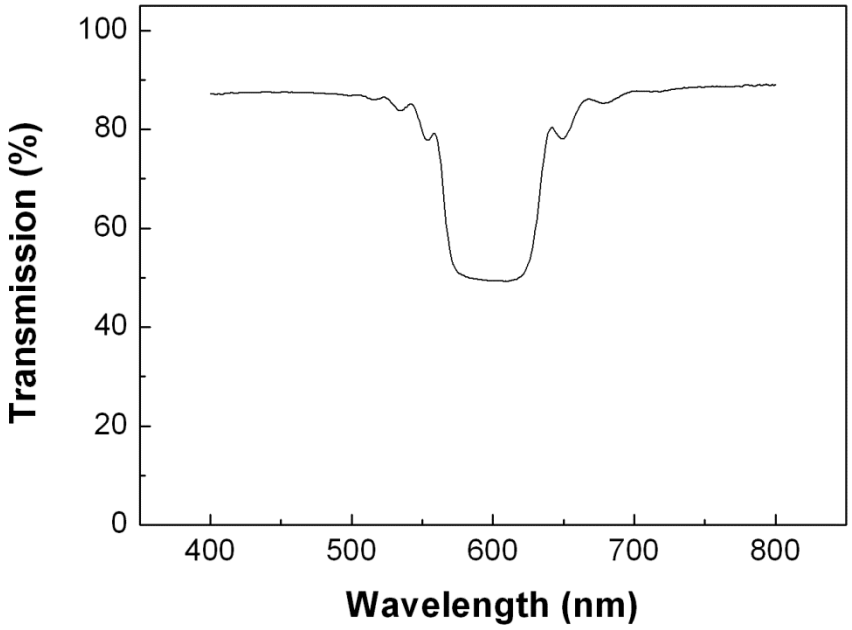

Figure 4-12 (a) Microscopy image in reflection mode without polarizer for an oriented PET/CLC coated film with presence of oily streak morphology characteristic of a CLC film with a planar alignment. Here the concentration of chiral dopant was adjusted to give a reflection band in the orange region. (b) Transmission spectrum recorded for the same film. Non-polarized light was used in this experiment resulting in a maximum reflection of 50%.

4.5 Conclusions

A CLC coating was applied to oriented PA6 films and fibres to generate colours based on selective reflection of light. Here the reflected light was centred in the green region of the visible spectrum. A planar cholesteric alignment was obtained for both films and fibres with the mesogens aligned parallel to the substrates' surface. By adjusting the optical retardation of the substrate, high reflection was achieved. The curved geometry of the fibres affected the reflected colour under oblique incidence. In the radial direction, the colour was isotropic and it was blue shifted in the longitudinal direction. Finally it was shown that the process is not restricted to oriented PA6 substrates but can be readily applied to PET tapes and fibres.

4.6 References

1 S. Kinoshita, S. Yoshioka, *Chemphyschem* **2005**, *6*, 1442-1459.

2 S. Kinoshita, S. Yoshioka, J. Miyazaki, *Rep. Prog. Phys.* **2008**, *71,* 1-30.

3 V. Sharma, M. Crne, J. O. Park, M. Srinivasarao, *Science* **2009**, *325*, 449-451.

4 B. Gauvreau, N. Guo, K. Schicker, K. Stoeffler, F. Boismenu, A. Ajji, R. Wingfield, C. Dubois, M. Skorobogatiy, *Opt. Express* **2008**, *16*, 15677-15693.

5 M. Dai, O. T. Picot, N. F. Hughes-Brittain, T. Peijs, C. W. M. Bastiaansen, *J Mater. Chem.* **2011**, *21*, 15527-15531.

6 P. G. d. Gennes, J. Prost, "*The physics of liquid crystals"*, 2nd edition, Clarendon Press ; Oxford University Press, Oxford New York, 1993, p. xvi.

7 S. Chandrasekhar, "*Liquid crystals"*, 2nd edition, Cambridge University Press, Cambridge England ; New York, NY, USA, 1992, p. xv.

8 W. D. Stjohn, W. J. Fritz, Z. J. Lu, D. K. Yang, *Phys. Rev. E* **1995**, *51*, 1191-1198.

9 D. K. Yang, X. Y. Huang, Y. M. Zhu, *Annu. Rev. Mater. Sci.* **1997**, *27*, 117-146.

10 S. Ishihara, *J. Disp. Technol.* **2005**, *1*, 30-40.

11 H. Aoyama, Y. Yamazaki, N. Matsuura, H. Mada, S. Kobayashi, *Mol. Cryst. Liq. Cryst.* **1981**, *72*, 127-132.

12 K. K. Chawla, "*Fibrous materials"*, Cambridge University Press, Cambridge, England, 1998, p. xv.

13 D. J. Broer, I. Heynderickx, *Macromolecules* **1990**, *23*, 2474-2477.

14 J. Lub, D. J. Broer, R. A. M. Hikmet, K. G. J. Nierop, *Liq. Cryst.* **1995**, *18*, 319-326.

15 D. J. Broer, H. Finkelmann, K. Kondo, *Makromol. Chem.* **1988**, *189*, 185-194.

16 G. P. Crawford, D. J. Broer, S. Zumer, "*Cross-linked liquid crystalline systems : from rigid polymer networks to elastomers"*, CRC Press, Boca Raton, FL, 2011, p. xv.

17 P. J. Collings, "*Liquid crystals : nature's delicate phase of matter*", 2nd edition, Princeton University Press, Princeton, N.J., 2002, p. xiv.

18 C. Sanchez, F. Verbakel, M. J. Escuti, C. W. M. Bastiaansen, D. J. Broer, *Adv. Mater.* **2008**, *20*, 74-78.

19 M. H. Song, B. C. Park, K. C. Shin, T. Ohta, Y. Tsunoda, H. Hoshi, Y. Takanishi, K. Ishikawa, J. Watanabe, S. Nishimura, T. Toyooka, Z. G. Zhu, T. M. Swager, H. Takezoe, *Adv. Mater.* **2004**, *16*, 779-783.

20 M. J. Escuti, D. R. Cairns, G. P. Crawford, *J. Appl. Phys.* **2004**, *95*, 2386-2390.

21 K. Lv, D. Z. Liu, W. Li, Q. X. Tian, X. Q. Zhou, *Dyes Pigment.* **2012**, *94*, 452-458.

22 J. Lub, D. J. Broer, R. T. Wegh, E. Peeters, B. M. I. van der Zande, *Mol. Cryst. Liq. Cryst.* **2005**, *429*, 77-99.

23 a) A.K. Bendiganale, V.C. Malshe, *Recent Patents on Chemical Engineering* **2008**, *1*, 67-79; b) B.J. Conolly, T.K. Hussey, C. Hurren, Heat Reflective Layered Garment System. WO 2012/073096 A1, **2012**.

Chapter 5

Optical strain sensor based on a CLC coating

5.1 Introduction

Detecting deformations in materials is of importance for a variety of applications, such as structural health monitoring of structures. Conventionally strain in engineering materials is detected by embedding fibre optics or by attaching an array of strain gauges onto the surface.[1, 2] Deformations are then monitored through changes in specific wavelengths reflected in the Fibre Bragg Grating (FBG) sensor fibre or by changes in electrical resistance of the metallic foil. Conductive polymer composites based on percolating networks of carbon nanomaterials like carbon nanotubes or graphene are also studied to sense mechanical deformations. Here, the exposure of these composites to external stimuli results in changes in electrical resistivity.[3, 4] In the present work we propose a different optical approach to detect deformations using a cholesteric liquid crystal (CLC) polymer. In the past few years,

CLCs that change colour dynamically have drawn much attention for detection and sensing applications.[5] CLCs selectively reflect a fraction of circularly polarized light which is directly related to the helical arrangement of the LC molecules.[6] CLC polymers are readily obtained by adding a chiral compound to nematic liquid crystal monomers.[7, 8] After aligning the mesogens on an oriented substrate, a cross-linked network is obtained through a photopolymerization step resulting in a film, which is glassy at room temperature (Young's modulus ~1-2 GPa).[9, 10] Mechanically induced colour changes in CLC polymers have already been predicted and demonstrated for CLC elastomers.[11-14] Here, the change in colour is attributed to a thinning of the elastomer that translates to a reduction in helix length thereby shifting the reflection band to lower wavelengths. Yet, the response of CLC elastomers is limited to large deformations and synthesis and processing is intricate. We have shown in Chapter 4 that a well-defined CLC organisation can be obtained by spray-coating a solution of CLC monomers onto oriented polymer tapes and fibres. Here we use the same process to fabricate an optical sensor to detect small uniaxial deformations in real time using an oriented polyamide 6 (PA6) substrate.

5.2 Experimental

5.2.1 Materials

A uniaxially oriented PA6 film with a thickness of 25 μm was purchased from Goodfellow. Monomers (Figure 5.1) C3M, C6M (Merck) and a chiral dopant (LC756 – BASF), were mixed together in the following proportions: 18.8%, 75.6%

and 4.6%, respectively. A small amount (1 wt.%) of 1-hydroxycyclohexyl phenyl ketone (Sigma Aldrich) was added as a photoinitiator.[15] The monomers and additives were dissolved in xylene in a 1 to 2.5 ratio.

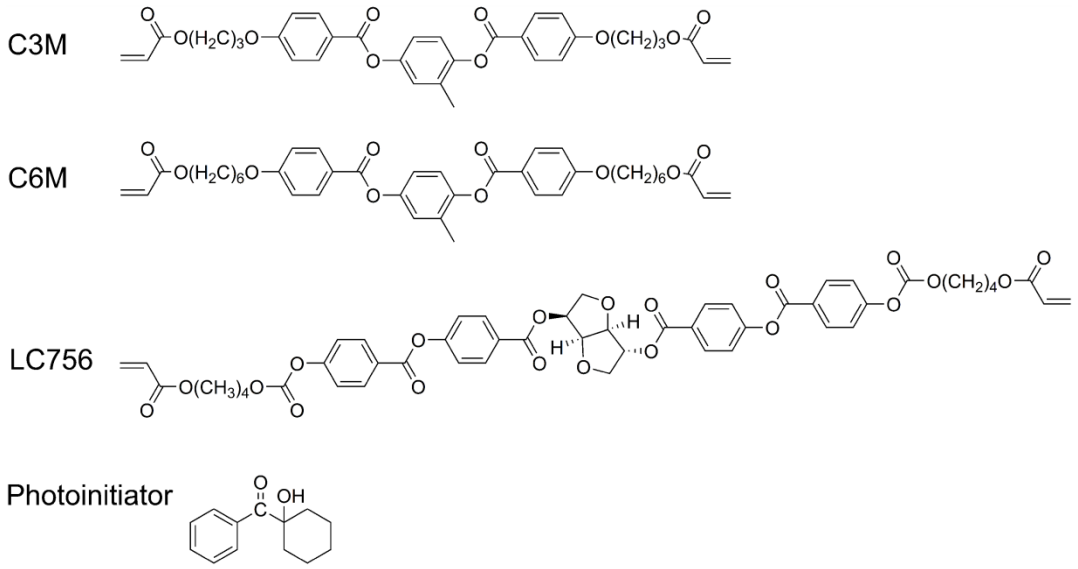

Figure 5-1 Chemical structure of the liquid crystal monomers.

5.2.2 Sensor preparation

PA6 films were cleaned with isopropanol and taped to a metal plate. The liquid crystal mixture was sprayed on the films using an Iwata airbrush (flow rate of 2 $mL.min^{-1}$ and a distance between nozzle and film of 10 cm). The coated films were placed in an oven (80 ^{o}C) for 60 s to remove residual traces of solvent and then cooled to room temperature. Photopolymerization was performed using a mercury lamp (EXFO Omnicure S2000, λ = 350-450 nm, 200 W) under nitrogen at room temperature for 200 s.

5.2.3 Characterization

Transmission measurements were performed using a Perkin Elmer Lambda 950 UV-Vis spectrophotometer equipped with left and right circular polarisers. To investigate the effect of strain, films were mounted on a custom-made strain rig. The frame enabled to apply uniaxial extension to the films and transmission measurements were performed for each extension values. The frame also prevented strain relaxation of the film during the measurements. Measurements were also performed during a loading-unloading cycle (Figure 5.2). During loading, extension was increased step-wise and the reflection band was measured for each step. Unloading was also done in a step wise fashion and the reflection band was measured in the same way. A TA Instrument DMA apparatus was used to follow the recovery of strain as a function of time. A load was applied to the film to obtain 11% of deformation. The load was kept constant for 2 min and released letting the film to recover to its initial length. Strain changes were monitored for 30 min after the load was released. Optical images were taken with a Leica microscope.

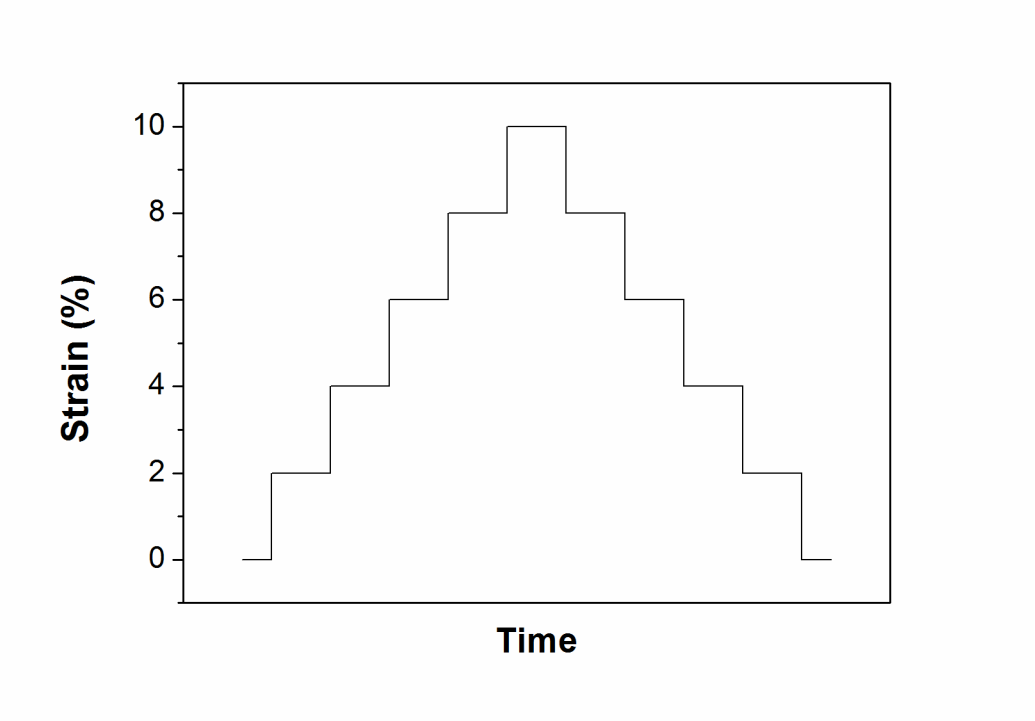

Figure 5-2 Illustration of the strain cycle

5.3 Results and discussion

The optical properties of the coating were first investigated when no strain was applied ($\varepsilon = 0$ %). Transmission measurements between 400 nm and 800 nm of left and right circular polarized light showed a strong polarization dependent reflection band centred at $\lambda = 601$ nm (Figure 5.3a).

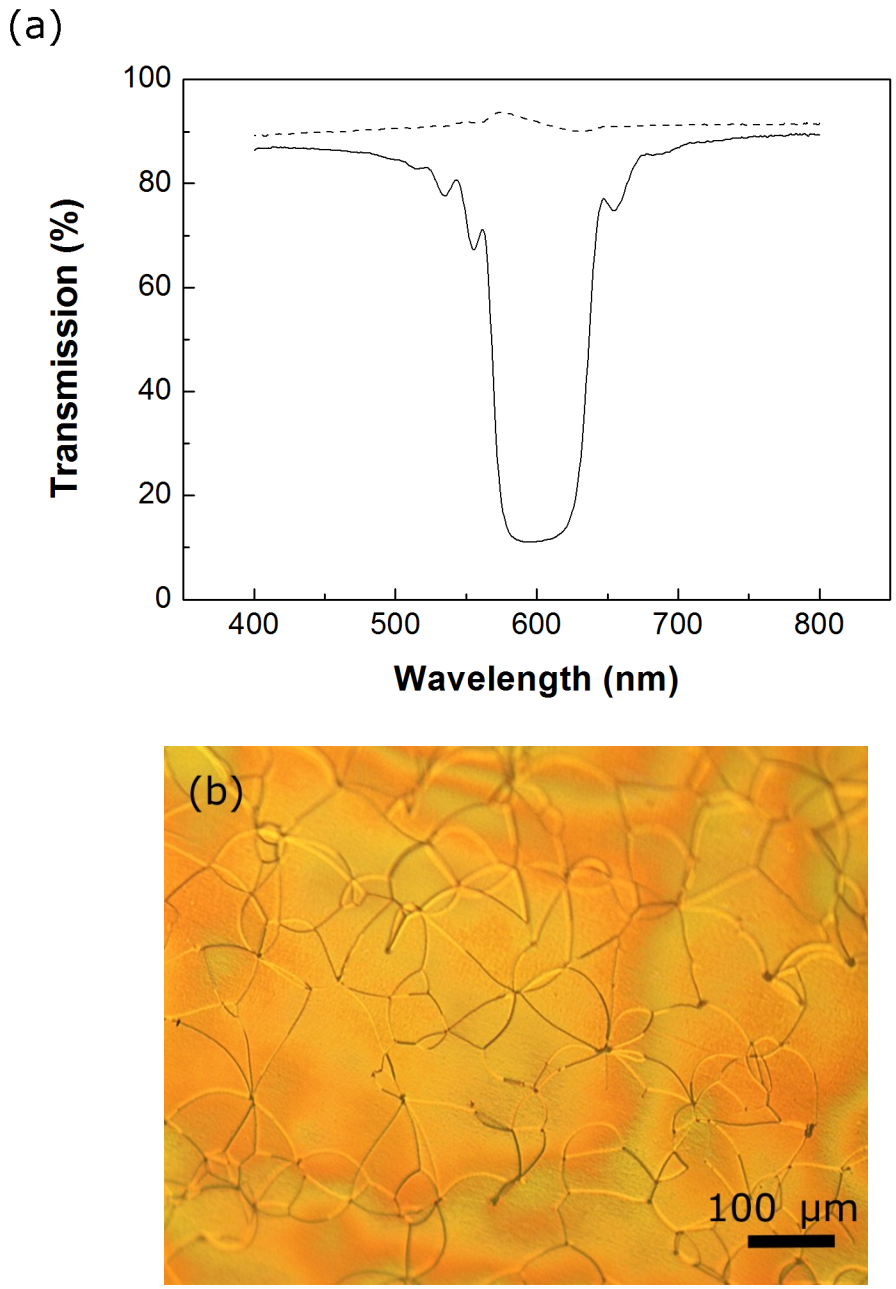

Figure 5-3 (a) Transmission spectra of the reflective film for two polarization states, (dash line) left-handed circular polarized light (LHCPL) and (solid line) right-handed circular polarized light (RHCPL). (b) Optical microscopy image taken in reflection mode for non-polarized light.

Observations of the coating under optical microscopy showed the characteristic oily streak morphology, typical of a planar CLC alignment (Figure 5.3b).[16] Transmission measurements using right-handed circular polarized light were then realised with uniaxial extension applied to the film. As strain increased, the reflection band was found to shift towards lower wavelengths (Figure 5.4a).

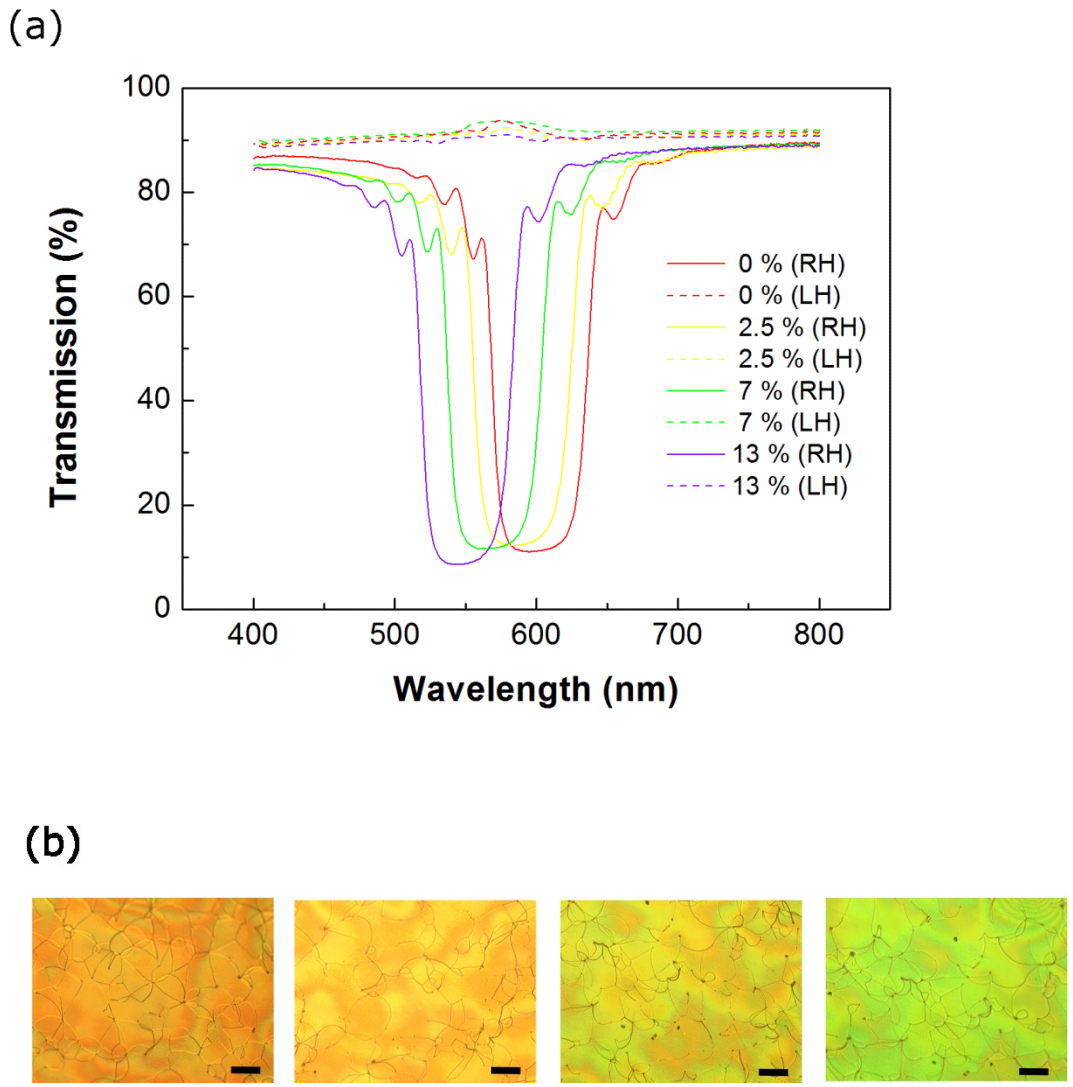

Figure 5-4 (a) Transmission spectrums of the bilayer film under extension for left-handed (LH) and right-handed (RH) circular polarized light. (b) Microscopy pictures in reflection mode showing the corresponding change in colour. The scale bars stand for 100 μm.

In this experiment, a maximal strain of 13% was imposed, resulting in an overall shift of 40 nm of the reflection band. This relatively large wavelength shift resulted in a colour change of the film from orange to green (Figure 5.4b). Measurements performed with left-handed circular polarized light showed no change under deformation. Surprisingly, further stretching of the sensor resulted in the opposite trend and the reflection band shifted towards its original position (Figure 5.5).

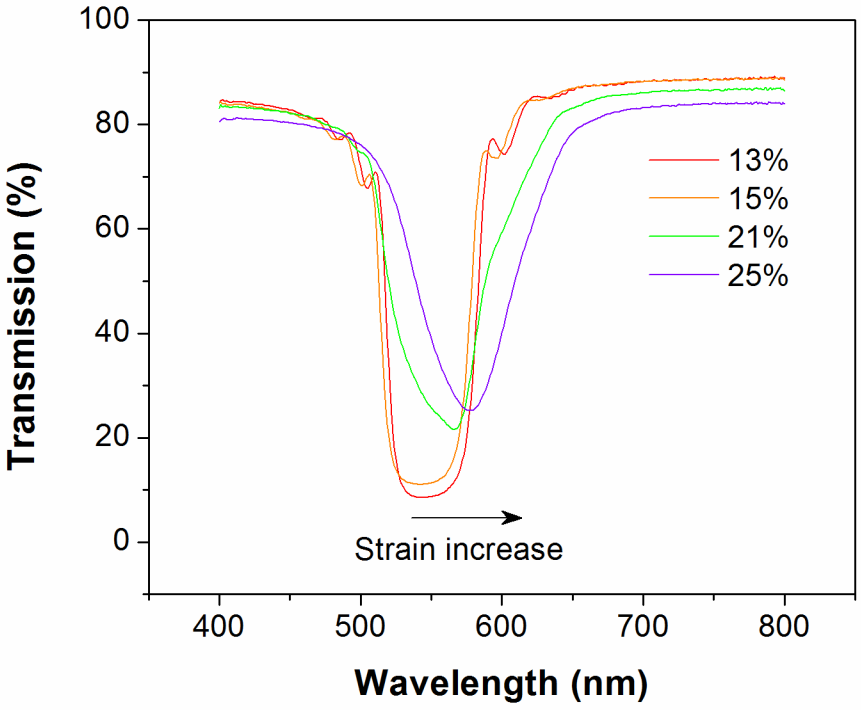

Figure 5-5 Transmission spectrum of the sensor for different extensions.

Optical microscopy images (Figure 5.6) revealed that above 10% strain, cracks appeared in the coating and in the vicinity of the crack the colour appeared orange.

Further stretching created larger and multiple cracks resulting in larger areas with an orange colour. These results indicate that at large strains, the colour shift is not homogenous in the coating layer. As the reflection band measurement is averaged on the area of the spectrophotometer beam spot, the resulting reflection band position is not indicative of the actual strain in the sensor.

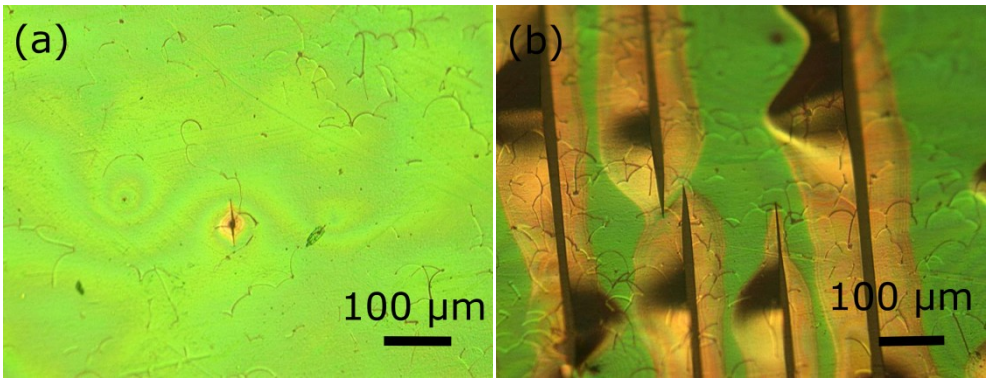

Figure 5-6 Optical microscopy images of the sensor taken in reflection. (a) ε = 14% and (b) ε = 19%

When the film was unloaded, the orange colour was restored. This reversible behaviour was further investigated by measuring the reflection band during a loading-unloading cycle. Figure 5.7 shows the wavelength shift (λ_0 - λ_x) as a function of strain. The wavelength shift is defined as the difference between the wavelength position for ε = 0% (λ_0) and the wavelength position for ε = x% (λ_x). Wavelength positions were measured at the mid-height of the reflection band. During loading the wavelength shift increased progressively to a maximum of 26 nm for 10% strain, while step-wise unloading of the film led to a reverse shift. From 10% to 4% strain, the shift was consistent between loading and unloading.

Interestingly, measurements below 4% strain showed a discrepancy for the loading and unloading data and upon unloading (ε = 0%) a shift of 5 nm remained. It is suspected that residual deformation in the polymer film did not allow full recovery of the reflection band.

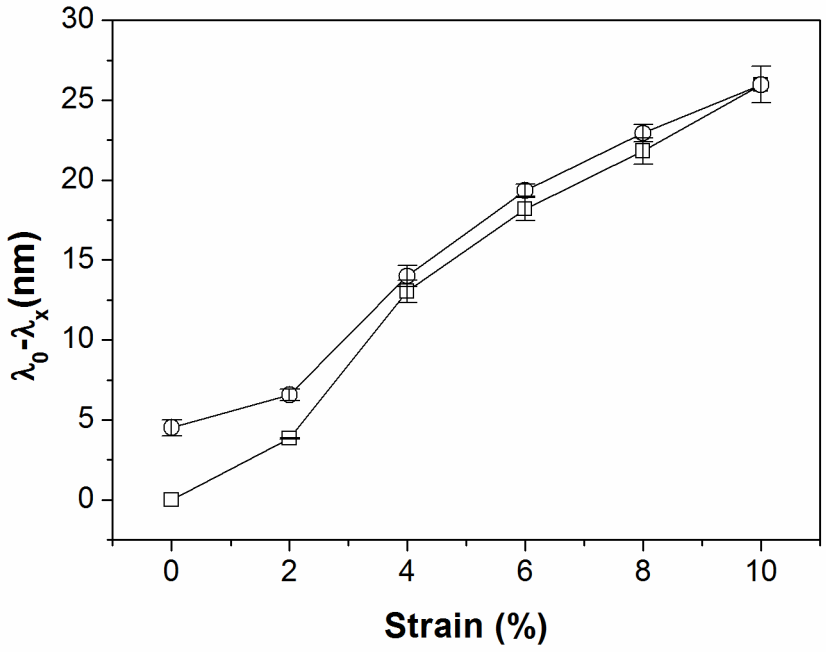

Figure 5-7 Wavelength shift as a function of strain during loading (□) and unloading (○) of the optical sensor.

Finally, in order to verify if the optical response correlates to the mechanical deformation behaviour of the substrate, the wavelength recovery process was further investigated. For this, the sensor was deformed to 11% for 2 min and then unloaded and left to recover. Transmission measurements were performed over time to follow the reflection band recovery.

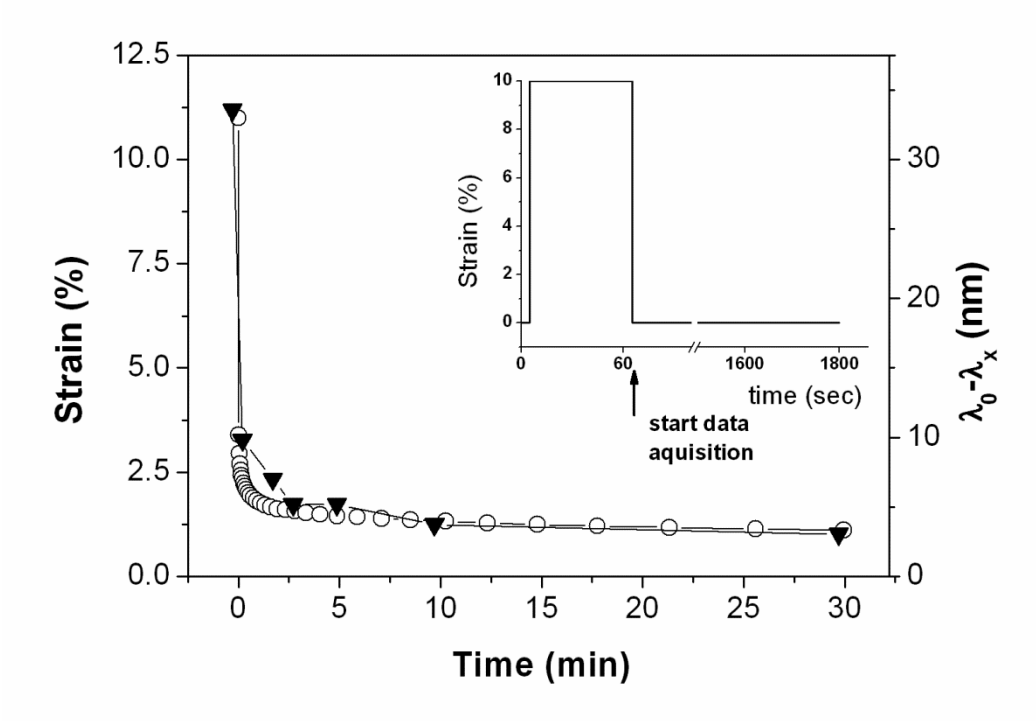

Figure 5-8 Strain (○) and wavelength shift (▼) as a function of time after unloading. Inset graph represents the strain cycle.

Wavelength shift as a function of time is shown in Figure 5.8. After unloading the film, the shift decreases drastically during the first few seconds and then levelled off. After 30 min of recovery, a residual shift of 3 nm remained. The same experiment was performed using a DMA apparatus. The DMA allowed following the change in strain in the polymer substrate as a function of time after unloading the sample (Figure 5.8). Here, as expected, the strain also decreased rapidly after unloading and finally levelled off. After 30 min recovery, 1.1% residual strain remained in the film. This amount of strain is in good agreement with the residual wavelength shift of 3 nm as measured optically.

5.4 Discussion

The strong Bragg reflection of the coating and oily streak morphology suggests that the helix axis is perpendicular to the surface of the substrate. When uniaxial strain was applied to the film along the orientation direction, a shift in the reflection was observed. For large deformations ($\varepsilon > 10\%$), the corresponding wavelength shift was large enough to result in a colour change visible by eye. On the other hand, deformations applied perpendicularly to the orientation direction showed limited colour change as necking of the PA6 substrate ($\varepsilon \sim 5\%$) resulted in delamination and failure of the coating.

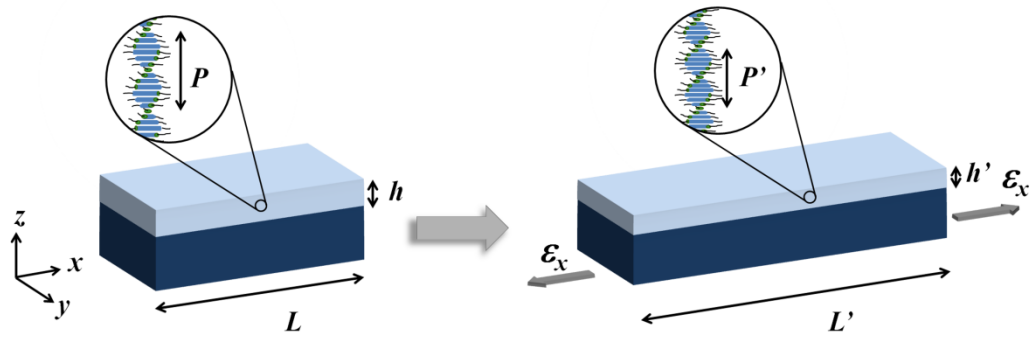

Figure 5-9 Schematic representation of the CLC strain sensing mechanism.

The colour change mechanism of the sensor (Figure 5.9) is very similar to the one reported for CLC elastomers.[12] During uniaxial extension of the bilayer film (ε_x), contraction of the CLC layer in the thickness direction ($h' < h$) leads to a reduction

in pitch length (P' < P). Previous reports on CLC elastomers reported a loss of chirality with increasing strain resulting in the development of a reflection band of opposite handedness.[11-12] Interestingly, no such observations were made in this case. We believe that, in comparison with elastomers, the higher cross-link density of the polymer prevents any reorientation of the mesogen units. This is further supported by reported work on highly cross-linked LC films with a planar alignment under deformation.[17] Additionally, it was shown that the colour shift was reversible, albeit the initial wavelength is not fully restored after unloading the film. It is presumed that the substrate has not fully recovered its initial length within the time frame of the experiment, resulting in a residual wavelength shift. This hypothesis was further confirmed by the results shown in Figure 5.8 where the recovery of both strain and wavelength shift follow the same trend. Moreover, the residual strain after 30 min recovery corresponded to the residual wavelength shift measured after the same recovery period. This result reflects the close correlation between the mechanical response of the polymer substrate to strain and the optical response of the CLC coating and thereby demonstrates the potential of our approach for real time strain sensing.

5.5 Conclusions

In summary an optical strain sensor has been produced by coating a mixture of CLC monomer onto a uniaxially oriented PA6 substrate followed by a photopolymerization step. When the substrate was stretched, a change in colour of

the coating was observed. This colour change is directly related to the decrease in the pitch of cholesteric helix. The optical response was found to be entirely dependent on the deformation of the substrate and upon unloading the wavelength shift was reversed. Additionally, residual plastic strain in the substrate resulted also in a residual shift in wavelength and colour.

5.6 References

1 T. G. Giallorenzi, J. A. Bucaro, A. Dandridge, G. H. Sigel, J. H. Cole, S. C. Rashleigh, R. G. Priest, *IEEE J. Quantum Elect.* **1982**, *18*, 626.

2 Z. Wisniewski, R. Wisniewski, J. L. Nowinski, *Rev. Sci. Instrum.* **2001**, *72*, 2829.

3 E. Bilotti, R. Zhang, H. Deng, M. Baxendale, T. Peijs, *J. Mater. Chem.* **2010**, *20*, 9449.

4 R. Zhang, M. Baxendale, T. Peijs, *Phys. Rev. B* **2007**, *76*.

5 T. J. White, M. E. McConney, T. J. Bunning, *J. Mater. Chem.* **2010**, *20*, 9832.

6 S. Chandrasekhar, "*Liquid crystals"*, 2nd edition, Cambridge University Press, Cambridge England ; New York, NY, USA, 1992, p. xv.

7 D. J. Broer, I. Heynderickx, *Macromolecules* **1990**, *23*, 2474.

8 J. Lub, D. J. Broer, P. van de Witte, *Prog. Org. Coat.* **2002**, *45*, 211.

9 R. A. M. Hikmet, D. J. Broer, *Polymer* **1991**, *32*, 1627.

10 J. Lub, D. J. Broer, R. T. Wegh, E. Peeters, B. M. I. van der Zande, *Mol. Cryst. Liq. Cryst.* **2005**, *429*, 77.

11 P. Cicuta, A. R. Tajbakhsh, E. M. Terentjev, *Phys. Rev. E* **2002**, *65*.

12 P. Cicuta, A. R. Tajbakhsh, E. M. Terentjev, *Phys. Rev. E* **2004**, *70*.

13 Y. Hirota, Y. Ji, F. Serra, A. R. Tajbakhsh, E. M. Terentjev, *Opt. Express* **2008**, *16*, 5320.

14 P. Palffy-Muhoray, H. Finkelmann, S. T. Kim, A. Munoz, B. Taheri, *Adv. Mater.* **2001**, *13*, 1069.

15 C. Sanchez, F. Verbakel, M. J. Escuti, C. W. M. Bastiaansen, D. J. Broer, *Adv. Mater.* **2008**, *20*, 74.

16 P. J. Collings, "*Liquid crystals : nature's delicate phase of matter*", 2nd edition, Princeton University Press, Princeton, N.J., 2002, p. xiv.

17 M. J. Escuti, D. R. Cairns, G. P. Crawford, *J. Appl. Phys.* **2004**, *95*, 2386.

Chapter 6

Light responsive actuators based on LC coatings

6.1 Introduction

In this chapter we aim at producing photoresponsive actuators for intelligent textile applications. While the previous chapter focused on an optical response, here it is intended to generate mechanical deformation in polymer tapes or fibres, in response to light using liquid crystal networks. Liquid crystal networks have been reported to deform in response to a variety of triggers such as temperature, humidity or light.[1-3] The present work focuses on photoresponsive LC networks. Light is an attractive stimuli as it is potentially clean, free and widely available in the environment. Photoresponsive LC networks are a class of responsive material that can undergo complex and reversible deformations upon exposure to light. Typically an azobenzene mesogen is incorporated into the network. Upon exposure to light,

usually in the UV range, the photoisomerisation from the *trans*- configuration to the *cis*- configuration takes place. Cooperative movement of neighbouring mesogens leads to contraction along the orientation direction and expansion in the direction perpendicular.[4] This simple response has been used to generate bending in LC polymer films.[5] The deformation is governed by molecular alignment, polarization, temperature, cross-linking density and concentration of azobenzene.[6-12] To date, UV actuating fibres have been obtained for elastomeric LC.[13] Here the intention is to develop UV responsive fibres using a bi-component fibre system. As demonstrated in Chapter 4, an oriented polymer core fibre allows aligning LC molecules and provides mechanical stability. In order to investigate the response, the system was simplified to a bilayer tapes. The bilayer tapes are produced via a simple spray coating step of an LC monomer mixture comprising a fixed amount of azobenzene moieties, on an oriented polymer film. The monomers are then converted to polymer network through a photopolymerization step.[14]

6.2 Experimental

6.2.1 Materials

A mixture of liquid crystal monomers and a reactive azobenzene liquid crystal (A3MA) were used. The azobenzene LC was kindly provided by TU Eindhoven, The Netherlands (Figure 6.1). A planar liquid crystal monomer mixture (RMM944) obtained from Merck was mixed with A3MA in different concentrations (2 wt.%, 4 wt.% and 8 wt.%) and 2 wt.% of photoinitiator phenylbis(2,4,6-

trimethylbenzoyl)phosphine oxide (Sigma Aldrich) was added for cross-linking. The mixture was dissolved in xylene in a 1:1 weight ratio for spin coated films and 1:2.5 in weight for spray coated films.

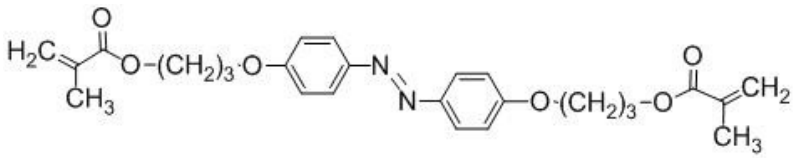

Figure 6-1 Chemical structure of the azobenzene dye A3MA.

6.2.2 Film preparation

Free standing LC actuators:

Free standing films were prepared for reference purposes. The LC solution was spin coated on a PVA coated glass slide. The PVA substrate was manually buffed prior to coating to generate a monodomain uniaxial alignment. The LC solution was spin coated at 2000 rpm for 30 s. The films were annealed at 80 ^{o}C in an oven for 60 s to remove residual traces of solvent and successively cooled to room temperature. Photopolymerization was performed using a mercury lamp (EXFO Omnicure S2000) in a nitrogen atmosphere at room temperature for 15 min. The lamp was equipped with a high-pass optical filter (Edmund Optics) in order to expose the film with $\lambda >$ 400nm. After curing, the glass slides were immersed in water and left overnight to allow the PVA layer to dissolve. The films were then carefully peeled off, rinsed with water to remove any residual PVA and left to dry in air.

Bi-layer LC actuators:

Bi-layer films were prepared using oriented PET and PA6 films as substrates. They were washed with isopropanol, dried with compressed air and taped to a metal plate. The LC solution was spray coated using an airbrush (Iwata) with a flow rate of 2 $mL.min^{-1}$. The distance from the nozzle to the film was 15 cm. The coated films were annealed and cured following the same procedure as described above for the free standing films.

6.2.3 Characterization

Alignment of the mesogens was checked visually using optical microscopy with crossed polarisers. The samples, with the rubbing direction aligned with the polariser, were rotated step wise by 45^{o} and images were taken for each step using a Leica camera. The absorption spectrums of the films were measured using a Perkin Elmer Lambda 950 UV-Vis spectrophotometer equipped with a linear polariser. Attenuated total reflectance (ATR) infra-red spectra were measured with a Varian 670 IR spectrometer. Measurements were performed on the LC/air surface of the coating and the LC/substrate surface of the coating with the IR beam polarized parallel and perpendicular to the stretching direction of polymer substrate. LC/substrate samples were prepared by gluing the coated side of the bi-layer to a glass slide. Then the polymer substrate was carefully peeling off leaving the LC coating on the glass slide. In this way it was possible to characterize the alignment at the LC/substrate interface. Phase transitions of the non-polymerized LC mixture were determined using differential scanning calorimetry (DSC) characterization with a heating and cooling rate of 5 $^{o}C/min$ (Mettler Toledo). The photoresponse of the bilayer films was characterized by clamping stripes (20 x 5 mm cut along the

orientation direction) at one end and irradiating them with UV light using a mercury lamp (EXFO Omnicure S2000) equipped with a filter to select the UV wavelength range: 280-390 nm (Andover 011FG09-50 filter). For each samples the response was filmed in real time and the bending radii were measured at 10 s intervals.

6.3 Results and discussion

Photoresponsive bilayer actuators were produced by spray coating the LC mixture on the oriented polymer substrate. DSC results (Figure 6.2) of the monomer prior to UV-polymerization were recorded. In the first scan a nematic phase was observed between 63 ^{o}C and 105 ^{o}C. During cooling at 5 ^{o}C/min, a single transition from isotropic to nematic was observed at 105 ^{o}C. The nematic phase was found to be stable over a broad range of temperature thereby allowing for photopolymerization of the LC at room temperature.

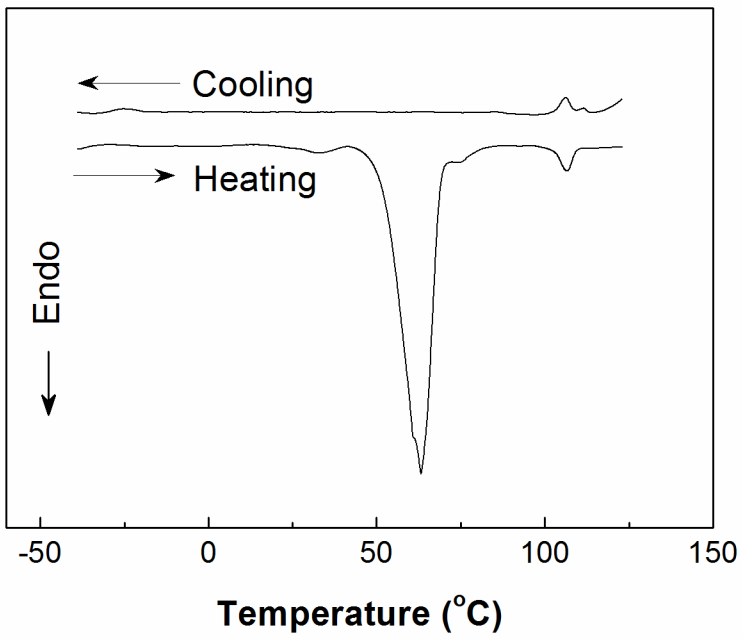

Figure 6-2 DSC thermogram of the LC host showing the nematic and isotropic transitions.

6.3.1 Liquid crystal coating morphology

The alignment of the mesogens was first checked by observing the coating (see the experimental section) in an optical microscope with crossed polarisers (Figure 6.3). Rotating the film by 45^{o} showed changes between dark and bright images revealing that the film is monodomain with the mesogens aligned preferably along the stretching direction of the polymer substrate.

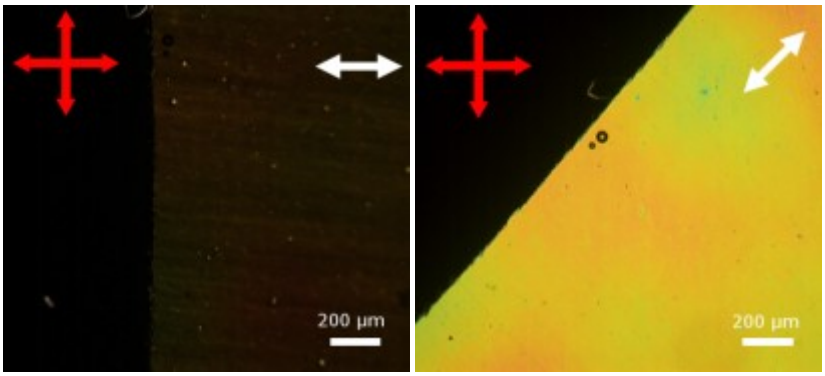

Figure 6-3 Polarized optical microscopy images of the coating after peeling it off the PET substrate. Pictures are taken at two different angles with respect to the polarization direction and the PET substrate's orientation. The red arrows indicate the orientation of the optical axis for the polariser and analyser. The white arrow indicates the orientation direction of the substrate.

These results were further confirmed by polarized absorption measurements performed on the bilayer film. Figure 6.4 shows the absorption of the bilayer from 600 nm to 320 nm for two polarisation states, *e.g.* parallel and perpendicular. A strong absorption peak centred on 363 nm corresponding to the absorption of the azobenzene in the *trans*-state is observed for light polarized parallel to the

orientation direction. On the other hand, the absorption was found to be lower when the polarisation is perpendicular to the orientation direction. This result supports the predominant alignment of the A3MA molecules along the stretching direction of the substrate.[21]

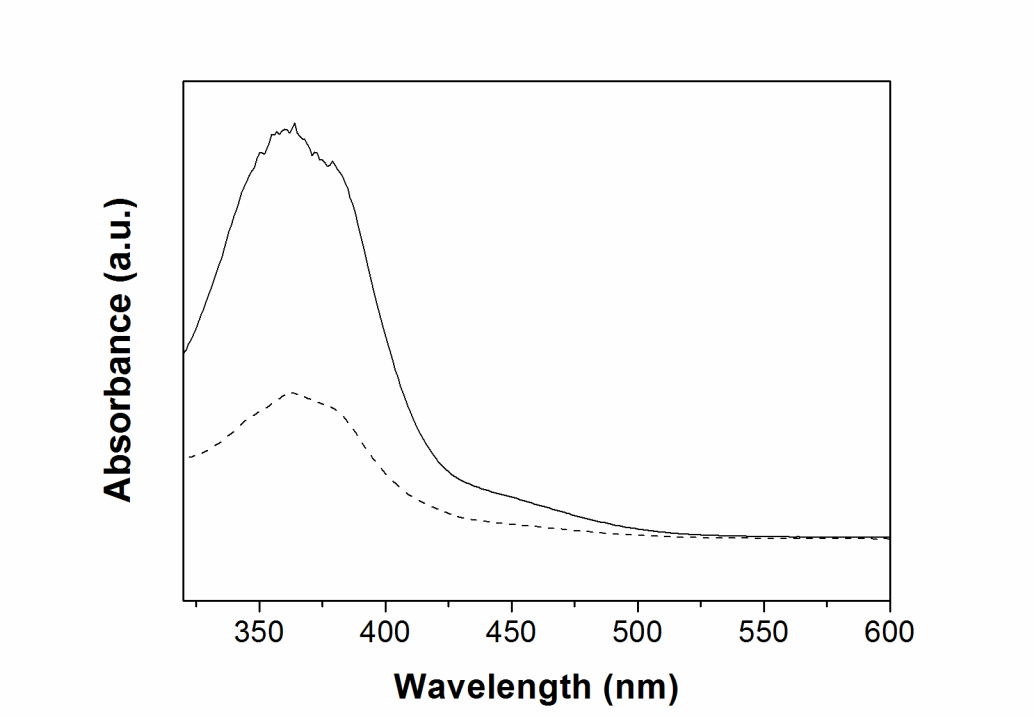

Figure 6-4 Polarized absorbance of the LC/PET film with 8% A3MA. The polarization direction is parallel (solid line) or perpendicular (dash line) to the orientation direction of the polymer substrate.

Polarised UV-Vis data was used to evaluate the LC network's order parameter *S*.[11, 21] This is of particular interest as the order parameter is known to influence the photoinduced bending.[10] Using the absorbance parallel ($A_{\parallel}$) and perpendicular ($A_{\perp}$) to the orientation direction, *S* could be calculated with Equation (6.1).

$$S = \frac{(A_{\parallel} - A_{\perp})}{(A_{\parallel} + 2A_{\perp})} \qquad 6.1$$

Table 6.1 gives the order parameter for the different PET actuators. The order parameter was almost the same for samples with PET-A2 and PET-A4 while it was slightly lower for PET-A8. Large concentrations (~10 wt.%) of A3MA have been reported to favour a multidomain LC morphology.[7] Although here we still have a monodomain morphology, it is suspected that the addition of 8 wt.% A3MA influences the order resulting in the lower *S* value.

Table 6-1 Order parameter for the three actuators PET-A2, PET-A4 and PET-A8

Sample	A3MA (wt.%)	S
PET-A2	2	0.46
PET-A4	4	0.46
PET-A8	8	0.37

The molecular alignment of the LC host was investigated with ATR-FTIR. This technique has previously been used to characterize molecular alignment at the surface of polymer films.[9, 22] Figure 6.5a show the spectra collected for the top surface of the coating (LC/air interface). The absorption band at 1759 cm^{-1} is assigned to the stretching vibration of carbonyl groups attached to the polymer backbone. It has been shown that no anisotropy is observed for this band.[9] On the other hand, bands at 1604 cm^{-1},1579 cm^{-1}, 1509 cm^{-1},1471 cm^{-1} assigned to the carbon-carbon stretching vibration in the benzene rings showed a large IR dichroism with the highest absorbance when the IR beam was polarized parallel to orientation direction of the polymer substrate, indicating that molecules were well aligned in this

direction. Similar spectra were collected for the other side of the coating which was attached to the polymer substrate (LC/substrate interface).

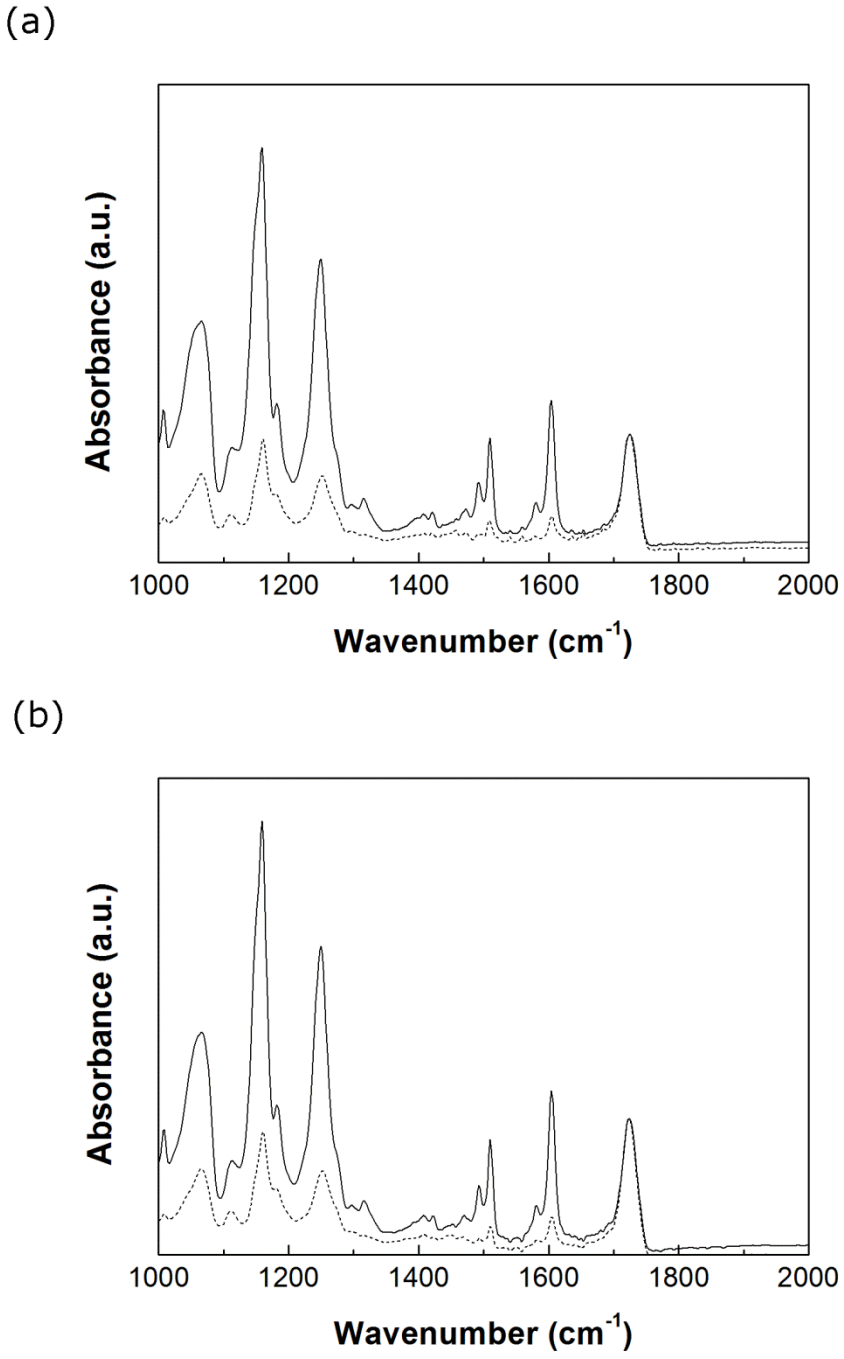

Figure 6-5 Polarized ATR FTIR spectrums of the LC coating at the LC/air interface (a) and the LC/substrate interface (b). The IR beam was polarized parallel (solid) and perpendicular (dash) to the substrate orientation.

The IR dichroic ratio was calculated using Equation (6.2).

$$D = \frac{A_{\parallel}}{A_{\perp}} \qquad 6.2$$

Where $A_{\parallel}$ and $A_{\perp}$ are the absorbance from the band at 1604 cm^{-1} for light polarized parallel and perpendicular to the orientation direction. At the LC/air interface, D was found to be 3.5 while it at the substrate/LC interface is was 4.3. A LC film with a planar alignment was taken as a reference. The dichroic ratio of this film was found to be 3, supporting that the LC molecules in the bilayer have a planar alignment.

6.3.2 Photoresponse of the bilayer

The photoresponse of the actuators was characterised by clamping a 10 mm long strip at one end and exposing it to UV light. The response was recorded with a digital camera. The films were exposed successively on both sides. All actuators showed a reversible bending in a distinctive direction according to the exposure side. Figure 6.6 shows a typical response for an actuator containing 8% of A3MA. Exposing the film on the LC coating side resulted in bending of the film towards the actinic light, while the opposite response was observed when exposing the substrate side. Such behaviour was also reported for elastomeric LC actuators laminated on polyethylene (PE) and PET substrates.[14-18, 23-24]

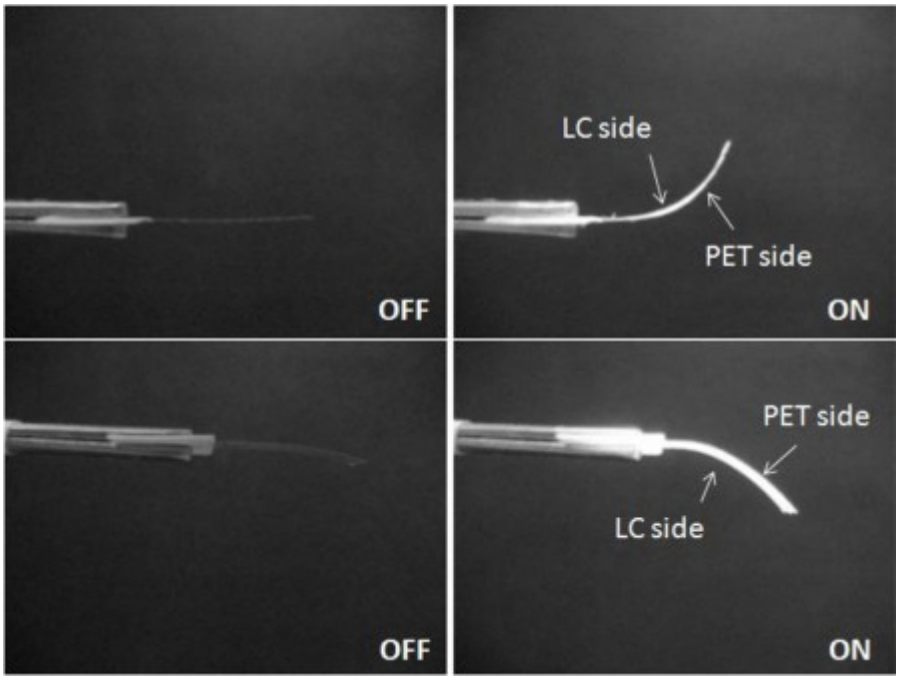

Figure 6-6 Response of a bilayer film containing 8 wt.% A3MA (10 mm x 4 mm) to UV illumination (200 $mW.cm^{-2}$). The top pictures are taken when exposing the PET side while the bottom pictures were obtained when exposing the LC side. The thickness of the polymer substrate was 25 μm and the coating thickness was 5 μm.

The bending radius 1/r of was also measured as function of time for the bilayer film. Figure 6.7 is a typical plot of the bending radius over time. Here the A3MA loading was 8%. As it can be seen, the film showed a large deformation occurring in the first few seconds of exposure. Then deformation levelled off after 30 s. A comparison was made for a bilayer film without the azobenzene LC. Surprisingly this film also showed a small response despite no azobenzene was added to the mixture. However, here the deformation was more linear and much smaller in magnitude. It is presumed that the observed response comes from heating of the oriented film by the lamp.[7]

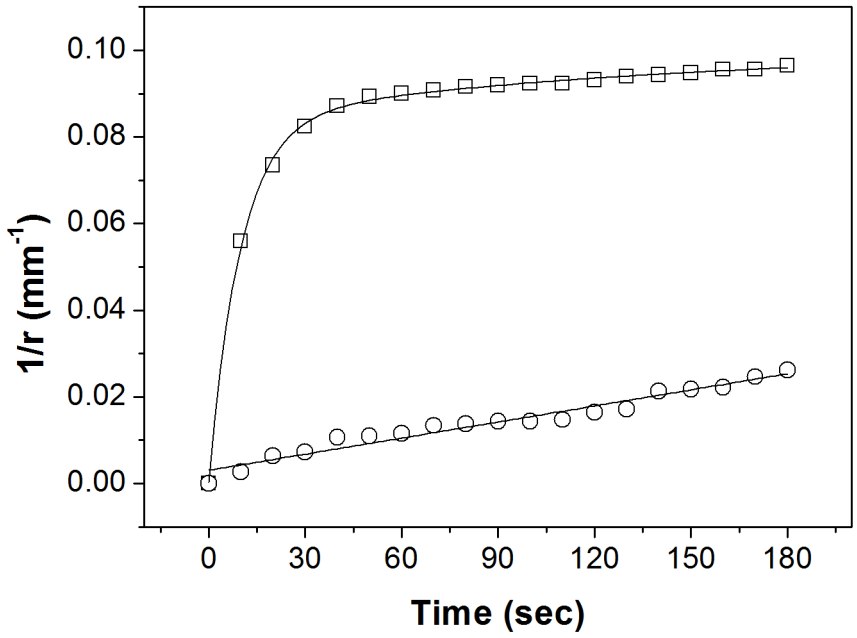

Figure 6-7 Bending radius as a function time for the actuator containing 8% A3MA (□), and the reference without any A3MA (○).UV intensity I = 200 mW.cm^{-2}. Solid lines are a guide for the eye.

The influence of substrate thickness and azobenzene content was also investigated. Firstly, a comparison was made between a bilayer with a 23 μm thick PET substrate and a bilayer with a 50 μm thick substrate (Figure 6.8). Increasing the thickness of the substrate largely affected the bending radius. After 180sec exposure it decreased by a factor 3. The concentration of A3MA was also varied and curvature was measured (Figure 6.8). Results show that a large bending (in comparison with the results obtained for 8% azobenzene) can be generated with the addition of only 2% azobenzene.

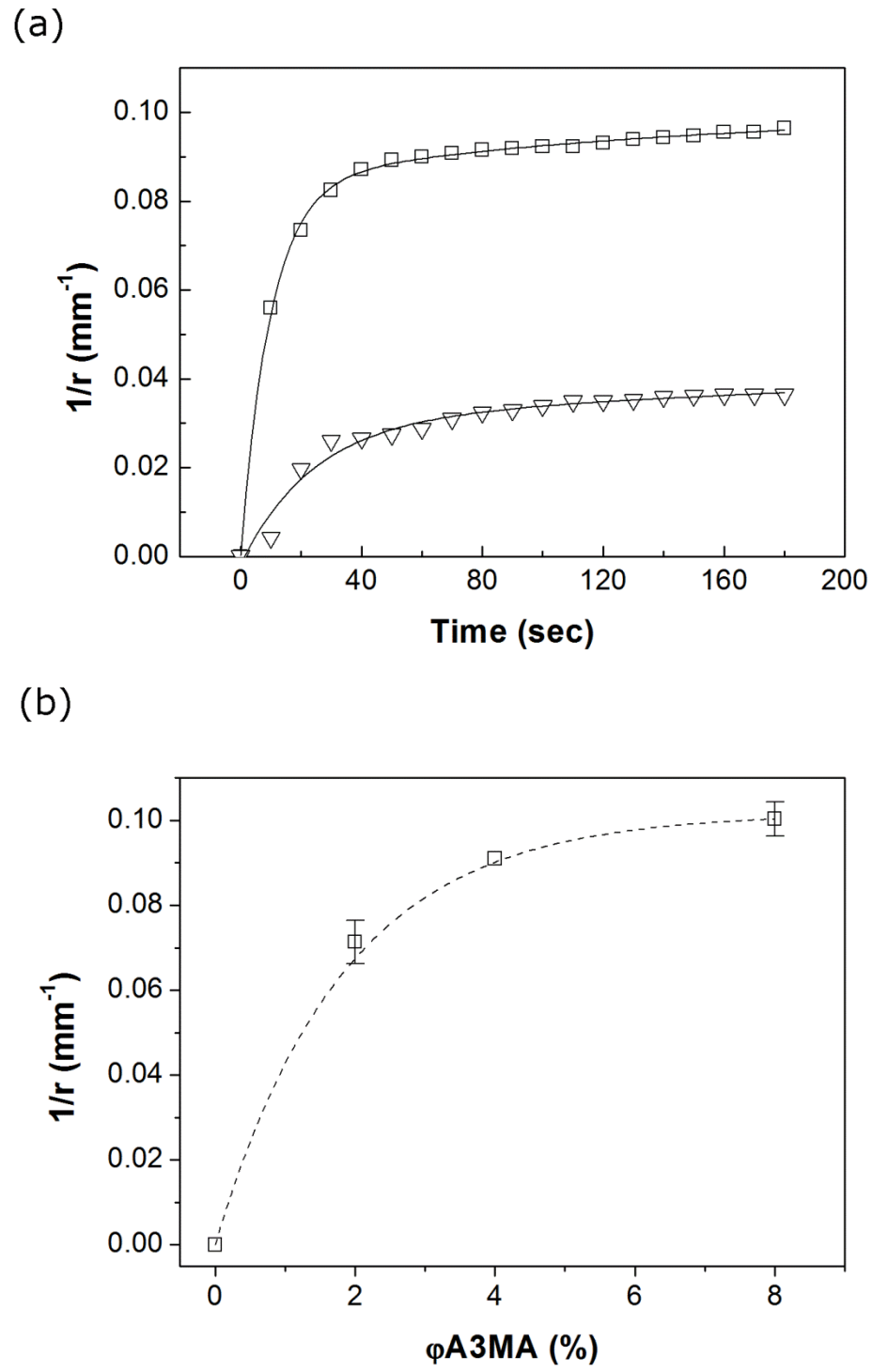

Figure 6-8 (a) Curvature of a PET/LC bilayer with different substrate thickness, 23 μm (□) and 50 μm (▽). UV intensity I = 200 mW.cm^{-2}. The solid lines are a guide for the eye. (b) Curvature of PET/LC bilayers with different concentrations of A3MA. UV intensity I = 200 mW.cm^{-2}. The dash line is a guide for the eye.

Additional experiments were also performed using oriented polyamide 6 (PA6) substrates as this polymer next to PET is one of the most widely used in the textile industry.[19] In Chapter 4 and 5 we successfully aligned mesogens on oriented PA6 substrates. The actuator preparation was done similarly to those for PET. After the photopolymerization step, the films were found to be curved with the LC coating always on the inside of the curvature (Figure 6.9a). This pre-bent shape is thought to originate from the polymerization shrinkage of the polymer network.[24] Surprisingly, the photoresponse of the PA6 system was different in comparison with the PET based actuator (Figure 6.9b). When the film was exposed to UV light the bending radius decreased during the first minute of exposure. As a result exposing the film from the LC side resulted in the actuator bending away from the light source. Prolonged exposure then resulted in a small increase of the bending radius as the film slightly bent back towards the light source. Such response is surprising, as we would expect the coating to contract upon UV exposure. On the other hand, absorption of λ=365 nm light by the azobenzene is usually accompanied by an increase in temperature.[7] As oriented polymers have a negative expansion coefficient, heating will induce contraction in the polymer substrate which may explain the observed response. In order to assess the thermal stability of the substrates, strain measurements during a temperature ramp were performed for the pure PA6 and pure PET films. It was found that the PET film was more stable with only -0.06% strain after heating the film to 50 ^{o}C. In contrast the PA6 substrate showed a -1.13% strain under the same heating conditions.

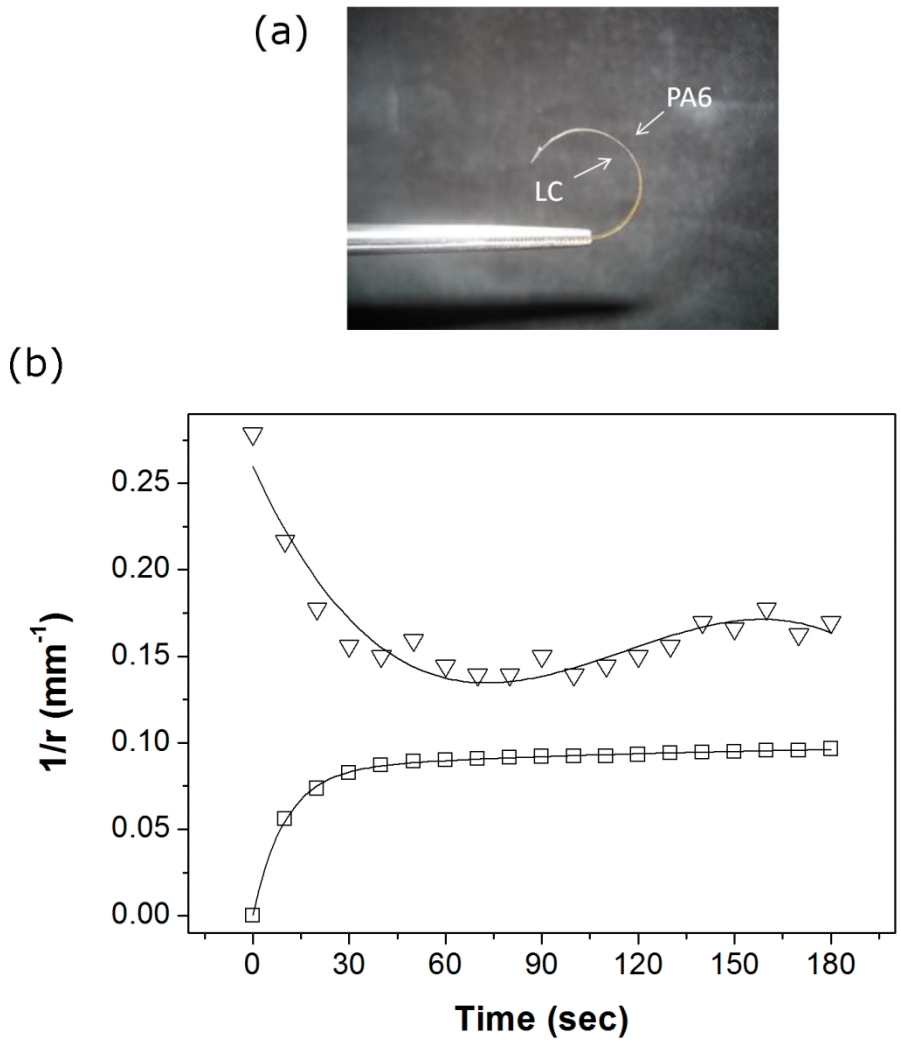

Figure 6-9 (a) Image of the bent shape of the PA6/LC bilayer after UV curing. (b) Bending radius as a function time for a PA6/LC bilayer (▽) and PET/LC bilayer (□). Both LC compositions contain 8% A3MA. UV intensity I = 200 mW.cm^{-2}. Solid lines are a guide for the eye.

6.4 Discussion

Morphological characterization of the coating revealed a well-organized LC layer was obtained on top of the oriented polymer substrate. The mesogens aligned preferentially along the orientation direction of the substrate. ATR FTIR spectroscopy supported a planar alignment. Polarized UV-Vis showed that the addition of A3MA caused a slight decrease in order at high concentrations. The same morphology was also found for PA6 based actuators. Exposure of the PET bilayer films to UV light resulted in a bending of the bilayer. Depending on the exposure side, the films bent towards or away from the light source. The bending mechanism is illustrated in Figure 6.10.

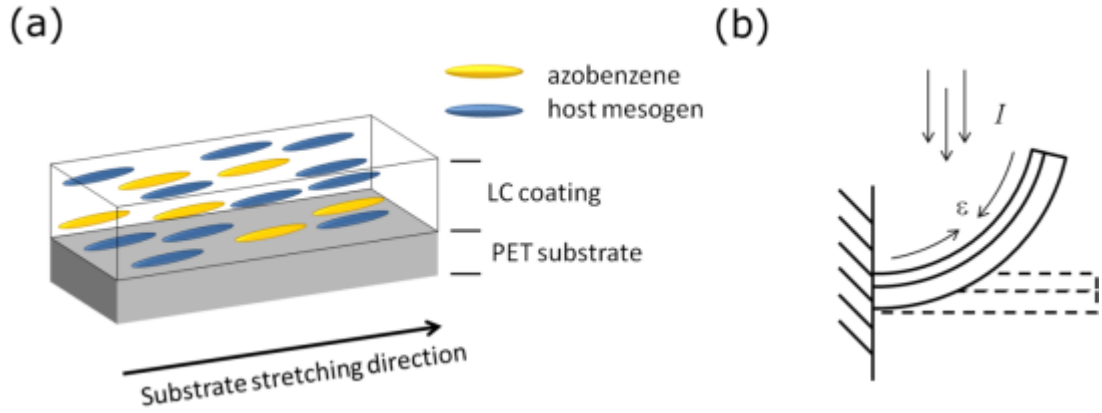

Figure 6-10 (a) Schematic representation of the LC/PET for a planar alignment. (b) Schematic illustration of a photoresponsive bilayer. Upon UV illumination trans- to cis-photoisomerisation induced contraction in the LC coating resulting in a bending moment in the bilayer film.

Upon exposure to $\lambda < 400$ nm, photoisomerisation of the azobenzene induces disorder in the LC network resulting in substantial contraction in the LC layer along the alignment direction. The resulting difference in contraction between the top and the bottom of the actuator bilayer induces a bending moment resulting in the observed deformation. The fact that bending was obtained with concentrations as low as 2% shows that the response comes from a cooperative motion of all the LC molecules induced by a subtle change in order. Additionally, the film deformed regardless of the exposure side (LC or substrate). As the polymer absorbs no or little light in the range of 360 nm, the contraction in the LC layer was of the same order of magnitude, resulting in bending for both situations. Additionally, mechanical deformation is greatly influenced by the thickness and more importantly by the thermomechanical properties of the substrate. It is believed that the response of the actuator results from a competition between contraction (UV induced through photo isomerisation) in the coating and contraction in the substrate (thermally induced resulting from the UV absorption). In the case of the LC/PA6 actuator, contraction in the substrate was pre-dominant over contraction in the coating. As a result the substrate response was the driving force for the actuation. On the other hand, heat had a minor impact on the PET substrate, and the deformation was solely ascribed to the contraction in the LC layer. In this work the bilayer is responsive to UV light which corresponds to the absorbance region of the azobenzene. Yet visible light or sunlight would be far more convenient from a textile application perspective. It is worth mentioning that using different azobenzenes molecules, actuation can be achieved with different wavelengths. Previous works have shown bending of LC networks in response to blue, green or red light as well as with sunlight.[26-29]

6.5 Conclusions

In summary, a photoresponsive actuator has been demonstrated, consisting of an oriented polymer substrate with a photoresponsive LC coating. The planar alignment of the mesogens resulted in substantial contraction in the LC layer when exposed to UV light causing unixaxial bending of the actuator. Different factors influencing the bending have been investigated, allowing optimising of the deformation. An important factor highlighted in this study was the importance of the thermal stability of the polymer substrate. As shown, this effect cannot be neglected and should be taken into account in the material selection for this type of actuators.

6.6 References

1 G. N. Mol, K. D. Harris, C. W. M. Bastiaansen, D. J. Broer, *Adv. Funct. Mater.* **2005**, *15*, 1155.

2 K. D. Harris, C. W. M. Bastiaansen, D. J. Broer, *Macromol. Rapid. Comm.* **2006**, *27*, 1323.

3 K. D. Harris, R. Cuypers, P. Scheibe, C. L. van Oosten, C. W. M. Bastiaansen, J. Lub, D. J. Broer, *J. Mater. Chem.* **2005**, *15*, 5043.

4 H. Finkelmann, E. Nishikawa, G. G. Pereira, M. Warner, *Phys. Rev. Lett.* **2001**, *87*.

5 Y. L. Yu, M. Nakano, T. Ikeda, *Nature* **2003**, *425*, 145.

6 K. M. Lee, H. Koerner, R. A. Vaia, T. J. Bunning, T. J. White, *Macromolecules* **2010**, *43*, 8185.

7 C. L. van Oosten, K. D. Harris, C. W. M. Bastiaansen, D. J. Broer, *Eur. Phys. J. E* **2007**, *23*, 329.

8 M. Kondo, Y. Yu, T. Ikeda, *Angew. Chem. Int. Edit.* **2006**, *45*, 1378.

9 M. Kondo, J. Mamiya, M. Kinoshita, T. Ikeda, Y. L. Yu, *Mol. Cryst. Liq. Cryst.* **2007**, *478*, 1001.

10 Y. L. Yu, M. Nakano, A. Shishido, T. Shiono, T. Ikeda, *Chem. Mater.* **2004**, *16*, 1637.

11 M. Kondo, M. Sugimoto, M. Yamada, Y. Naka, J. Mamiya, M. Kinoshita, A. Shishido, Y. L. Yu, T. Ikeda, *J. Mater. Chem.* **2010**, *20*, 117.

12 Y. L. Yu, M. Nakano, T. Ikeda, *Pure Appl. Chem.* **2004**, *76*, 1467.

13 T. Yoshino, M. Kondo, J. Mamiya, M. Kinoshita, Y. Yu, T. Ikeda, *Adv. Mater.* **2009**, *21*, 1

14 D. J. Broer, R. G. Gossink, R. A. M. Hikmet, *Angew. Makromol. Chem.* **1990**, *183*, 45.

15 M. Yamada, R. Okutsu, J. Mamiya, M. Kinoshita, T. Ikeda, Y. L. Yu, *Mol. Cryst. Liq. Cryst.* **2007**, *470*, 93.

16 M. Yamada, M. Kondo, R. Miyasato, J. Mamiya, M. Kinoshita, Y. L. Yu, C. J. Barrett, T. Ikeda, *Mol. Cryst. Liq. Cryst.* **2009**, *498*, 65.

17 M. Yamada, M. Kondo, J. I. Mamiya, Y. L. Yu, M. Kinoshita, C. J. Barrett, T. Ikeda, *Angew. Chem. Int. Edit.* **2008**, *47*, 4986.

18 M. Yamada, M. Kondo, R. Miyasato, Y. Naka, J. Mamiya, M. Kinoshita, A. Shishido, Y. L. Yu, C. J. Barrett, T. Ikeda, *J. Mater. Chem.* **2009**, *19*, 60.

19 F. Cheng, R. Yin, Y. Zhang, C.-C. Yen, Y. Yu, *Soft Matter* **2010**, *6*, 3447.

20 K. K. Chawla, "*Fibrous materials"*, Cambridge University Press, Cambridge, England ; New York, 1998, p. xv.

21 A. Shimamura, A. Priimagi, J. Mamiya, T. Ikeda, Y. L. Yu, C. J. Barrett, A. Shishido, *Acs Appl. Mater. Inter.* **2011**, *3*, 4190.

22 C. L. van Oosten, D. Corbett, D. Davies, M. Warner, C. W. M. Bastiaansen, D. J. Broer, *Macromolecules* **2008**, *41*, 8592.

23 B. L. Wang, Y. You, Y. Z. Huo, *Thin Solid Films* **2011**, *519*, 5310.

24 Y. Yue, X. Changwei, W. Binglian, J. Lihua, H. Yongzhong, *International Journal of Smart and Nano Materials* **2011**, *2*, 245.

25 R. A. M. Hikmet, B. H. Zwerver, D. J. Broer, *Polymer* **1992**, *33*, 89.

26 T. J. White, N. V. Tabiryan, S. V. Serak, U. A. Hrozhyk, V. P. Tondiglia, H. Koerner, R. A. Vaia, T. J. Bunning, *Soft Matter* **2008**, *4*, 1796.

27 C. L. van Oosten, C. W. M. Bastiaansen, D. J. Broer, *Nat. Mater.* **2009**, *8*, 677.

28 R. Y. Yin, W. X. Xu, M. Kondo, C. C. Yen, J. Mamiya, T. Ikeda, Y. L. Yu, *J. Mater. Chem.* **2009**, *19*, 3141.

29 S. Serak, N. Tabiryan, R. Vergara, T. J. White, R. A. Vaia, T. J. Bunning, *Soft Matter* **2010**, *6*, 779.

Chapter 7

Conclusions and Future work

7.1 Conclusions

Smart textiles have recently received much interest from both industry and academia with areas of application as diverse as military, architecture or medical and an on-growing market for consumer goods (Figure 7.1).[1] In this work conventional fibres and textiles have been combined with optics and LCD technologies to enhance their functionalities. The thesis has focused on three main aspects which are (i) perception, (ii) sensing and (iii) responsiveness. In the first part, perception of fibres was addressed using two different approaches, one based on photolithography to generate colours by diffraction of light. The other approach is based on a self-organising cholesteric liquid crystal (CLC) coating that generates structural colours through selective reflection of light. The second part, explored the potential for sensing strain optically using a CLC polymers combined with a flexible polymer

carrier. Finally, in the last part, the work aimed at demonstrating how responsiveness could be introduce into textiles by producing light driven actuating bilayer film. These actuators consisted of an oriented polymer carrier with a photoresponsive liquid crystalline network.

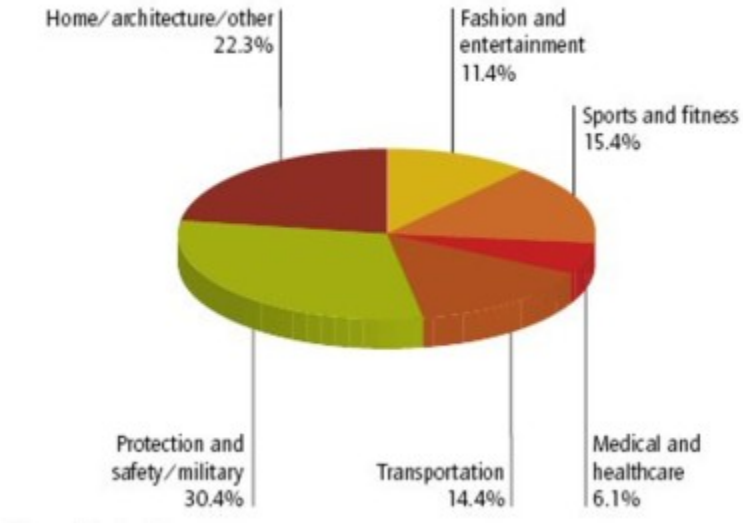

Figure 7-1 Smart fabrics end-use markets, 2011 (Source: Intertech Pira, Smithers Apex).[1]

7.1.1 Perception in textiles based on diffraction and reflection of light

Fibres and films with striking, angular dependent colours originating from reflective or diffractive effects were produced. For the latter, diffractive features were created on the surface of a polymer substrate using photoembossing. This soft lithographic process allows generating surface relief structures through a UV photopatterning step followed by a thermal development step. Generally a step wise process, its application to fibres is limited due to the low through-put of the technique. In

Chapter 3 it was demonstrated that by using pulsed holography, photoembossed structures could be successfully generated in flat films in static and/or dynamic conditions, *i.e.* moving films. The latter is attributed to the short exposure time (5 ns pulse) allowing the film to move without losing contrast in areas exposed to UV light. This continuous process greatly improved the throughput of photoembossing with a maximum speed of 0.21 $m.s^{-1}$. Although far from speeds encountered in fibre spinning processes (> 100 $m.s^{-1}$) it is mainly limited by laser specifications and therefore higher line speeds are to be expected for lasers with higher frequency pulsing rate and/or higher output energy.

Structural colours based on reflection of light were also produced in oriented polymer films and fibres using a cholesteric liquid crystal (CLC) network. Melt processed fibres and films were drawn and spray-coated with a cholesteric liquid crystal monomer mixture. The coating was then cured through a photopolymerization step. Films exhibited strong angular dependent colours due to their two dimensional shape while fibres, which can be considered as 1D objects, showed angular dependence in one dimension only. The curved geometry of the fibre impacted on the reflection band, as it was broader and the reflectivity only reached 26%. In comparison, films showed a sharp reflection band that could reach up to 80% reflectivity when the coating was applied on both sides of the polymer film. CLCs are intrinsically limited to 50% reflection of un-polarized light; here the high reflection was attributed to the half wave retardation induced by the oriented polymer substrate. The coating process was also done in a continuous fashion, and PA6 filaments were successfully coated. The as-produced fibre was then woven into a conventional weaving pattern (8 harness-satin) to demonstrate the textile application.

7.1.2 Optical strain sensing

In Chapter 4 it was demonstrated that a well-defined planar CLC arrangement can be obtained on oriented PA6 films. In Chapter 5, the optical response to deformation of these coated PA6 films was then investigated. It was found that uniaxial stretching of the PA6 substrate resulted in a pitch decrease in the CLC layer due to Poisson's contraction. In this study it was shown that 10% strain resulted in a 25 nm shift towards lower wavelengths. This shift was enough to result in change in colour, in this case from orange to green. It was also demonstrated that the colour changed accordingly to the mechanical behaviour of the PA6 substrate making this type of sensor particular suited for real-time strain sensing.

7.1.3 Light driven actuation

In the last part of the thesis, the intention was to produce fibres that respond to an environmental stimulus such as temperature, humidity or light; for adaptive textiles. In Chapter 6 we developed a bilayer LC/polymer film that deformed in response to UV-light. This bilayer structure was produced by spray coating a liquid crystal monomer mixture comprising an azobenzene mesogen, onto an oriented PET substrate followed by a photopolymerization step to cross-link the LC network. Extensive characterization of the coating was carried out to establish the morphology of the coating. It was found that the mesogens were organized in a monodomain planar alignment, with its director oriented along the stretching direction of the polymer substrate. Exposure of the bilayer to UV light ($\lambda < 400$ nm) resulted in the deformation of the film from a flat shape to a bent shape. This deformation was

attributed to a photoinduced contraction along the orientation direction in the LC layer. The contraction originated from a cooperative motion of the mesogens resulting from the photoisomerisation of the azobenzene moieties present in the LC polymer network. The effect of substrate thickness and azobenzene contraction on the bending behaviour of the bilayer system was also investigated. Experiments were also performed with oriented PA6 substrates. Here, the behaviour was somewhat unexpected as it showed an opposite bending response to the PET bilayer system. The results pointed out the importance of thermally induced contraction of the substrate as was confirmed by measuring thermal shrinkage of the substrate. Heating the PA6 film to 50 ^{o}C showed a large shrinkage of 2.6% while for PET heating resulted in minor shrinkage ($\varepsilon < 0.1\%$). In comparison the photoinduced contraction in the LC layer was only 0.6%. Therefore in this case, the observed response was primarily driven by the substrate behaviour.

7.2 Future work

Throughout this thesis it has been shown that a liquid crystal polymer coating is a promising approach to produce functional fibres. Some of the work has demonstrated its application to textiles with the production of a fabric demonstrator. However, further textile specific characterizations are needed. Some are as simple as putting the fabric through repeated washing cycles to demonstrate the robustness of the coatings, while others are more specifically related to adhesion and abrasion resistance of the coating for durability testing, water/gas permeability for breathability and/or comfort.[2] In this work wavelength specific reflective fibres were

produced which had a metallic effect that changed colour in a single dimension, *i.e.* when the viewer moved along the fibre axis. These optical effects suggest interesting applications for fashion, apparel and entertainment. However, reflective fibres based on CLC networks have also great potential for applications in areas such as architecture or cosmetics. In Chapter 4 it has been mentioned that the reflected wavelength is easily tuned by adjusting the amount of chiral mesogens in the CLC monomer mixture. Thus reflection bands can be generated for instance in the near IR region. Figure 7.2 shows preliminary results of three different reflection bands in the near IR region.

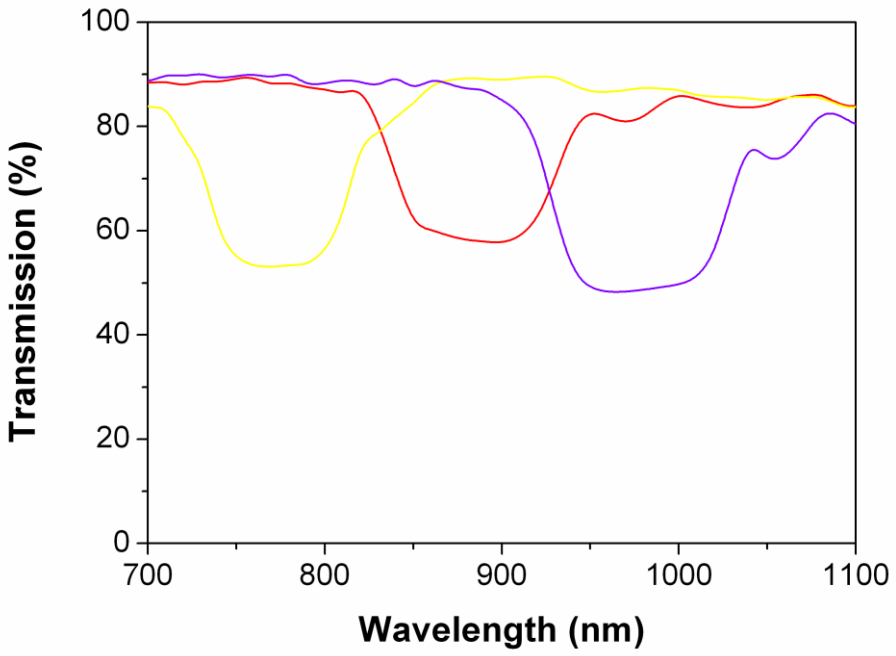

Figure 7-2 Transmission spectrum of CLC coatings with different amounts of chiral mesogens(yellow, red and purple curves correspond to 3.8, 3.3 and 2.9 wt.% of chiral dopant). Each reflection band is centred on a different wavelength in the near IR region

A promising area for such fibres is for heat management in buildings where the energy demand for cooling is constantly increasing.[3] Near IR reflecting fibres woven into fabrics would act as functional curtains reflecting heat radiations from the sun while remaining transparent to visible and UV wavelengths. Additionally, using round cross-sectional fibres, the reflection band will remain invariant of the incident angle around the fibre axis. This presents the advantage of reflecting the same wavelength throughout the day regardless of the position of the sun.

Finally, light driven moving bilayer films were produced. Yet the potential for smart actuating garments in response to an environmental stimulus still needs to be explored and adaptive Gore-Tex® materials spring to mind. From a textile perspective, curling or coiling deformations might be more relevant as they may enhance the macroscopic actuation of the fabric. Films that coil in response to temperature or light rather than bend are readily obtained by introducing a twist in the LC director through the thickness of the film.[4-5] By introducing a small twist in the molecular orientation using for instance a chiral compound, out of plane bending leading to curling can be generated. In our preliminary work we obtained such response in PET/LC bilayer films (Figure 7.3b). The offset orientation of the mesogens was obtained by adding a small portion of LC756 to the LC mixture. The resulting twist in molecular orientation can be controlled through the chiral dopant concentration resulting in a more or less pronounced curling response (Figure 7.3b).

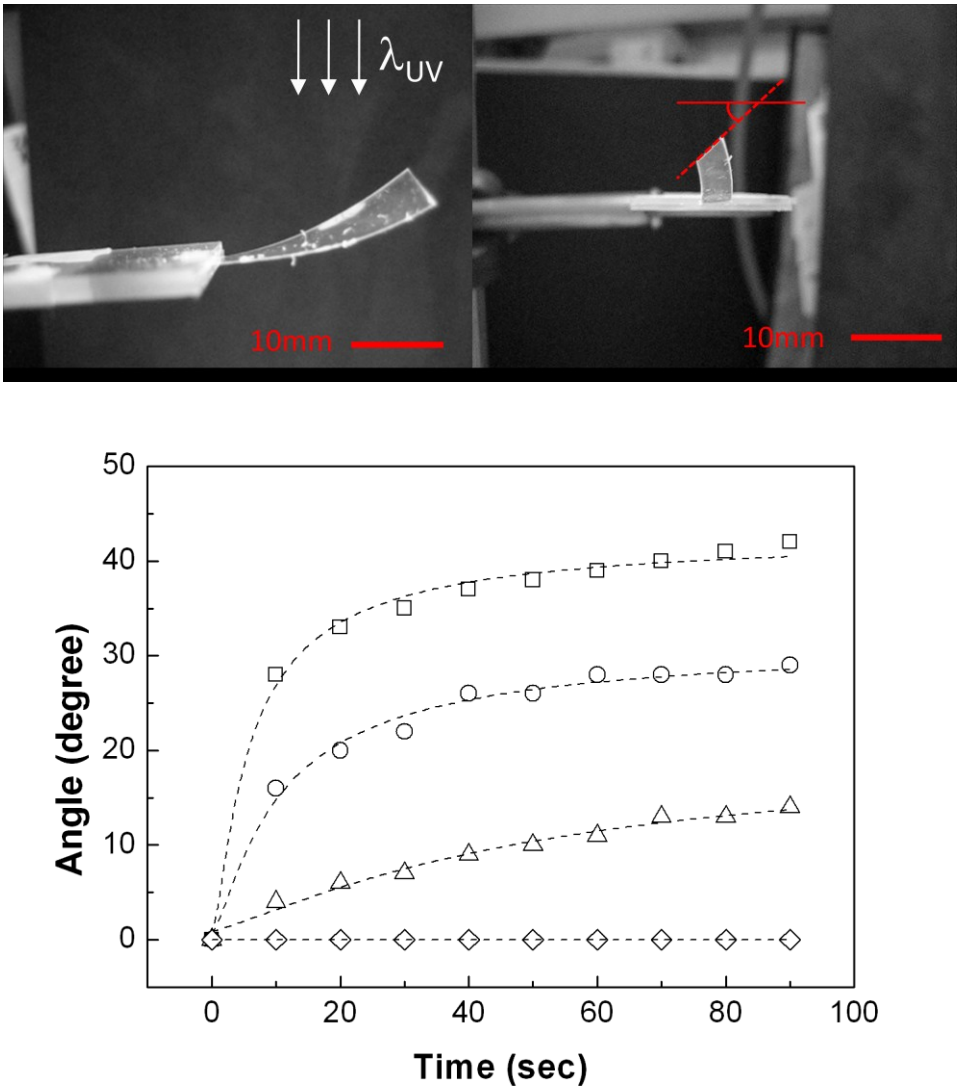

Figure 7-3 a) Curling response of a bilayer film (10 mm x 4 mm) to UV (100 mW.cm^{-2}). The thickness of the polymer substrate was 25 μm and the coating thickness was 5 μm. B) Influence if chiral dopant content on the twist angle: 0 wt.% (◇), 0.1 wt.% (□), 0.2 wt.% (○) and 0.4 wt.% (Δ).

Although complete twisting over 360^{o} was not obtained it is worth mentioning that substrate thickness and stiffness will affect the actuation as it has been shown in Chapter 6. Nevertheless, curling response is achievable in bilayer LC/polymer films with this approach.

References

1 https://www.smithersapex.com/smart-textiles-to-see-rapid-growth-to-2021.aspx.

2 W. Fung, "*Coated and laminated textiles"*, CRC Press ; Cambridge, 2002, p. 250.

3 H. Breesch, A. Bossaer, A. Janssens, *Sol. Energy* **2005**, *79*, 682.

4 Y. Sawa, F. F. Ye, K. Urayama, T. Takigawa, V. Gimenez-Pinto, R. L. B. Selinger, J. V. Selinger, *P. Natl. Acad. Sci. USA* **2011**, *108*, 6364.

5 K. D. Harris, R. Cuypers, P. Scheibe, C. L. van Oosten, C. W. M. Bastiaansen, J. Lub, D. J. Broer, *J. Mater. Chem.* **2005**, *15*, 5043.